Dissertation

Deciphering the role of intestinal DGAT1 in lipid and energy homeostasis

submitted by

Vinay Vasudev SACHDEV

for the Academic Degree of

Doctor of Philosophy

(Ph.D.)

at the

Medical University of Graz

Institute of Molecular Biology and Biochemistry

Under the Supervision of

Prof. Dr. Dagmar Kratky

2017

Acknowledgement

I want to express sincerest gratitude to my supervisor and mentor Prof. Dagmar Kratky for her constant and strong support for all this time. I am indebted for her efforts, time and guidance to carve a scientist out of me. It is commendable how she encourages, teaches and nurtures scientific thinking in students. It helped me tremendously to trust my instincts. Thanks a lot! I specially thank Anton Ibovnik and Silvia Rainer for their impeccable technical assistance and help throughout this research work.

This doctoral thesis was a fantastic journey, one that I cherished and relished the steep learning curve. It was a pleasure to work on a scientific and personal front alongside such wonderful people throughout this period. A special thanks to present and former colleagues at Institute of Molecular Biology and Biochemistry, Medical University of Graz, for maintaining such friendly and conducive environment at work. Each one of them has left a special impression which has helped me mold for better.

I like to thank all our collaborators in Graz as well as abroad for their valuable support at different stages of this research. A special token of thanks to Prof. Albert K. Groen, University of Groningen, Groningen and Prof. Mahmood M. Hussain, SUNY DOWNSTATE MEDICAL CENTER, New York for hosting and supporting me during my research stay abroad. It was a great learning experience and had an amazing time working with colleagues at both laboratories.

I am thankful to our funding sources, FWF, Medical University of Graz and DK-Program “Metabolic and Cardiovascular Disease”. Sincere thanks to Karin Osibow for all her help and superb administration of student affairs.

Great cheers to all friends for the fun times we had in last years. Special thanks to Sumitra for being my pillar during good part of this thesis. Finally, words will not suffice to appreciate the support and love of my family: mom, dad, sisters and now a beautiful inclusion, my fiancée, Madalina Duta-Mare!

This work is dedicated to

My family

On their shoulders I stand tall

Table of contents

Declaration

I hereby declare that this thesis is my own original work and that I have fully acknowledged by name all of those individuals and organizations that have contributed to the research for this thesis. Due acknowledgement has been made in the text to all other material used. Throughout this thesis and in all related publications I followed the “Standards of Good Scientific Practice and Ombuds Committee at the Medical University of Graz”

Graz, 11.05.2017

…….

Vinay Sachdev

Please note that parts of this thesis have been published and/or are under preparation for future publications.

Novel role of a triglyceride-synthesizing enzyme: DGAT1 at the crossroad between triglyceride and cholesterol metabolism

Sachdev V, Leopold C, Bauer R, Patankar JV, Iqbal J, Obrowsky S, Boverhof R, Doktorova M, Scheicher B, Goeritzer M, Kolb D, Turnbull AV, Zimmer A, Hoefler G, Hussain MM, Groen AK, Kratky D.

Biochim Biophys Acta. 2016 Sep;1861(9 Pt A):1132-41.

Triglyceride synthesis by DGATs is essential for lipid fuel replenishment in cold- acclimated mice

Sachdev V, Duta-Mare M, Huber K, Saurug P, Bogner-Strauss JG, Kratky D

Manuscript under preparation

Zusammenfassung

Fettleibigkeit und die damit in Verbindung stehenden Erkrankungen verbreiten sich weltweit mit steigender Tendenz und erhöhen damit auch die Häufigkeit des metabolischen Syndroms. Charakteristisch für das metabolische Syndrom sind erhöhte Triglyzerid- und Cholesterinwerte im Plasma. Acyl-CoA Diazylglyzerol Acyltransferasen (DGATs) katalysieren den letzten und geschwindigkeitbestimmenden Schritt in der Triglyzeridbiosynthese. Die zwei bekanntesten Vertreter dieser Enzyme sind DGAT1 und DGAT2. Ein systemischer DGAT1 Verlust in Mäusen hat positive Auswirkungen auf den Phänotyp und ist charakterisiert durch eine Resistenz gegenüber Diät-induzierter Fettleibigkeit, hepatischer Steatose und geht einher mit einem erhöhtem Energieumsatz. Diese metabolischen Vorteile gehen allerdings verloren, wenn DGAT1 nur im Darm exprimiert wird. Zusätzlich haben DGAT1-defiziente Mäuse auf Apolipoprotein E-defizienten Hintergrund, durch reduzierte Plasma Cholesterinwerte sowie eine reduzierte Aufnahme von Cholesterin aus dem Darm positive Auswirkungen auf die Entstehung von Atherosklerose.

Im ersten Teil dieser Arbeit verwendeten wir darmspezifische DGAT1-defiziente (I-DGAT1$^{-/-}$) Mäuse um die Beteiligung der darmspezifischen DGAT1 Aktivität auf den Triglyzerid- und Cholesterinhaushalt zu untersuchen. Die Cholesterinabsorption, die mittels akuten und fraktionellen Cholesterinabsorptionsstudien gemessen wurde, war im Dünndarm und der Leber von I-DGAT1$^{-/-}$ Mäusen deutlich reduziert. Nach Fütterung der Mäuse mit einer fett- und cholesterinreichen Diät (HF/HCD) zeigten I-DGAT1$^{-/-}$ Mäuse eine Resistenz gegenüber Diät-induzierter Fettleibigkeit sowie reduzierte Plasmakonzentrationen an Cholesterin im Vergleich zu den Kontrolltieren. Dieselben Ergebnisse beobachteten wir auch in globalen DGAT1$^{-/-}$ und mit DGAT1 Inhibitor behandelten Mäusen. Weiters ist der postprandiale Chylomikronen-Metabolismus in I-DGAT1$^{-/-}$ Mäusen verändert. Durch eine gleichzeitige Gabe von [^{3}H]Triolein und [^{14}C]Cholesterin zeigte sich sowohl eine reduzierte Chylomikronensekretion als auch weniger Chylomikronen im Plasma und in der Lymphe. Defizienz als auch Inhibierung von DGAT1 resultierte außerdem in kleineren Chylomikronen und erhöhter trans-intestinaler Cholesterinausscheidung (TICE). Ergebnisse aus dieser Dissertation zeigen, dass ein verbesserter

Cholesterinmetabolismus einerseits durch reduzierte Cholesterinsekretion aus den Enterozyten und andererseits durch eine veränderte Aufnahme von freien Fettsäuren aus der Nahrung resultiert. Zusammenfassend deuten die Ergebnisse auf eine bislang unbekannte Rolle von DGAT1 hin. DGAT1 Defizienz/ Inhibierung beeinflusst den Cholesterin- und Chylomikronenmetabolismus und führt zu einer Erhöhung von TICE.

Im zweiten Teil dieser Arbeit untersuchten wir die Auswirkungen der DGAT Enzyme auf die Wärmeregulierung während akuter und chronischer Kälteexperimente. Speziell in Zeiten eines erhöhten Energiebedarfs spielen zirkulierende Lipoproteine wie z.B. Chylomikronen eine wesentliche Rolle für die Bereitstellung von Energie für das braune Fettgewebe. Ich untersuchte daher, ob die zuvor gefundenen reduzierten Cholesterinkonzentrationen im Plasma sowie Chylomikronengrößen in I-DGAT$^{-/-}$ Mäusen Auswirkungen auf die Wärmeregulierung während Kälteexpositionen hat. Ich beobachtete eine erhöhte Aufnahme Chylomikronen-induzierter Lipide im braunen Fettgewebe von I-DGAT$^{-/-}$ Mäusen, die der Kälte ausgesetzt waren. Zusätzlich war die akute Wärmeregulierung in I-DGAT$^{-/-}$ Mäusen, die ein fett- und cholesterinreiches Futter erhielten, leicht verbessert, während die adaptive Wärmeregulation mit den Kontrolltieren vergleichbar war. Darüber hinaus zeigte eine pharmakologische DGAT1 und DGAT2 Inhibierung, *in vitro* und *in vivo*, dass die Triglyzeridbiosynthese über die DGAT Enzyme im braunen Fettgewebe wesentlich für die Aufrechterhaltung des freien Fettsäurenachschubs ist.

Abstract

Obesity and its associated disorders have risen to epidemic proportions globally and thus concomitantly increased the prevalence of the metabolic syndrome. Elevated circulating plasma triglyceride (TG) and total cholesterol (TC) concentrations are characteristic features often associated with the metabolic syndrome. Acyl-CoA:diacylglycerol acyltransferases (DGATs) catalyze the final and only dedicated step of TG biosynthesis. DGAT1 and DGAT2 are two known forms of DGAT enzymes. DGAT1 deficiency in mice results in a metabolically beneficial phenotype of resistance to diet-induced obesity and fatty liver disease and increased energy expenditure, which is reversed when DGAT1 is expressed only in the intestine. Furthermore, DGAT1 deficiency in apolipoprotein $E^{-/-}$ mice has an athero-protective role partially due to lower plasma cholesterol concentrations and reduced intestinal cholesterol absorption.

In the first part of this thesis, we used intestine-specific DGAT1 knockout (I-$DGAT1^{-/-}$) mice to elucidate the contribution of intestinal DGAT1 (I-DGAT1) activity in TG and cholesterol homeostasis. Cholesterol absorption, as measured by acute and fractional cholesterol absorption assays, was severely reduced in the small intestine and liver of I-$DGAT1^{-/-}$ mice. When challenged with high-fat/high cholesterol diet, I-$DGAT1^{-/-}$ mice exhibit resistance to diet-induced obesity coupled with lower plasma TC and cholesteryl ester concentrations compared to control littermates. Observations of I-DGAT1 deficiency phenocopy findings in whole body $DGAT1^{-/-}$ and DGAT1 inhibitor-treated mice. The postprandial chylomicron metabolism is altered in I-$DGAT1^{-/-}$ mice as simultaneous gavage of [^{3}H]triolein and [^{14}C]cholesterol revealed a reduced chylomicron secretion rate and radiotracer counts in plasma and lymph chylomicrons. In addition, deficiency/inhibition of DGAT1 results in smaller chylomicron size and increased trans-intestinal cholesterol excretion. We show that the improved cholesterol phenotype is a result of decreased enterocyte cholesterol secretion and altered dietary FA metabolism. In summary our findings provide insight into a novel role of DGAT1 and identify a pathway by which I-DGAT1 deficiency affects whole-body cholesterol homeostasis in mice by altering chylomicron metabolism and increasing TICE.

In the second part, we explored the contribution of DGAT enzymes in the maintenance of thermoregulation upon acute and chronic cold exposure. Circulating lipoproteins like chylomicrons play a significant role towards fuel replenishment in the brown adipose tissue during high energy demand conditions. Therefore, we determined whether reduced circulating cholesterol concentrations and smaller chylomicron size observed in I-DGAT1$^{-/-}$ mice affects thermoregulation upon acute or chronic cold exposure. We observed increased uptake of chylomicron-derived lipids in the BAT of cold-exposed I-DGAT1$^{-/-}$ mice. Furthermore, acute thermogenesis was slightly improved in I-DGAT1$^{-/-}$ mice but the adaptive thermogenesis was comparable between control and I-DGAT1$^{-/-}$ mice. In addition, using *in vitro* and *in vivo* pharmacological DGAT1 and DGAT2 inhibition studies, we determined that TG biosynthesis via DGAT enzymes in BAT is fundamental for the replenishment of the FA pool to sustain thermogenesis during shivering as well as non-shivering thermogenesis.

Chapter I

Role of intestinal DGAT1 in regulation of cholesterol homeostasis

1. Introduction

1.1. Metabolic syndrome

1.1.1 Definition of the metabolic syndrome

The metabolic syndrome (MetS), also referred to as syndrome X or insulin resistance syndrome, is a cluster of clinical abnormalities manifesting the risk for cardiovascular disease, stroke, vascular dysfunction, and diabetes. The characteristic features of the pathogenesis include central obesity and insulin resistance as major causative factors in combination with several other predisposing risk factors (1). The constellation of metabolic abnormalities and their 'cut-off' points are still a matter of debate; nevertheless, the guidelines issued by the World Health Organization define MetS as combination of insulin resistance/diabetes plus any of the following two conditions:

(a) Obesity: waist/hip ratio >0.9 in males and >0.85 in females or body mass index >30kg/m^2,

(b) Dyslipidemia: triglycerides (TG): ≥150 mg/dL and high-density lipoprotein cholesterol (HDL-C) <35 mg/dL in males and <39 mg/dL in females,

(c) Microalbuminuria: urine albumin ≥20µg/min or albumin: creatinine ratio ≥ 30 MAG/g,

(d) Blood pressure: ≥140/90mm Hg (2).

By this definition, 20–25% of the world's population suffers from MetS. The prevalence of MetS varies from 8% to 43% in men and from 7% to 56% in women around the world (3). Individuals with MetS are five-fold more susceptible to develop insulin resistance, which further elevates the risk for type 2 diabetes mellitus (T2DM) and cardiovascular diseases (CVD). The presence of these features results in an increased risk of developing fatty liver, cholesterol gallstones formation, polycystic ovary syndrome, asthma, apnoea, and certain forms of cancer, such as breast, pancreatic, colorectal, and prostate cancer (4, 5). The pathophysiology of MetS is extremely intricate, involving multiple organs and has been only partially elucidated.

1.1.2 Insulin resistance and the metabolic syndrome

Insulin resistance and T2DM are often associated with dyslipidemia characterized by elevated triglyceride-rich lipoproteins (TRLs), decrease in HDL-C and metabolically altered low-density lipoprotein (LDL). Increased free FA (FFA) flux from adipocytes induces visceral TG deposition in peripheral tissues such as skeletal muscles and liver, which triggers increased production of glucose and hepatic release of TRLs such as very low-density lipoproteins (VLDL) contributing to insulin resistance and its associated diseases (6). Apolipoprotein B (apoB), a major protein moiety of lipoproteins, is stabilized by FFAs and is degraded in an insulin-dependent manner via the phosphoinositide 3-kinase pathway. Increased FFAs leading to insulin resistance stimulate VLDL production by inhibiting apoB degradation leading to an atherogenic dyslipidemia (7). Another hallmark of insulin resistance is decreased capacity of lipoprotein lipase (LPL), the rate-limiting enzyme to cleave TGs from VLDL and other lipoproteins to facilitate their clearance from circulation. Thus, insulin resistance increases VLDL concentrations by increasing its production in the liver, and by preventing its clearance from circulation, hence accelerating the manifestations of CVD (6, 8).

VLDL is further catabolized to remnant lipoproteins and small dense LDL, an established athergonic lipoprotein (9). These particles accelerate atheroma formation due to their higher capacity to be taken up by macrophages, decreased hepatic clearance due to low affinity for the LDL receptor, more profanity to enter the arterial wall due to higher binding affinity to proteoglycans, and being more susceptible to oxidation (10).

Because LPL is less active in insulin-resistant states, an expanded plasma TG pool induces accelerated exchange of TGs and cholesteryl esters (CEs) between VLDL and lipoproteins, including LDL and HDL. This process results in the enrichment of TGs and depletion of CEs from both LDL and HDL. The specific TG enrichment in the core of HDL particles could explain the impairment of their antioxidative properties (8).

1.1.3 Obesity and the metabolic syndrome

An imbalance between energy intake and energy expenditure due to excessive intake of calorie-rich, nutrient-dense food and lack of physical activity has led to obesity in today's population to epidemic proportions (11). The plasticity of adipocytes allows them to increase in size to accommodate increased influx of calories. However, over the period of time, increased adipocyte hypertrophy and hyperplasia result in decreased blood supply to the tissue and increased adipocyte cell death. Macrophages are recruited in high numbers to clear the apoptotic cells, which leads to low-grade inflammation along with secretion of various pro-inflammatory markers like tumor necrosis factor alpha and interleukin-6 and adipokines such as adiponectin, leptin, plasminogen activator inhibitor-1, and angiotensinogen (12). Ectopic lipid deposition in peripheral tissues combined with systemic inflammation result in insulin resistance and subsequently in MetS as shown in Fig. 1.

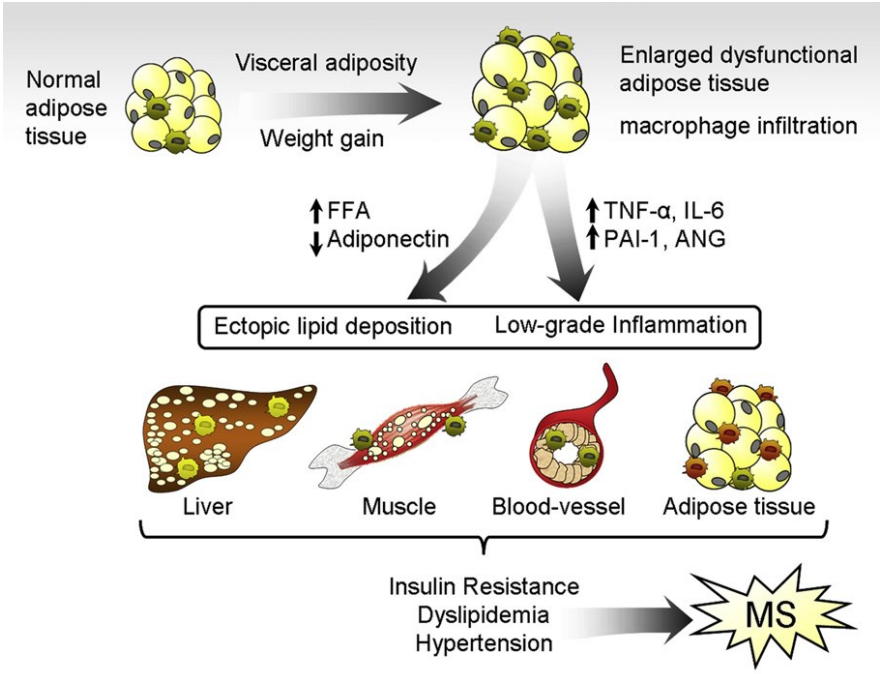

Figure 1: Adipose tissue expansion, insulin resistance, and the metabolic syndrome. Access calorie intake and ectopic fat accumulation result in bigger and less active adipocytes. Increased flux of FFA release into the periphery, reduced adiponectin functions, and elevated secretion of pro-inflammatory markers are characteristic feature of dysfunctional adipocytes. Over the period of time, these characteristics manifest into obesity and systemic low-grade inflammation, the known casual factors for the development of insulin resistance. The cascade of events often result in dyslipidemia and hypertension leading to the MetS phenotype (12). Requisite permission to use this figure was obtained (Appendix).

1.1.4 Treatment of the metabolic syndrome

MetS is a complex conglomeration of various physiological manifestations leading to elevated risk of atherosclerotic CVD, T2DM, and all-cause mortality. Thus, the treatment options vary dramatically based on the environmental exposure, genetic predisposition, and composition (age, sex, and ethnicity). However, improvement of lifestyle is recommended as first choice of therapy combined with increased physical activity and diet modifications. Various studies recommend weight loss of 10% reduction in body weight in the first six months to a year and continued thereafter until a BMI less than 25 has been recorded (10). In order to control hypertension, a recommended daily sodium intake between 65–100 mmol should be supplemented with the intake of fruits and vegetables enriched with potassium, with a goal of 90–120 mmol of potassium per day (13). Pharmacological intervention is considered where lifestyle modifications are unable to decrease the apparent risk factors. Drugs prescribed for weight loss include two main classes: appetite suppressants such as phentermine derivatives and Sibutramine and nutrient absorption inhibitor such as the gastrointestinal lipase inhibitor Orlistat (14). Angiotensin converting enzyme inhibitors or angiotensin receptor blockers is the first-line of pharmacological treatment in the MetS, especially in the setting of diabetes or nephropathy (15). Statins are choice of drugs for reducing LDL-C concentrations in patients suffering from acute coronary syndrome (16). Statins act by inhibiting 3-hydroxy-3-methyl-glutaryl (HMG-CoA) reductase, the rate limiting enzyme in cholesterol biosynthesis and exhibit few pleotropic effects. They have also been shown to increase HDL-C by 5–10%, and reduce TGs concentrations by 7–30% primarily with moderate to high doses (16). Nevertheless, the treatment regimen is often aimed at maintenance rather than curing the syndrome. Thus, to better understand the MetS and develop targeted strategies for its treatment we need to look at organs which regulate nutrient handling, its absorption, and assimilation, namely the intestine.

1.2 Overview of intestinal lipid absorption

Virtually, absorption of all nutrient lipids across the blood stream is carried out by highly dynamic epithelial mucosa of the intestine. The immense amounts of dietary lipids in our calorie-dense modern diet are processed with effective ease by the

small intestine. Along with nutrient digestion and absorption, its roles extend to energy and nutrient expenditure and maintaining immunological competence. The sufficiently 'fed' intestine facilitates energy nourishment in a series of orderly and interrelated steps; however, it is the 'overfed' intestine which has been in the focus of clinical and basic efforts (17). Dietary lipids are processed and packaged into chylomicrons and released into the blood stream. An imbalanced calorie intake and expenditure leads to overproduction of these lipoproteins, their accumulation and/or defective clearance from plasma resulting in dyslipidaemias, a predominant catalyst for obesity, insulin resistance, and cardiovascular diseases. Thus, understanding the mechanisms of intestinal lipid absorption is important as it not only sustains life but is also the root cause of modern-day life threatening diseases (17). A brief overview of dietary lipid transport is shown in the cartoon below (Fig. 2).

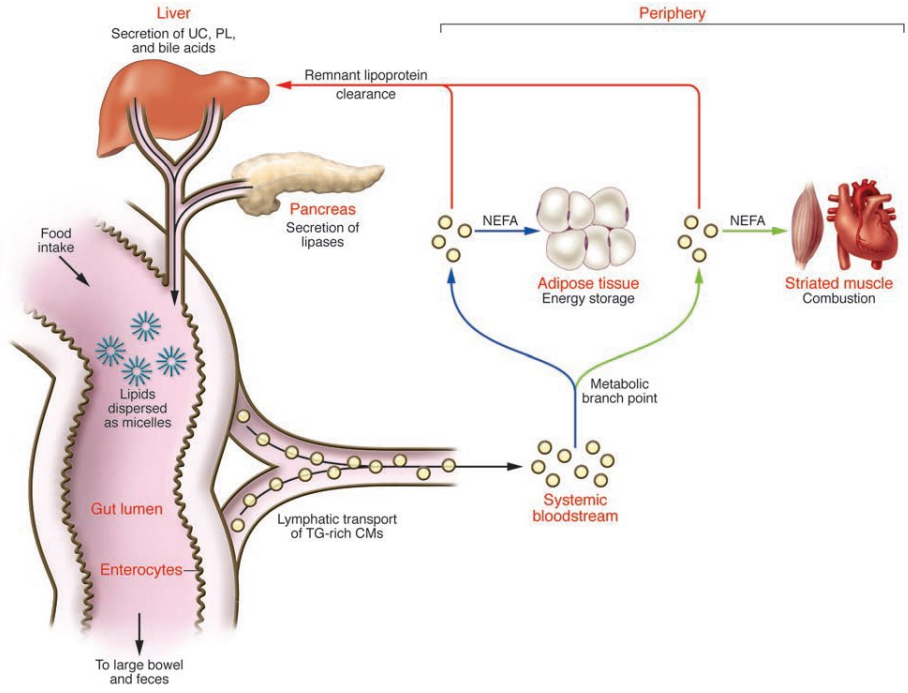

Figure 2: Cartoon depicting dietary lipid transport from intestinal lumen to peripheral tissues. Dietary lipids are processed by gastric and pancreatic lipases, emulsified by hepatic bile acids, and packaged into chylomicrons (CM), which are released into the blood stream to provide non-esterified free FAs (NEFA) for peripheral tissues like adipose tissues and muscles. Resultant remnant lipoproteins are transported to the liver for clearance (17). Requisite permission to use this figure was obtained (Appendix).

1.2.1 Intestinal triglyceride absorption

Dietary TGs form the bulk of animal fats and plant oils along with trace amounts of phospholipids, sterols, lipophilic vitamin, and other components. Due to its highly hydrophobic nature, TGs are unable to pass readily through cellular membranes. Thus, they are solubilized into micelles by the action of bile acids (BA) and hydrolyzed by lingual, gastric, and pancreatic lipases into basic components like FAs (FAs) and monoglycerides (MGs). This absorption occurs primarily in the absorptive enterocytes of proximal half of the intestine and very less in the distal intestine. The process is so well tuned that, after any given meal, more than 95% of ingested dietary fats are absorbed by the intestine (18). The processing of fat is metabolically more efficient and thus requires less energy expenditure after its consumption compared to other nutrient sources like carbohydrates and proteins (19). In addition, intestinal fat absorption triggers enteroendocrine and neural mediators to govern signals indicating the nutritional status, which, in turn, regulates the systemic metabolism. Thus, intestinal TG homeostasis is pivotal for overall energy metabolism *in vivo* (20).

The absorption of FAs and MGs across the enterocytes is majorly carried out through concentration gradient-dependent passive diffusion. The brush border membrane (BBM) of enterocytes harbors an unstirred water layer which, creates an optimum acidic microenvironment for diffusion of large amount of FAs through the lumen (21). Although various proteins are implicated in facilitating FA uptake, their role as key mediators of transmembrane FA transport is still controversial (20, 21). FA transport protein 4 (FATP4) is proposed to regulate long-chain FA uptake as it shares sequence homology with the acyl-coenzyme A synthetase (ACSL) family and is speculated to transfer FAs in form of fatty acyl-coenzyme A (21). FATP4 knockdown in isolated enterocytes, however, exhibited decreased FA uptake comparable to results obtained from heterozygous $FATP4^{+/-}$ mice (22, 23). Moreover, global deficiency of FATP4 in mice is embryonically lethal, which was speculated to be due to its critical role in skin lipid metabolism (23). However, its function in intestinal FA transport was found to be dispensable (22). FA translocase, otherwise known as cluster of differentiation 36 (CD36), is a highly expressed protein on the BBM of the proximal intestine. Despite its role in FA uptake *in vitro* and transgenic mouse models, its importance as a classical

transmembrane transporter is still controversial (24). CD36$^{-/-}$ mice exhibit impaired proximal intestinal lipid uptake; however, absorption *per se* is unchanged partly due to increased lipid absorption in the distal intestine of these mice (25). CD36 overexpression in a cell culture model indicated increased TG synthesis but did not increase FA transport across the plasma membrane (26). There was also no gross lipid malabsorption reported in CD36-deficient humans (27). Together, these reports suggest that CD36 regulates FA metabolism through additional systemic pathways, for instance, by increasing the secretion of two gut hormones, secretin and cholecystokinin, and not by maintaining the flux of FA within cell compartments (28). Several other proteins are reported as FA transporters. Most recently, the plasma membrane lipid raft protein caveolin-1 was shown to mediate FA absorption both *in vitro* and *in vivo*, possibly due to its interaction with CD36 (29-31). Another intestinal microvilli plasma membrane-associated FA-binding protein (FABP) has been studied extensively (32). Though, it shares high protein homology with mitochondrial aspartate aminotransferase, its role in intestinal FA transport is still not proven (20, 33, 34).

Once taken up by the enterocytes, FAs and MGs are transported from the cytoplasm to the endoplasmic reticulum (ER) aided by cytoplasmic-associated FABPs (35). The most abundantly expressed FABPs in the proximal intestine are intestinal-specific FABP (IFABP or FABP2) and liver-specific FABP (LFABP or FABP1) which is also expressed in the liver and kidney (36). Genetic mutation in IFABP gene in humans is often associated with detrimental phenotype of hypertriglyceridemia, insulin resistance, and diet-induced obesity (37-39). I*n vitro* studies have suggested a role of IFABP to transport long-chain FAs in 1:1 ratio across the ER to aid TG biosynthesis (21). Further, LFABP is proposed to maintain FA flux between the plasma membrane and cytoplasm compartments (40). IFABP$^{-/-}$ and LFABP$^{-/-}$ mice, however, lack lipid malabsorption, which suggests that these proteins only play minor role in intestinal lipid absorption (40-42). It is plausible that these proteins play multifactorial roles as e.g. LFABP is shown to regulate MG channeling for TG synthesis, FA oxidation and budding of pre-mature chylomicrons (43).

There are thirteen known long-chain fatty acyl—CoA ligases (ACSLs) capable for providing long-chain acyl-CoAs for TG synthesis (20). These long-chain acyl-CoA

groups are essential for the functioning of TG synthesis enzymes (22). One of them, ACSL5, is abundantly expressed in the proximal intestine and its deficiency in mice leads to almost 60% decrease in total ACSL activity in the intestine. However, unchanged post-prandial lipid absorption or diet-induced obesity in ACSL5$^{-/-}$ mice suggests that the role of ACSL5 is dispensable in intestine and other ACSLs can compensate for its deficiency (44).

In the ER, the re-esterification of FAs for TG biosynthesis is mediated through well-orchestrated pathways which are recognized based on their initial acyl acceptor: glycerolphosphate or MG pathway. Both these pathways converge on the final acylation step and utilize thioesters as donors for long-chain acyl-CoAs (45). Glycerolphosphate pathway is commenced by conversion of dietary glucose to glycerol-3-phosphate which is further acylated by glycerol-3-phosphate acyl-transferase (GPAT) 3 and 4 at the sn-1 position resulting in lysophosphatidic acid. The sequential acylation by 1-acylglycerol-3-phosphate acyltransferase (AGPAT) 1-5, and lipin 1-3 and subsequent removal of phosphate moiety results in synthesis of the diglycerides (DG) (46, 47). Along with generating precursors for cellular membranes, the glycerolphosphate pathway plays an important role in re-esterification of around 30% of TG synthesized in the enterocytes (47). The glycerolphosphate pathway is more important for FA esterification in the intestine in the absence of MG during prolonged digestion, when MG is converted into FAs and glycerol by the action of several lipases (47).

The majority of TG biosynthesis in the enterocytes is carried out by the MG pathway in which dietary MGs and FA acyl-CoAs are covalently bound to form DG. This reaction is catalyzed by monoglyceride acyltransferase (MGAT) enzymes. The MG pathway plays a prominent role in facilitating TG biosynthesis especially after heavy influx of dietary lipids during the post-prandial phase (48). It is also speculated that in human infants the MG pathway regulates the absorption of the long-chain saturated FA palmitate, which is a major component of breast milk (49).

The final and rate-limiting step for TG biosynthesis, similar for both pathways, is carried out by diglyceride acyl transferase (DGAT) enzymes, which acylate DG to synthesize TG (45). In the intestine, both pathways are proposed to generate TG destined for specific cellular compartments. TG synthesized by the MG pathway is

mostly incorporated for chylomicron formation, whereas glycerolphosphate-mediated TG is stored in the cytoplasm of the enterocytes (20). The detailed steps for TG biosynthesis in enterocytes are summarized in Fig. 3.

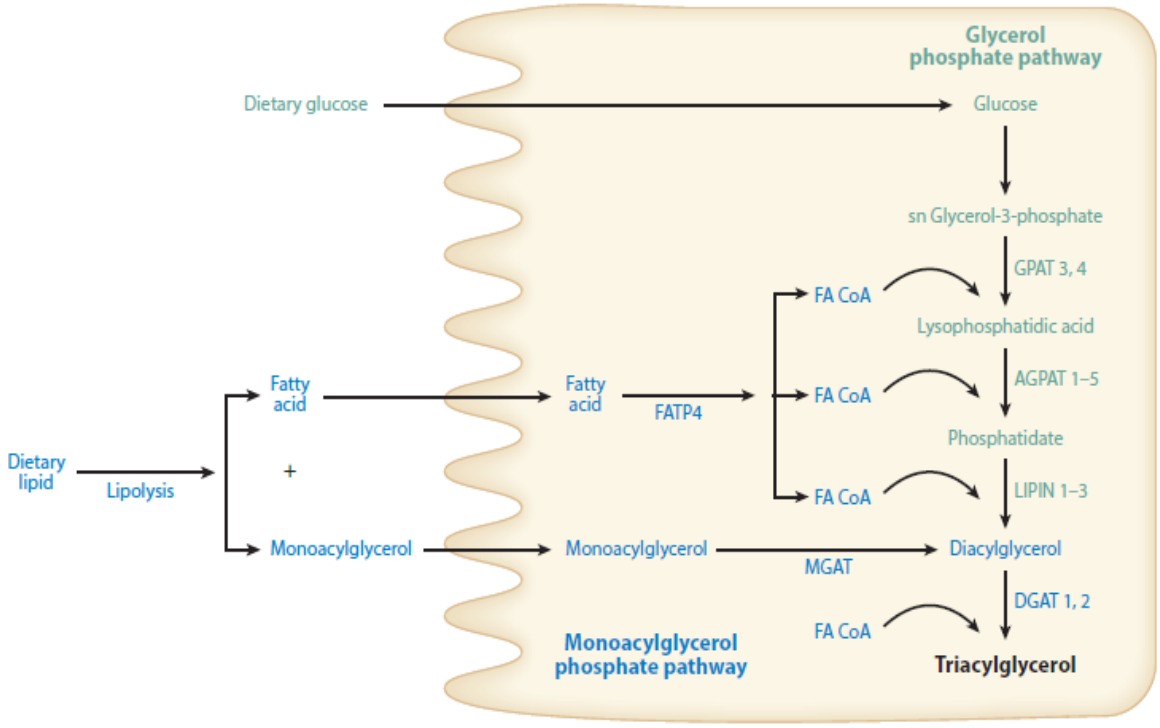

Figure 3: Triglyceride synthesis in the enterocyte: The two major TG synthesizing pathways, monoglyceride and glycerolphosphate pathways are responsible for 75-80% and 15-20% of total TG biosynthesis, respectively. Dietary components are broken down into basic components like FA and monoglyceride which can pass through the apical surface of enterocytes via diffusion or by transporters. Once taken up inside the enterocytes, FA is converted to fatty acyl-CoA by FATP4. Fatty acyl-CoA and monoglyceride can be converted to diglyceride, catalyzed by MGAT, which can be further converted to triglyceride by DGATs. Glycerolphosphate pathway: Triglyceride can also be synthesized from glucose and fatty acyl CoA. Dietary glucose taken up in the enterocytes is converted into sn Glycerol-3-phosphate, which sequentially generates lysophosphatidic acid, phosphatidate, and diglyceride by the addition of fatty acyl-CoA catalyzed by GPAT, AGPAT, and lipin, respectively. Diglyceride is converted to Triglyceride as described above. Abbreviations: AGPAT, 1-acyl-*sn*-glycerol-3-phosphate acyltransferase; CoA, coenzyme A; DGAT, diglyceride acyltransferase; FA, FA; FATP4, FA–transport protein 4; GPAT, glycerol-3-phosphate:acyl-CoA acyltransferase; MGAT, monoglyceride acyltransferase (6). Requisite permission to use this figure was obtained (Appendix).

1.2.2 Intestinal cholesterol absorption

The intestine is exposed to cholesterol either in form of biliary cholesterol or dietary cholesterol. The bile predominantly contains free cholesterol (FC) and

enters the intestine at the proximal end where it forms mixed micelles (50). Dietary cholesterol consists of FC and CEs. Hydrolysis of CE by pancreatic lipase results in FC and FA release, which get mixed with biliary micelles and are introduced at the BBM of enterocytes. FA uptake into the enterocyte has been explained before in section 1.2.1. FC transport into the enterocyte is mediated by the glycosylated protein Niemann Pick C1 like 1 protein (NPC1L1) which is abundantly enriched on plasma membrane rafts of enterocytes (50, 51). NPC1L1 was identified as a cholesterol transporter as part of the quest to determine the mechanism of ezetimibe, a potent drug for the treatment of diet-induced hypercholesterolemia (51). Cholesterol binds to the N-terminal binding site of NPC1L1, thereby changing its conformation and facilitating the C-terminus domain bind to Numb. These changes allow the interaction of NPC1L1 with Clathrin, which assists the internalization of the cholesterol-bound NPC1L1 to the endosomes where cholesterol is released to be transported to other organelles, including the ER (52). However, the mechanism/s regulating intracellular cholesterol transport is still elusive. As expected, NPC1L1$^{-/-}$ mice exhibited reduced fractional cholesterol absorption and increased loss of fecal sterols (53).

The ATP-binding cassette (ABC) proteins ABCG5 and ABCG8 are also involved in intestinal cholesterol uptake (54). These efflux proteins function as a heterodimer and can transport absorbed cholesterol from the enterocyte back to the intestinal lumen (55). Genetic mutation in ABCG*5* and ABCG8 genes results in β-sitosterolemia due to increased plant sterol accumulation in the tissues and systemic circulation, tendon xanthomas and premature coronary artery disease in patients (54, 56, 57). ABCG5/G8$^{-/-}$ mice have reduced biliary cholesterol secretion along with enhanced phytosterol absorption but the efficiency of cholesterol absorption remain unchanged (58-60). These observations indicate that ABCG5 and ABCG8 are more important for phytosterol than cholesterol homeostasis.

Scavenger receptor class B type 1 (SR-B1) has been implicated in mediating intestinal cholesterol absorption. The expression of SR-B1 on both the apical and basolateral surface of enterocytes makes it particularly an interesting candidate. However, studies have shown varied results as intestinal overexpression of SR-B1 in mice leads to increased cholesterol absorption (61). *In vitro* studies in Caco-2 cells treated with SR-B1 antibodies also lead to decreased cholesterol absorption

(62). In contrast, targeted deletion of SR-B1 deletion in mice resulted in unchanged cholesterol uptake and secretion, suggesting that this protein might not be a critical cholesterol transporter (63-65). A similar paradigm has surrounded the role of CD36 in cholesterol metabolism. *In vitro* studies indicated increased cholesterol uptake in CD36 overexpressing mammalian cells (66). Cholesterol uptake from the proximal intestine and its transport to the lymphatic system was significantly decreased in $CD36^{-/-}$ mice. Although cholesterol absorption is delayed in these mice, the cholesterol absorption *per se* was unchanged (67).

The intestinal HDL pathway plays a significant role in maintaining FC homeostasis by regulating its secretion from the intestinal lumen to the peripheral circulation. In this pathway, apolipoprotein A1 (APOA1) and ABCA1 have been shown to play an important role (68). *In vitro* studies showed that secretion of cholesterol by HDL increased when cells were treated with the liver X receptors (LXRs) and retinoid X receptors (RXRs) agonists by increasing the expression of ABCA1 (69, 70). Reduced cholesterol secretion by HDL was reported when cells were treated with glyburide, an ABCA1 inhibitor (71). Cholesterol secretion in intestine-specific $ABCA1^{-/-}$ mice was decreased by around 27% (72). It is proposed that ABCA1 could enhance either the transport of intracellular cholesterol to the plasma membrane or its efflux to extracellular transporters (73). Ex vivo cholesterol absorption studies using isolated enterocytes deficient in either apoA1 or ABCA1 further indicated individual deficiencies of either apoAI or ABCA1 had no significant effect on the uptake of cholesterol despite significantly decreased cholesterol secretion compared to controls specifically in the HDL fraction (69, 74). These studies suggest that intestinal HDL plays a pivotal role in intestinal cholesterol metabolism. The other major pathway for cholesterol and TG secretion into lymphatics is through chylomicrons.

1.2.3 Chylomicron assembly and secretion

Lipids absorbed by the intestine and transported to the intracellular ER are packaged into large, spherical TG-rich lipoproteins called chylomicrons. Their synthesis is initiated in the ER by scaffolding a large hydrophobic apolipoprotein B48 (APOB48) with lipids in a microsomal transfer protein (MTP)-dependent

manner (6). MTP, which is a heterodimer of a 97 kDa catalytic subunit and protein disulphide isomerase, is mainly found in the ER of hepatocytes and intestinal epithelial cells. Its interaction with APOB is critical for the transfer of lipids to the hepatic and intestinal lipoprotein core (6, 20).

APOB-48 is the major, nonexchangeable apolipoprotein of chylomicrons which is encoded by the APOB gene. Unlike in the liver, where translation of APOB gene generates the full-length APOB-100 protein, a post-transcriptional modification of APOB gene by Apobec-1 in the intestine leads to insertion of a stop codon resulting in a translated protein of 48% of its total length (APOB-48) (75).

In the absence of lipids or MTP, apoB-48 undergoes proteosomal degradation, whereas lipid supply induces physical interaction of APOB-48 with MTP in the inner leaflet of the ER. These processes help APOB to fold into a configuration conducive to accepting more lipids (76). Thus, lipidated apoB-48 is detached from the ER membrane forming a “primordial particle” that contains TG, CE, fat-soluble vitamin, and phospholipids in its core. The “core expansion” of primordial particles by addition of neutral lipids during the post-prandial condition or by the fusion of preformed lipid droplets results in the formation of larger pre-chylomicrons (77).

APOB-48 is a non-exchangeable apolipoprotein on chylomicrons though several exchangeable apolipoproteins (which are synthesized in enterocytes) mark the surface of the chylomicron, including APOAI, APOAIV, and APOCs. APOAIV is speculated to assist in the stabilization of the surface of expanding chylomicron particles (78). It is still elusive how APOAIV regulates MTP expression but reports suggest that APOAIV overexpression is associated with elevated MTP expression in the ER lumen leading to increased packaging of TG into nascent chylomicrons as well as enhanced CM synthesis (29). In agreement, APOAIV$^{-/-}$ mice have lower intestinal MTP levels (79).

Intracellular transport of chylomicrons is a dynamic process orchestrated by several proteins. The pre-chylomicrons from the ER membrane are exported by pre-chylomicron transport vesicles (PCTVs) to the cis-Golgi for further maturation. These vesicles, which are about 250 nm in diameter, are larger in size than vesicles responsible for intracellular protein transport and are characterized by the presence of distinctive vesicle-associated membrane protein 7, APOB-48, CD36,

and L-FABP (80). Although certain members of the coat protein complex II (COPII)-interacting proteins (such as Sar1, Sec 23/24 and Sec 13/31) are necessary for the lipid vesicular formation required for fusing of PCTVs with the Golgi complex, the PCTV transport itself is not subjective to the COPII-mediated transport (81, 82). Using recombinant FABP1 in murine studies, it was shown that L-FABP is sufficient to initiate synthesis and budding of PCTVs from the ER (41). However, L-FABP generated PCTVs lacking COPII proteins are unable to fuse with the Golgi (83). PCTV biogenesis is an energy-dependent process, which requires ATP-mediated phosphorylation of Sar1b, which in turn triggers binding of L-FABP to the ER thus initiating PCTV synthesis and budding from the ER (84). Together these studies show that to necessitate PCTV biogenesis two sets of proteins are critical: (i) proteins to initiate its formation and budding from the ER and (ii) proteins to facilitate its binding to the Golgi (83). Proteomic studies have identified several candidates which might be involved in PCTVs transport however, their role still remains elusive (85, 86).

After budding from the ER, the PCTVs then fuse with the cis-Golgi. This process requires interaction of VAMP7 on PCTVs with the Golgi membrane proteins syntaxin 5, rbet1, and vit1a (29). In the Golgi, pre-chylomicron gains APOAI and APOB48 which undergoes glycosylation (87, 88). It is well accepted that chylomicrons are transferred from trans-Golgi to the basolateral membrane via vesicles, however, the mechanism/s involved in their release from the Golgi or their fusion with the basolateral membrane, subsequent exocytoses into the lamina propria, and release into lymphatic system are still undefined (89). In the lymphatic system, chylomicrons are concentrated before being delivered to the blood circulation at the thoracic duct. The steps involved in chylomicron assembly and secretion are summarized in Fig. 4.

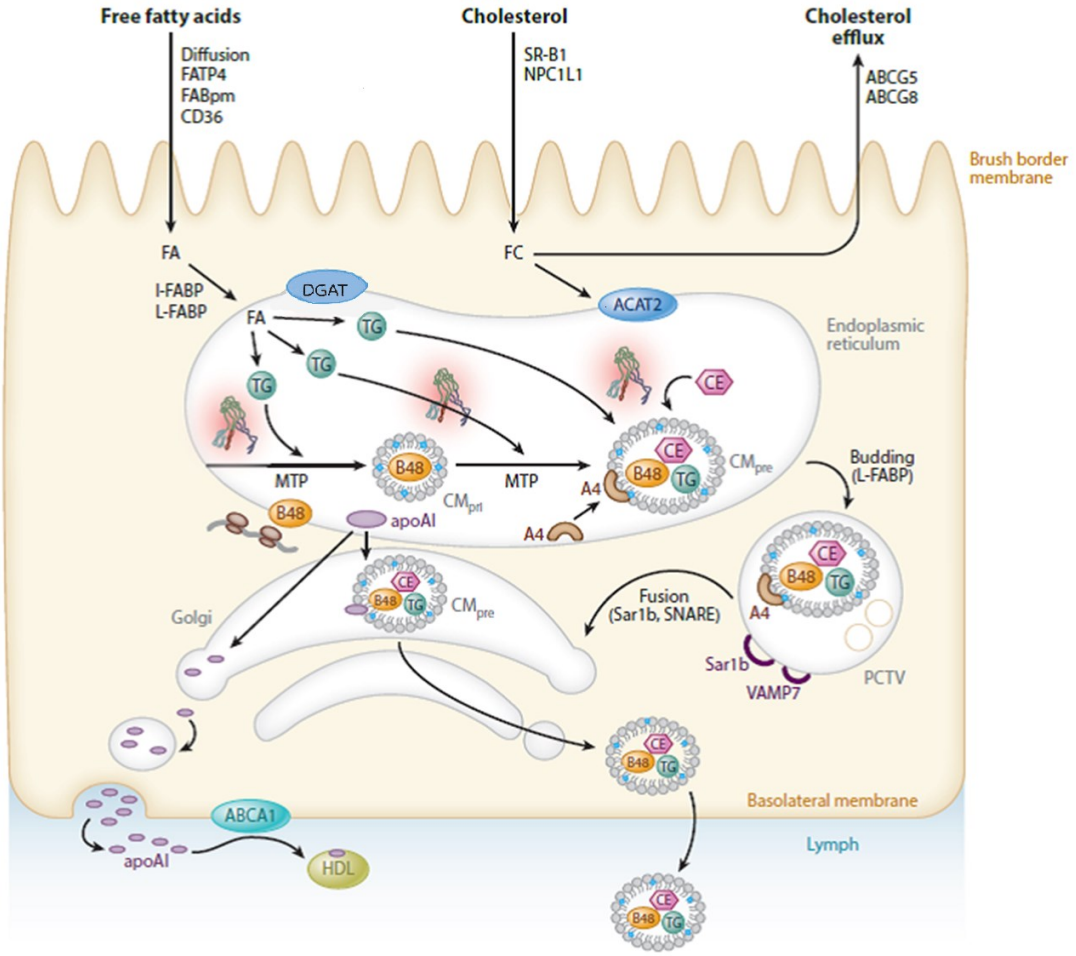

Figure 4: Chylomicron assembly and secretion. Hydrolyzed products of dietary lipids such as FAs and FC are taken up by enterocytes by passive diffusion or various transporters and transported to the ER where FAs are resynthesized into TG by DGAT as described in Figure 3. FC can be either excreted back to the lumen via ABCG5/G8 or effluxed to blood circulation by ABCA1 and APO-AI mediated HDL particles. Alternatively, FC is esterified by ACAT2 and transported to the ER where lipidation of APOB-48 with neutral lipids and phospholipid in MTP-dependent manner forms a primordial chylomicron. After acquiring APOAIV, these pre-chylomicrons are exported in a pre-chylomicron transport vesicle (PCTV) by budding from the ER (aided by L-FABP) and fuse with the cis-Golgi (aided by several proteins). In the Golgi, the pre-chylomicron acquires APOA1. Mature chylomicrons are exported from the Golgi in vesicles and released from the basolateral surface of the enterocyte into the lymphatic circulation. Abbreviations: ABCA1, ATP–binding cassette transporter A1; ABCG5/G8, ATP-binding cassette transporter G5/G8; DGAT, acyl-CoA:diacylglycerol-acyltransferase; ACAT2, acyl-CoA:cholesterol acyltransferase 2; CD36, cluster of differentiation 36; FABPpm, FA–binding protein plasma membrane; FATP4, FA–transport protein 4; HDL, high-density lipoprotein; I-FABP, intestinal FA–binding protein; L-FABP, liver FA–binding protein; VAMP7, vesicle-associated membrane protein 7. Adapted from (6) with requisite permission (Appendix).

1.2.4 Intestinal lipid droplets

The lipids synthesized in the intestinal ER membrane can either become part of cytosolic lipid droplets (CLDs) and stored or transported to the ER for secretion (73). These CLDs constitute as a temporal reservoir for lipid storage in conditions where high dietary lipid influx overwhelms chylomicron mediated clearance of lipids and thus are critical for efficient lipid absorption (90). The dietary fat content directly regulates the amount of TG in the CLDs present mostly in the proximal small intestine and these CLDs are cleared within 12 h post-feeding. The length of the predominant FA in the intestinal CLD correlates with the FA concentration of the diet consumed (20). Hence, the CLD metabolism is closely linked to the dietary fat absorption.

CLDs are large, heterogeneously sized, spherical particles with a dense lipid core mainly consisting of neutral lipids (TG and CE) surrounded by a phospholipid monolayer (91-94). The surface harbors proteins mainly from the Perilipin family (93). CLD biogenesis is widely elucidated as a resultant product of increased accumulation of newly synthesized TG between the two leaflets of the ER phospholipidbilayer (92, 94). The nascent CLDs then bud off from the ER to the cytoplasm. This process, however, is different in lipoprotein-synthesizing cell types such as hepatocytes and enterocytes, where CLDs are shown to also partition towards the ER lumen (73).

CLDs are implicated to maintain lipid homeostasis especially during nutrient-starved conditions by TG hydrolysis through a lipolysis/re-acylation cycle. In enterocytes, the chain of events would involve TG hydrolysis in CLD and mobilization of FAs to the ER followed by TG re-synthesis for subsequent secretion with lipoproteins (95). Adipose TG lipase (ATGL) and its activator, comparative gene identification-58 (CGI-58), are crucial for TG hydrolysis to DG and FAs followed by the actions of hormone sensitive-lipase (HSL) and mono glyceridelipase (MGL) to generate monoglycerides, glycerides and FAs (95). In enterocytes, cytosolic TG mobilization into the ER may also require other proteins such as cell death-inducing DFF45 -like effector b (Cideb) (20, 96). The lipid storage in CLDs to be released during fasting conditions might also explain the mechanisms involved in increased plasma TG concentrations observed just before

the digestion of food (97). Thus, CLDs may play a physiological role in optimizing fat absorption, as suggested by phenotypes of mice that fail to mobilize their TG core (Table 1).

Table 1: Selected mouse-models of intestinal TG metabolism (adapted from (20) with requisite permission (Appendix).

Gene	Tissues with High Expression	Genetic Manipulation	Phenotype
Mgat2	Small intestine	Global knockout	Delayed fat absorption Increased energy expenditure Protection from obesity induced by diet or the agouti mutation
		Intestine-specific deletion	Delayed fat absorption Partial protection from diet-induced obesity
		Intestine-specific expression	Restored fat absorption rate Partial recovery of weight gain and metabolic efficiency when fed a high-fat diet
Dgat1	Small intestine, adipose tissue and mammary gland	Global knockout	Delayed fat absorption Increased energy expenditure Protection from obesity induced by diet or the agouti mutation
		Intestine-specific expression	Restored fat absorption rate Recovery of weight gain and hepatic steatosis induced by high-fat feeding
Dgat2	Liver, adipose tissue and mammary gland	Global knockout	Death shortly after birth with severe deficiency in energy substrates and skin barrier defect
		Intestine-specific over-expression	Increased TG secretion Exacerbated hepatic steatosis
MTP	Liver and intestine	Conditional intestine-specific deletion	Reduced chylomicron secretion Large lipid droplets in enterocytes Steatorrhea
ApoB	Liver and intestine	Intestine specific deletion	Defect in chylomicron production Fat malabsorption
ATGL	Adipose tissue	Intestine specific deletion	Increased cytosolic lipid droplets in enterocytes Increased fecal fat
CGI-58	Adipose tissue and testes	Intestine specific deletion	Decreased fat absorption Increased fecal fat TAG accumulation in enterocytes
Cideb	Liver and intestine	Global knockout	Protection from diet-induced obesity Increased energy expenditure Reduced chylomicron secretion

1.2.5 Cholesterol efflux and trans-intestinal cholesterol excretion

Intestinal-derived chylomicrons or HDL particles transport dietary cholesterol to the peripheral tissues as per their systemic requirements. In order to get rid of excess of cholesterol, extrahepatic (peripheral) tissues return cholesterol to the liver for subsequent excretion into bile, which is released into the intestinal lumen to be excreted through the feces. This process is called reverse cholesterol transport (RCT) and the hepatobiliary route of cholesterol degradation and its excretion has been very well elucidated (98). Nevertheless, there is mounting evidence of the existence of an alternate pathway that directly secretes cholesterol from the circulation via enterocytes into the intestinal lumen. This pathway is termed as trans-intestinal cholesterol excretion (TICE), which contributes to almost 30% of total cholesterol excretion in mice (99, 100). Recently, its activity was also proved in healthy human volunteers where TICE-mediated fecal cholesterol excretion ranged from 22-35% of total fecal neutral sterol (NSL) (100). Thus, the non-biliary cholesterol excretion pathway is an important player in maintenance of whole-body lipid metabolism.

The molecular mechanisms regulating the TICE pathway are still incompletely understood. Pharmacological manipulations in rodent models revealed that activation of LXR and peroxisome proliferator activated receptor δ (PPAR-δ) leads to augmented TICE (99). Studies in transgenic mouse models also have shed some light on the regulation of TICE. In ABCG5/G8$^{-/-}$, multi-drug resistant factor 2$^{-/-}$ and NPC1L1$^{liver\text{-}tg}$ (hepatic NPC1L1 overexpression) mice, biliary cholesterol secretion is severely impaired, however, the fecal NSL remains grossly unaltered which indicates that the non-biliary cholesterol excretion pathway can compensate for diminished biliary cholesterol excretion (58, 101-103). These studies also hint at the liver in regulating the TICE pathway. In mouse models that exhibit increased hepatic FC accumulation, such as hepatic-ACAT2-knockdown (on LDLR$^{-/-}$ background) and NPC1L1$^{liver\text{-}tg}$ mice, liver-derived nascent APOB containing lipoproteins can repackage FC to be released into the bloodstream (101, 104). These lipoproteins then can be taken up by the proximal intestine partially through LDLR-mediated uptake and also through other unknown mechanisms given that TICE is still active in LDLR$^{-/-}$ mice (103-105). Although the characterization of these lipoproteins as either modified VLDL or unknown lipoproteins is still elusive,

however, it is suggested that APOB-containing lipoproteins can deliver cholesterol for TICE (103). A proposed model of enterocyte cholesterol flux is shown in Fig. 5.

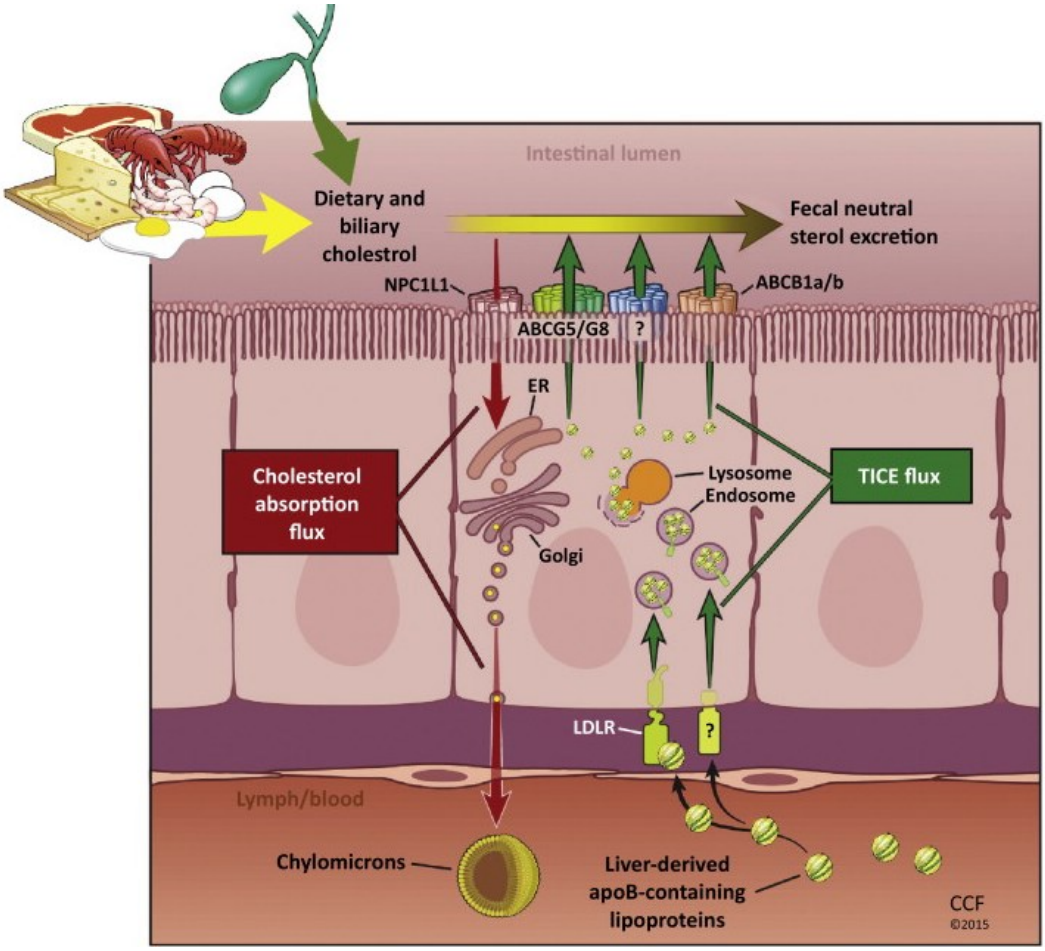

Figure 5: The proposed model for cholesterol flux across the intestinal enterocyte. The intestinal enterocyte processes cholesterol delivered to the apical or basolateral surface by two different pathways. First, the dietary and biliary cholesterol is taken up at the apical surface of the enterocyte in the Niemann–Pick C1-like 1 (NPC1L1)-dependent manner and transfered to the endoplasmic reticulum (ER), where it is incorporated into the chylomicrons for delivery into the lymphatics. In contrast to absorptive pathway, transintestinal cholesterol excretion (TICE) flux is mainly mediated at the basolateral surface of the enterocyte. Liver derived APOB-containing lipoproteins from the bloodstream are taken up in part by lipoprotein receptors present on the enterocyte surface for e.g. low-density lipoprotein (LDL) receptor (LDLR) and by still unknown receptors. In the enterocyte, these lipoproteins are processed by endosomal and lysosomal compartments and are subsequently effluxed from the apical surface partly by the action of the ATP-binding cassette transporters ABCG5/ABCG8 and ABCB1a/b and by still unknown receptors. Once secreted into the intestinal lumen, a part of this effluxed cholesterol can be excreted into the feces. The precise mechanisms underlying the TICE pathway are still unclear. ?, unknown receptor mediating the uptake of TICE lipoproteins (103). Requisite permission to use this figure was obtained (Appendix).

Irrespective of the lipoproteins delivering cholesterol to the small intestine, the receptors regulating its uptake or secretion to the intestinal lumen are critical to be determined. These receptors are still undefined. The ABCG5/G8 heterodimer is the most likely candidate due to its role in cholesterol efflux in the enterocytes. Indeed, LXR agonist treatment did not increase fecal NSL or macrophage to liver RCT in ABCG5/G8$^{-/-}$ mice (58). However, cholesterol absorption was unaltered in ABCG5/G8$^{-/-}$ mice and the TICE was only slightly decreased in ABCG5$^{-/-}$ mice. These findings indicate that ABCG5/G8 might be important but not necessary for TICE (106). SR-B1, due to its expression on the intestinal basolateral membrane, was also implicated in the regulation of TICE. By using an intestinal perfusion system, TICE was found to be significantly increased, not decreased, in SR-B1$^{-/-}$ mice (107). Thus, the search for the mediators and regulators of TICE is still an open arena.

1.3 Intestinal triglyceride synthesis and systemic energy balance

Our understanding of how the gut TG synthesis regulates overall energy metabolism has advanced considerably in the last few decades. Genetically modified rodent models provide a fantastic opportunity to study the physiological roles of individual genes. Murine models with impaired chylomicron assembly such as intestine-specific MTP$^{-/-}$ or APOB$^{-/-}$ mice demonstrate severe malabsorption of dietary fats phenocopying the results observed in humans with loss of function mutations in these genes (20, 108, 109). Unlike impaired chylomicron assembly, reduced intestinal TG synthesis in mice due to single deletions of enzymes involved in its synthesis does not result in severe dietary fat malabsorption, which indicates redundancy of enzyme function or adaptability (6). However, the systemic metabolism is altered due to decreased intestinal TG synthesis as observed in mouse models with deletion of genes involved in the MAG pathway.

1.3.1 DGAT1, a major intestinal DGAT enzyme

Although DGAT activity was reported already in 1960 (110) , it has been only in the last two decades that DGAT genes were cloned (111-113), paving the way to study TG synthesis in detail. In the small intestine, DGAT activity is highest in the

proximal region and decreases distally across the length of the intestine (114, 115) The two unrelated DGAT enzymes, DGAT1 and DGAT2, have been identified and investigated for their role in intestinal lipid metabolism. These genes catalyze the same reaction but do not share significant sequence homology at the level of DNA or protein sequences and also differ from one another in terms of structure, expression pattern, and biochemical properties (45). The mammalian DGAT1 belongs to the membrane-bound O-acyltransferase superfamily and was identified due to its sequence similarity to ACATs, whereas DGAT2 shares sequence homology with members of MGAT and wax synthases family (112, 113). DGAT1 also possesses retinol acyl transferase activity and is speculated to regulate retinol absorption whereas DGAT2 is more specific and active in catalyzing DGAT activity (20, 116). They have wide tissue expression pattern including the small intestine, liver, adipocytes, mammary glands, and testis with both being integral ER membrane proteins (45). In certain cell types, however, DGAT2 is reported to be associated with CLDs and mitochondria (117, 118) . Thus, it is likely that DGAT1 and DGAT2 might determine synthesis of TG for storage versus secretion in enterocytes (114).

Global DGAT1 deficient mice are lean, resistant to high-fat diet induced obesity, hepatic steatosis and exhibit increased energy expenditure in spite of similar food intake as summarized in Fig. 6 (45). DGAT1 deficiency also has pleotropic effects as indicated by the observation that female DGAT1$^{-/-}$ mice do not produce milk due to a mammary gland defect in TG production and DGAT1 deficiency in both sexes leads to increased fur loss and sebaceous gland degeneration (119). Further, DGAT1$^{-/-}$ mice are highly insulin and leptin sensitive which is likely due to DGAT1-mediated TG metabolism in the adipose tissue (120). DGAT1 is expressed quite ubiquitously in many tissues but its expression is highest in small intestine in comparison to other murine or human tissues (113, 114) However, DGAT1$^{-/-}$ mice do not undergo dietary fat malabsorption, impaired chylomicron assembly and have similar fecal fat balance compared to control mice (121). A transient lipid accumulation in the proximal intestine of DGAT1$^{-/-}$ mice after an oral lipid bolus is observed but it is cleared after overnight fasting. However, fat stimulus in DGAT1$^{-/-}$ mice delays the gastric emptying with slower but sustained release of TG into the circulation in part due to increased glucagon-like peptide 1 (GLP-1) (121, 122).

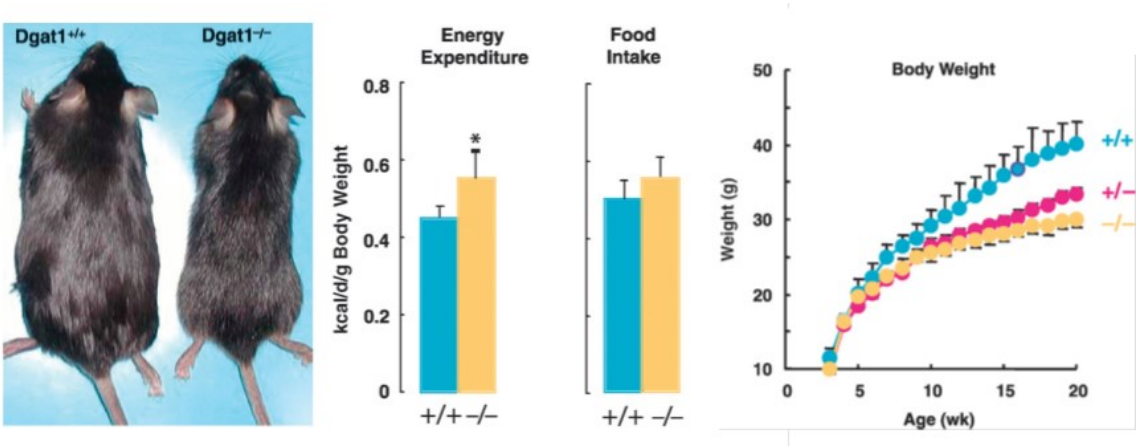

Figure 6: Effects of DGAT1 deficiency on energy metabolism. Male mice (10 weeks old) fed a high-fat diet for 2 weeks. DGAT1$^{-/-}$ mice have leaner appearance compared to wild-type mice, increased energy expenditure, and comparable food intake. Weight curves for high-fat diet-fed wild-type, Dgat1$^{+/-}$, and Dgat1$^{-/-}$ mice (92). Requisite permission to use this figure was obtained (Appendix).

DGAT1 in the intestine is considered to be an important component in maintaining whole-body energy homeostasis. Intestine-only expression of DGAT1 in DGAT1$^{-/-}$ mice reverses most of the metabolically beneficial phenotype observed in DGAT1$^{-/-}$ mice (121). Unlike DGAT1$^{-/-}$ mice, intestine-only DGAT1 mice, upon oil bolus, did not accumulate excess TG in CLDs of enterocyte nor was their postprandial TG secretion different compared to control mice. The most important observation was that intestine-only DGAT1 mice had restored susceptibility to high-fat diet induced fatty liver disease and obesity (121). These results strongly indicate the importance of I-DGAT1 (I-DGAT1) in conferring the improved metabolic phenotype in DGAT1$^{-/-}$ mice. Our group previously has reported that DGAT1 deficiency in apolipoprotein E$^{-/-}$ mice has an athero-protective role along with reduced plasma circulating cholesterol concentrations and cholesterol absorption (123). It is likely that DGAT1 in the intestine not only regulates TG metabolism but also mediates cholesterol homeostasis due to its important role in chylomicron synthesis.

1.3.2 Pharmacological inhibition of DGAT1 activity

Numerous DGAT1-specific inhibitors have been tested in mouse models and some also in human studies in search of therapeutic benefits of increased insulin sensitivity and resistance to diet-induced obesity as observed in DGAT1$^{-/-}$ mice

(124). Many of the pharmacological DGAT1 inhibitors used in mice generated positive and predictable results similar to those in DGAT1$^{-/-}$ mice like delayed chylomicron secretion, delayed gastric emptying, increased GLP-1 and peptide YY levels, decreased postprandial TG secretion, improved plasma TG and TC concentrations, resistance to fatty liver disease, improved insulin action, and resistance to weight gain (125-131).

Similar to studies in rodents, pharmacological inhibition of DGAT1 in clinical trials successfully replicated the favorable outcomes of increased weight loss and gastric emptying. However, the development of DGAT1 inhibitors as therapeutic target is hampered due to severe gastrointestinal side-effects observed in inhibitor-treated patients. Unlike rodent models, which have both DGAT1 and DGAT2 expression in the small intestine, human intestine is speculated to have DGAT1 as a prominent DGAT. Thus, it is likely that complete inhibition of DGAT1 in human intestine results in fat malabsorption due to an inability of synthesize TG, thus leading to severe diarrhoea (132-134). The idea is supported by the observations that null or missense mutations in the DGAT1 gene are linked to congenital diarrheal disorders and protein losing enteropathy (133, 134). However, the utility of DGAT1 inhibitors has recently been strengthened by studies with the DGAT1 inhibitor pradigistat, in patients suffering from familial chylomicronemia. The drug has been shown to decrease plasma TG concentrations and, most importantly, is well tolerated by patients suffering from familial chylomicronemia (135). The mechanism why complete DGAT1 inhibition in these patients does not lead to unwanted side-effects is still unclear. Nevertheless, it strengthens the possibility that DGAT1 inhibition in humans is still a viable therapeutic target for the treatment of MetS-related disorders.

1.3.3 Other genes involved in intestinal TG synthesis

DGAT2 is expressed in the small intestine of mice. Lack of malabsorption and unchanged plasma TG concentrations in DGAT1$^{-/-}$ mice suggest that DGAT2 can compensate for TG synthesis in mice. However, not much is known about the role of DGAT2 in intestinal lipid metabolism as DGAT2$^{-/-}$ mice are lipopenic (Fig 7.) and die within a day after birth due to a defect in skin barrier function (136).

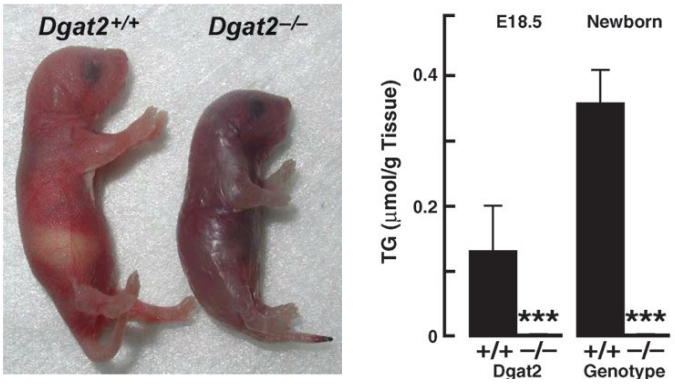

Figure 7: Phenotype of DGAT2 deficiency in mice. Mice deficient in DGAT2 are smaller, have abnormal skin and impaired skin barrier, and die early in the postnatal period due to severe lipopenia. Reduced carcass TG observed in Dgat2$^{-/-}$ mice (45). Requisite permission to use this figure was obtained (Appendix).

DGAT2 is most robustly expressed in the liver and adipose tissues of mice as well as in humans and its role is suggested to maintain hepatic lipid droplet biogenesis (136, 137). How DGAT2 regulates intestinal lipid metabolism is still unclear. Intestine-specific DGAT2 overexpression in DGAT1$^{-/-}$ mice did not increase postprandial TG secretion or altered TG content in intestinal CLD, indicating that two intestinal DGATs in mice have separate and non-redundant function (138).

MGAT2 is also highly expressed in murine and human intestines and has been suggested as an interesting candidate to regulate intestinal TG biosynthesis (139). MGAT2$^{-/-}$ mice exhibit delayed gastric emptying and reduced postprandial TG secretion but the overall TG absorption remains unaltered even on high-fat diet. Decreased TG secretion was in line with increased TG accumulation in enterocyte CLD of MGAT2$^{-/-}$ mice (140). A similar phenotype was observed in intestine-specific MGAT2$^{-/-}$ and pharmacological MGAT2 inhibitor-treated mice (141, 142). Thus, MGAT2 is not critical for TG absorption but can mediate intestinal TG storage and secretion balance (114).

1.4 Aim of the study

TG and cholesterol metabolism is distinctive yet intercalated at several critical regulatory check-points. Beginning from their entry into the gastro-intestinal tract to their incorporation into lipoproteins and subsequent catabolism, these lipids follow a similar metabolic fate. We previously observed that DGAT1 deficiency in apolipoprotein $E^{-/-}$ mice attenuates atherosclerosis partially due to reduced plasma circulating cholesterol concentrations and intestinal cholesterol absorption (123). Thus, we hypothesize that their might exist an interdependency between TG and cholesterol metabolism and that I-DGAT1 might be at the crossroads of these two metabolisms. We therefore performed murine studies using intestine-specific $DGAT^{-/-}$ ($I\text{-}DGAT1^{-/-}$) mice and compared them to $DGAT1^{-/-}$ and DGAT1 inhibitor-treated (DGAT1-Inh) mice to address the following aims:

Specific aim 1:

To study the impact of I-DGAT1 deficiency on plasma lipids, lipoprotein assembly and overall lipid homeostasis.

Specific aim 2:

To determine the contribution of I-DGAT1 in regulation of intestinal cholesterol absorption.

Specific aim 3:

To examine whether I-DGAT1 deficiency alone is sufficient to phenocopy the resistance to diet-induced obesity and improved insulin sensitivity observed upon global DGAT1 deficiency or pharmacological DGAT1 inhibition.

Specific aim 4:

To delineate the molecular pathways mediating the observed lipid metabolism upon I-DGAT1 deficiency.

2. Materials and Methods

2.1 General techniques, buffers and equipment

2.1.1 Equipment

Table 2: Equipment used for various procedures

Equipment	Company
Centrifuge (5471R)	Eppendorf, Wien, Austria
ß-counter	Packard, Dayton, UK
Power supply (Power Pac 300)	Bio-Rad, Hercules, CA
Lightcycler 480	Roche, Palo Alto, CA
Sonicator	B.Braun, Hessen, Germany
Lyophilisator	Virtis, Warminter, PA
Nano Drop Spectrophotometer	Peqlab, Darmstadt, Germany
Thermal cycler C1000	Bio-Rad, Hercules, CA
Microwave	Whirlpool, Benton Harbor, MI
Precellys	Peqlab, Darmstadt, Germany
Anthos 2000	Anthos, Toulouse, France
Viktor 1420 Multilabel counter	Wallac, Saskatchewan, Canada

2.1.2 Western blotting buffers

a) Lysis buffer:

Fifty mM Tris HCl, 150 mM NaCl, 1% Triton X-100 and 0.5% deoxycholate, 1:2000 protease cocktail inhibitor cocktail were mixed and pH 7 was adjusted with KOH.

b) Sample buffer:

In 25 ml H_2O, 2.3 g SDS, 0.6 g Tris, pH was adjusted to 6.8 with HCl, then 10 ml glycerol was added and volume made up to 45 ml. One drop of bromophenolblue and mercaptoethanol (3%) was added followed by incubation for 10 min in hot water.

c) Separating gel buffer:

1.5 M Tris and 0.4% SDS were mixed in 80 ml H_2O. pH 8.8 was adjusted with HCl and volume made up to 100 ml.

d) Stacking gel buffer:

Six g Tris was dissolved in 90 ml ddH_2O. pH was adjusted to 6.8 with HCl and volume was made up to 100 ml with ddH_2O.

e) Separating gel

Ingredients were mixed in the order shown in Table 3.

Table 3: Seperating gel

Reagents	**10% SDS-gel**
Acrylamide	2866.25 µl
Seperating gel buffer	2712.5 µl
ddH2O	5171.25 µl
10 % SDS	100µl
TEMED	4.4 µl
10% APS	7.6 µl
Final volume	87804.4 µl

f) Stacking gel

Stacking gel was prepared according to Table 4.

Table 4: Stacking gel

Reagents	**4% SDS-gel**
Acrylamide	326 µl
Buffer 2	500 µl
ddH2O	1650 µl
10 % SDS	21.5µl
TEMED	1.25 µl
10% APS	19 µl
Final volume	2517.75 µl

2.1.3 Real-time PCR including cDNA generation

a) cDNA preparation

Total RNA from tissues was extracted using TriFast (Peqlab, Erlangen, Germany) according to the manufacturer's protocol. Two µg RNA in a final volume of 10 µl were reverse transcribed by using High-Capacity cDNA Reverse transcription kit (Applied Biosystems, Carlsbad, CA). High-Capacity cDNA Reverse transcription kit's master mix composition is as shown in Table 5.

Table 5: cDNA Reverse transcription kit's master mix

Component	Volume (µl)/reaction
10 X Buffer	2
25 X dNTP Mix (100 mM)	0.8
10 X RT Random Primers	2
Multiscribe reverse transcriptase	1
RNase inhibitor	0.7
Nuclease-free water	3.5
2 µg RNA/10 µl water	10
Total volume / reaction	20

The reverse transcription reaction of sample was carried out in thermocylcer C-1000 (Bio-Rad, Hercules, CA) using the program shown in Table 6.

Table 6: Thermocycler conditions for reverse transcription:

	Step 1	Step 2	Step 3	Step 4
Temperature	25°C	37°C	85°C	4°C
Time	10 min	120 min	5 s	∞

b) Real-time PCR

cDNA was diluted 1:50 in ddH_2O. Three µl of diluted cDNA and 1 µl of each forward and reverse primer (as shown in Table 7.) were mixed with 5 µl Quantifast SYBR Green master mix (Qiagen, Hilden, Germany). Samples were analyzed in duplicate and normalized to the expression of the house-keeping gene peptidylprolyl isomerase A *(*Ppia, also known as cyclophilin A). Real-time PCR

was performed on a Roche LightCycler 480 (Roche Diagnostics, Palo Alto, CA) using the program shown in Table 8. Expression profiles and associated statistical parameters were calculated using the public domain program Relative Expression Software Tool – REST 2008 (http://www.genequantification.com/download.html).

Table 7: Primers for real time PCR:

Gene	Forward primer (5`-3`)	Reverse primer (5`-3`)
CD36	GCAGGTCTATCTACGCTGTG	GGTTGTCTGGATTCTGGAGG
ABCG8	CTGTGGAATGGGACTGTACTTC	GTTGGACTGACCACTGTAGGT
NPC1L1	GCAAGGTGATCAGGAGGTTGA	ATCCTCATCCTGGGCTTTGC
FATP4	ACTGTTCTCCAAGCTAGTGCT	GATGAAGACCCGGATGAAACG
SRB1	GAGCACGTTCTACACGCAG	GGTCTGACCAAGCTATTCAGGTT
SREBP1c	CCATCGACTACATCCGCTTCTT	ACTTCGCAGGGTCAGGTTCTC
MTTP	CACACAACTGGCCTCTCATTAAAT	TGCCCCCATCAAGAAACACT
ABCA1	CTCTTCATGACTCTAGCCTGGA	ACACAGACAGGAAGACGAACAC
PDK4	CCGCTGTCCATGAAGCA	GCAGAAAAGCAAAGGACGTT
HMGCR	TAGCTCGTGGAATGGCAATC	CTCTAGGACCAGCGACACAC
CYP7A1	AGACCTCCGGGCCTTCCT	ATCACTCGGTAGCAGAAGGCAT
PPIA	CCATCCAGCCATTCAGTCTT	TTCCAGGATTCATGTGCCAG
FGF15	GCCATCAAGGACGTCAGCA	CTTCCTCCGAGTAGCGAATCAG
DGAT1	TCCGCCTCTGGGCATTC	GAATCGGCCCACAATCCA
DGAT2	AGTGGCAATGCTATCATCATCGT	TCTTCTGGACCCATCGGCCCCAGGA

Table 8: PCR program for real time PCR:

Denaturation and Amplification	95°C 60°C	10 s 30 s	40
Melting curve	95°C 60°C 95°C	10 s 20 s continuous	1 1
Cool down	4°C	20 s	1

2.2 Animals and diets

I-DGAT1$^{-/-}$ (125) and DGAT1$^{-/-}$ (143) mice and their respective controls used in this study were a kind gift by Dr. Robert Farese, Jr. (Harvard T.H. Chan School of Public Health, Boston, MA). DGAT1$^{-/-}$LDLR$^{-/-}$ mice were generated by breeding LDLR$^{-/-}$ mice (purchased from Jackson Laboratory, Bar Harbor, ME) and DGAT1$^{-/-}$ mice. For all experiments, age-matched male mice between 3-4 months of age were used. Mice were fed either regular chow diet (11.9% caloric intake from fat; Altromin 1324, Lage, Germany) or were switched to high-fat/high-cholesterol diet (HF/HCD; 30% caloric intake from fat plus 1% cholesterol; Ssniff, Soest, Germany) or high-fat diet (HFD; 60% caloric intake from fat; Research Diet Services, Wijk Bij Duurstede, The Netherlands) one month after weaning. The FA composition of the special diets used in this study is shown in Table 9. Housing conditions were maintained under a 12 h light/12 h dark cycle in a hygienic, temperature-controlled environment with unlimited access to water and food (144).

Experiments conducted for the measurement of cholesterol fluxes after prolonged DGAT1 inhibition in mice were performed at the University of Groningen, The Netherlands, as part of my research stay abroad. These experiments were conducted in accordance with the local laws and requisite permissions were obtained by the Ethical Committee of the University of Groningen. For all other experiments, required permissions were approved by the Austrian Federal Ministry of Science, Research, and Economy, Vienna, Austria, in accordance with the Council of Europe Conventions.

Table 9: **FA composition of experimental diets used in the study (% of total FAs)**

FA	HF/HCD	HFD
C 10:0	-	0.03
C 12:0	0.09	0.07
C 14:0	3.32	1.1
C 15:0	-	0.07
C 16:0	26	19.67
C 16:1	2.51	1.33
C 17:0	1.22	0.35

C 18:0	17.09	10.56
C 18:1	39.12	34.02
C 18:2	8.22	28.72
C 18:3	2.06	2.04
C 20:0	0.12	0.15
C 20:1	0.03	0.58
C 20:2	-	0.78
C 20:3	-	0.11
C 20:4	0.22	0.27
C 22:5	-	0.07
SFA	47.84	32
MUFA	41.66	35.93
PUFA	10.50	31.99

2.3 Blood biochemical analyses

Blood was collected via retro-bulbar puncture from 4 h fasted mice and plasma was prepared within 20 min of blood collection by centrifugation at 5,200 g for 7 min at 4°C. TG, TC, and FC concentrations were measured enzymatically using commercially available kits according to manufacturer's instructions (DiaSys, Holzheim, Germany). Two hundred µl pooled plasma from each group were separated by fast protein liquid chromatography (Pharmacia P-500, Neuss, Germany) equipped with Superose 6 column (Amersham Biosciences, Piscataway, NJ). Isolated fractions were used to measure TC concentrations enzymatically (144).

2.4 HDL particle size analysis

HDL (5 µg protein per lane) was separated by native gradient gel electrophoresis (4%–16% NativePage; Life Technologies, Carlsbad, CA). Gels were run for 120 min at a constant voltage of 150 V in NativePage running buffer (Life Technologies, Carlsbad, CA). Gels were then fixed with a mixture of 25% isopropanol/10% acetic acid for 10 min and stained overnight with Coomassie Brilliant Blue G-250 (Thermo Fisher Scientific, Vienna, Austria). Plasma HDL particle size analysis was performed by the group of Dr. Gunther Marsche, Medical University of Graz.

2.5 Acute pharmacological DGAT1 inhibition

The DGAT1 inhibitor used in this study was a kind gift by Dr. Andrew Turnbull, AstraZeneca R&D, Moelndal, Sweden and has previously been characterized as compound 2 (144, 145). The regimen of treatment and the doses for the *in vivo* treatment of mice were adapted from a previous report (125). Inhibitor dosage treatment was initiated 24 h before starting the experiment at 8 a.m. upon removal of food for 2 h and were continued every 24 h during the course of the experiment. Wild-type C57BL/6 mice were orally dosed with either vehicle composed of 0.5% w:v of hydroxypropylmethylcellulose (Sigma-Aldrich, St. Louis, MO) in 0.1% v:v Tween 80 or DGAT1-Inh (5 mg/kg body weight) dissolved in vehicle. Mice had access to food 2 h post treatment. On the day of short-term or fractional cholesterol absorption experiments (described below), mice were gavaged with corn oil containing the respective radiotracer 2 h post treatment before getting access to food (144).

2.6 DGAT activity assay

The DGAT activity assay was performed as described previously (146). Briefly, the substrate containing 0.2 mM diglyceride (*sn*-1,2, Sigma-Aldrich, St. Louis, MO) in Tris buffer (50 mM, 20mM $MgCl_2$, pH 7.4) and 0.8 mM phosphatidylcholine was sonicated (Virsonic 475, Ontario, Canada). To the emulsified substrate, cold-oleoyl-CoA (Sigma-Aldrich, St. Louis, MO) and [^{14}C]oleoyl-CoA (55 µCi/µmol, ARC Inc., St Louis, MO) were added to a final concentration of 30 and 20 µM, respectively. The sample in its final volume of 100 µl Tris buffer contained 50 µg of intestinal microsomal fraction in the presence or absence of the DGAT1 inhibitor (5 µM). The substrate and sample were mixed 1:1 (v:v) to give a final volume of 200 µl and incubated for 10 min at room temperature. Catalysis was terminated by adding chloroform/methanol (2:1, v:v) and the extracted lipids were subjected to thin-layer chromatography (TLC) using hexane/diethyl ether/acetic acid (70/29/1, v:v:v) as solvent. The band corresponding to TG was scraped off carefully, and radioactivity was determined by liquid scintillation counting. This experiment was performed in collaboration with Dr. Thomas Eichmann, University of Graz.

2.7 Short-term cholesterol absorption

Cholesterol absorption studies were performed as described previously (123). Briefly, mice fed chow diet were fasted for 4 h in the morning and gavaged with 200 µl corn oil containing 2 µCi [^{3}H]cholesterol (ARC Inc., St Louis, MO) and 200 µg cholesterol (Sigma-Aldrich, St. Louis, MO). After 4 h of radiotracer gavage, blood was collected to isolate plasma see 2.2 and mice were euthanized for tissue collection. Isolated liver and three parts of the small intestine (duodenum, jejunum and ileum) were rinsed with cold-PBS to remove blood and luminal contents respectively. The tissues were dissolved in 1 M NaOH at 65°C overnight and then subjected to liquid scintillation counting (144).

2.8 Fractional cholesterol absorption

Fractional cholesterol absorption was measured by the fecal dual-isotope ratio method as described (123). Chow diet-fed mice were housed in single cages 2 days before the commencement of the experiment. On the day of the experiment, mice were fasted for 4 h in the morning and gavaged with a single dose of 200 µl corn oil containing 0.2 µCi [^{3}H]sitostanol (ARC Inc., St. Louis, MO) and 0.1 µCi [^{14}C]cholesterol (ARC Inc., St. Louis, MO). Fecal samples were collected for 2 days post-gavage and mice were euthanized. Fecal lipids isolation was carried out using the Folch extraction method (144). Radiotracer counts were measured by liquid scintillation counting. Fractional cholesterol absorption was calculated using the following formula: % absorption = dose [^{14}C]:[^{3}H]-fecal [^{14}C]:[^{3}H])/dose [^{14}C]:[^{3}H] x 100 (VS).

2.9 Uptake and secretion of cholesterol by primary enterocytes

Primary enterocytes were isolated from overnight fasted C57BL/6 mice, suspended in 4 ml of DMEM, and incubated at 37°C as described (69). Either vehicle (DMSO) or DGAT1 inhibitor (EC50 = 0.03 µm, dissolved in DMSO) was added to suspended enterocytes. For radiotracer cholesterol uptake measurements, micelles were mixed with 1 µCi/ml [^{3}H]cholesterol. The composition of uptake micelles was as followed: 0.14 mM sodium cholate, 0.15 mM sodium deoxycholate, 0.17 mM phosphatidylcholine, and 0.19 mM mono-

oleoylglycerol. Cholesterol uptake was measured at regular intervals, after which enterocytes were washed with PBS. Cellular lipids from the enterocytes were extracted by overnight incubation with chloroform/methanol (1:1 v:v), and isolated lipids were subjected to liquid scintillation counting. For determination of cholesterol secretion, isolated enterocytes were first pulsed for 1 h with uptake micelles and then chased with DMEM containing secretion micelles in the absence and presence of the DGAT1 inhibitor. Secretion micelles consisted of 1.4 mM oleic acid, 0.14 mM sodium cholate, 0.15 mM sodium deoxycholate, 0.17 mM phosphatidylcholine, and 0.19 mM mono-oleoylglycerol. Post 2 h of chase, enterocytes were centrifuged at 2000 rpm for 10 min at 4°C, lipids were extracted using chloroform:methanol (1:2, v:v) and isolated into individual species by TLC. FC and CE fractions were scraped and radioactivity was determined by liquid scintillation counting (69, 144). These experiments were performed in collaboration with Dr. Jahangir Iqbal at the laboratory of Dr. Mahmood Hussain, SUNY Downstate Medical Center, New York, as part of the research stay abroad.

2.10 Chylomicron secretion

Chylomicron secretion rates using [^{3}H]triolein (Perkin Elmer, Boston, MA) and [^{14}C]cholesterol (ARC Inc., St. Louis, MO) were measured according to previous reports (125, 144) with minor modifications. Briefly, HF/HCD-fed mice were fasted for 4 h starting at 6 a.m. LPL-mediated lipolysis was blocked by intraperitoneal injection with Polamer-407 (P-407) (1 g/kg body weight, Sigma-Aldrich, St. Louis, MO) in PBS. Mice were gavaged with 200 µl corn oil containing 1 µCi [^{3}H]triolein, 0.5 µCi [^{14}C]cholesterol, and 200 µg cholesterol. Blood samples were taken at indicated time-points and plasma radiotracer counts were measured. Mice were anaesthetized and lymph from the lymph duct was surgically removed as described (144, 147) with modifications. Briefly, mice were subjected to a left subcostal incision and the abdominal cavity was opened carefully. The cisterna chyli and the thoracic duct were exposed by systematically maneuvering a self-retaining retractor. Lymph was carefully sucked up using glass micro-capillary tubes and radioactivity was measured in 100 µl lymph by liquid scintillation counting (144).

2.11 Gastric emptying and gut transit

Gastric emptying and intestinal transit were determined by assessing the distribution of a 70 kDa FITC conjugate dextran marker (Sigma-Aldrich, St. Louis, MO) throughout the gastrointestinal tract of the mice, as described previously (21). Briefly, 12 h fasted mice were gavaged with 0.1 ml of 5 mM FITC-dextran, 30 min post-gavage, mice were sacrificed and the stomach and small intestine were carefully removed. The small intestine was divided into five segments of equal length. The stomach was taken as segment No 1 and the five segments were numbered consecutively from 2 to 5. Each segment was flushed carefully with 3 ml of 50 mM Tris buffered saline solution (pH 10.3). Samples were centrifuged at 2000 rpm for 10 min, and fluorescent activity of the supernatant was measured using a fluorimeter (Perkin-Elmer, Cedex, France). %Gastric emptying was measured using the formula: [(total dextran (stomach + intestine) – dextran (stomach))/total dextran (stomach + intestine)] x 100. Gut transit was determined as a factor of the intestinal geometric centre (IGC) based on the equation: IGC = (fraction of amount of FITC in each segment) x (segment number). The dextran concentration in each segment was expressed as a fraction of total dextran recovery (148).

2.12 Chylomicron size measurement

HF/HCD-fed mice were injected with P-407 to block lipolysis and gavaged with 200 µl corn oil. Postprandial plasma chylomicrons were isolated 90 min after gavage by density-gradient centrifugation as described previously (144, 149). Briefly, 0.4 ml of plasma was mixed with 0.9 ml PBS (containing 2 mM benzamidine) and 0.7 g KBr (4 M final concentration, density 1.3 g/ml). The top fraction containing chylomicrons was carefully eluted and particle size was estimated using Zetasizer Nano ZS (Malvern Instruments Ltd, Malvern, UK) at 25°C in triplicate and values were averaged. Data were represented as a mean hydrodynamic diameter in nanometer scale (Z-Average d_{nm}) (144). Measurement of particle size was performed in the laboratory of Dr. Andreas Zimmer with assistance of Dr. Bernhard Scheicher, University of Graz.

2.13 Oral glucose tolerance test (OGTT)

Mice were fasted for 6 h in the morning without access to drinking water. Blood was taken from the tail vein before and 15, 30, 60, 120, and 180 min after an oral gavage of D-glucose (2.0 g/kg body weight, (Sigma-Aldrich, St. Louis, MO). Glucose concentrations from tail vein blood were determined using glucometer AccuCheck-active (Roche Diagnostics, Palo Alto, CA) (150).

2.14 Intra-peritoneal insulin tolerance test (IPITT)

Insulin stock solution (Actrapid, Novo Nordisk, Denmark) was diluted with saline to 0.5 U/ml (1/200 dilution) by adding 5 µl stock (100 U/ml) to 995 µl 0.9% (w:v) sterile saline to prepare the working solution. Mice were fasted for 6 h in the morning without access to drinking water. Insulin (0.5 U/kg) was injected intraperitoneally using a 27G needle and blood was collected from the tail vein before and 15, 30, 60, 120, and 180 min after injection. Glucose concentrations from blood were determined using glucometer AccuCheck-active (Roche Diagnostics, Palo Alto, CA).

2.15 Hematoxylin and eosin staining

Tissues from overnight fasted HF/HCD-fed DGAT1$^{fl/fl}$ and l-DGAT1$^{-/-}$ mice were fixed in 4% neutral-buffered formaldehyde for 24 h and subsequently embedded in paraffin. Sections (5 µm) were deparaffinized and subjected to hematoxylin and eosin staining using standard protocols as described (144).

2.16 Oil-red O staining

Oil red O (Sigma-Aldrich, St. Louis, MO) was mixed with 100 ml isopropanol. The working reagent was prepared by mixing 30 ml stock solution with 20 ml distilled water stirred for 10 min. Liver sections were dipped in 4% paraformaldehyde-PBS for 10 min, followed by 60% isopropanol treatment for 5 min and incubated with working oil red O stain for 15 min. Samples were quickly dipped in 60% isopropanol for 1 s and counter-stained with hematoxylin stain (0.1%) for 5 min, and washed in running water. Sections were dried and mounted with glycerine

jelly. The sectioning and subsequent hematoxylin and eosin and Oil red O staining was performed in collaboration with Ms. Silvia Schauer and Prof. Gerald Hoefler, Medical University of Graz.

2.17 Freeze-fracture transmission electron microscopy

Five microliters of postprandial lymph and plasma chylomicrons from HF/HCD-fed mice were used to perform freeze-fracture transmission electron microscopy as described previously (144, 151). Briefly, frozen samples were subjected to freeze substitution and ultrathin sections (75 nm) were dissected using Leica UC 7 Ultramicrotome, followed by staining with lead citrate (5 min) and uranyl acetate (15 min). Using a FEI Tecnai G2 20 transmission electron microscope (FEI, Eindhoven, The Netherlands) with a Gatan ultrascan 1000 CCD camera (acceleration voltage 120 kV), high resolution images were acquired. This experiment was performed by Dr. Dagmar Kolb, Medical University of Graz.

2.18 Quantification of fecal neutral sterol loss, bile acid and FA concentrations

Feces were collected for 72 h from individually housed mice. Fifty micrograms of dried feces were used for determination of fecal neutral sterol loss (NSL), bile acid (BA) concentrations, and FA composition by gas chromatography as described recently (152, 153). Briefly, feces were homogenized in 200 µl PBS, extracted with 250 µl 1 M sodium hydroxide and 750 µl 1 M methanol in a tube under constant vortexing. Tubes were heated for 2 h at 80°C in a heating block. Extraction was carried out thrice with 3 ml petroleum ether followed by centrifugation for 10 min at 2000 rpm. Organic fractions were collected and dried under a nitrogen stream. Samples were derivatized using mixture of N,O-bis(trimethylsilyl)trifluoroacetamide: pyridine : trimethylchlorosilane in a ratio of 5:5:0,1 (v:v:v) for 1 h at room temperature, evaporated under a nitrogen stream, extracted in 1000 µl hexane, and measured using gas chromatography as described previously (152, 153). All reagents were purchased from Sigma-Aldrich, St. Louis, MO). Fecal BA and FA composition were measured according to protocols previously reported (152, 153).

2.19 Measurement of TICE

C57BL/6 mice were acquired from Harlan (Horst, The Netherlands) and fed high-fat diet (HFD; 60% caloric intake from fat; Research Diet Services, Wijk Bij Duurstede, The Netherlands) supplemented with either vehicle or the DGAT1 inhibitor (5 mg/kg diet) for 4 weeks. Cholesterol flux experiments for TICE estimation were performed as described (154). Briefly, three days before the start of the experiment, the animals were housed individually. Before any intervention, baseline parameters were measured. Feces were collected for a period of 48 h before starting the experiment as well as a basal blood sample from the tail tip. On day 1 at 9:00 am, the mice received an intravenous (retro-orbital) injection of 0.7 µmol D5-cholesterol (Cambridge Isotope Laboratories, Inc. Andover, MA) dissolved in 150 µL intralipid (20%, Fresenius Kabi, Den Bosch, The Netherlands) and an oral dose (by gavage) of 1.5 µmol D7-cholesterol (Medical Isotopes, Inc., Pelham, NH) dissolved in 200 µL medium chain TG oil (Pharmacy UMCG, Groningen, The Netherlands). At time points 0, 3, 6, 12, 24, 48, 72, 96, 120, 144, and 168 h after labeled cholesterol administration: bloodspots were collected by tail-vein (~ Ø 5 mm). To estimate cholesterol synthesis on day 7 of the experiment at 9:00am (=168 h), the mice were switched to tap water containing 2% (w:w) 1-^{13}C-acetate (NEN Life Science, Zaventem, Belgium). The mice had *ad libitum* access to the 1- ^{13}C-acetate drinking water for at least 3 days. At time points 180, 192, 204, 216, 228, and 240 h further bloodspots were collected to estimate *de novo* cholesterol synthesis. Feces were collected once daily over the 10 days period. To obtain bile characteristics at day 10 (=240 h), mice were anesthetized with isoflurane and kept warm at 37°C. The common bile duct was cannulated and bile was collected. The bile from the first 5 min was discarded (this is mostly originating from the gallbladder), after which the hepatic bile was collected in a weighed eppendorf-tube during the next 20 min. At the end of the experiment, mice were sacrificed by cardiac puncture and cervical dislocation and subsequently plasma and tissues were collected. Fecal NSL, BA, and FA concentrations were measured as described above. Quantification of fecal NSL, BA, and FA concentrations and measurement of TICE were performed at the laboratory of Dr. Albert Groen, University Medical Center Groningen, Groningen, as part of the research stay abroad.

2.20 Western blotting analysis

Scrapings from intestinal mucosa or tissue lysates were sonicated (Labsonic B. Braun, Melsungen, Germany) in RIPA buffer, and protein concentrations were determined by Bradford assay. Tissue lysates were seperated on 10% SDS-PAGE and transferred onto a PVDF membrane using Transblot turbo (Bio-Rad, Hercules, CA) according to the manufacturer's instructions. Non-specific binding sites were blocked for 2 h at RT by incubating the membrane with 5% non-fat dry milk in 1x TBS-T buffer, which consisted of 150 mM NaCl, 10 mM Tris, 0.1% Tween 20 (pH 8). An overnight incubation of blots with rabbit polyclonal primary antibodies against NPC1L1 (1:200), CD36 (1:1,000), SR-B1 (1:1,000), and mouse monoclonal antibody against ABCG8 (1:1000) was carried out. All primary antibodies were purchased from Novus Biologicals, Littleton, CO. Monoclonal anti-mouse β-actin (1:5,000, Santa Cruz Biotechnology, Heidelberg, Germany) was used as loading control. HRP-conjugated goat anti-rabbit (1:2,500, Dako, Glostrup, Denmark) and rabbit anti-mouse antibodies (1:500, Dako, Glostrup, Denmark) were visualized by enhanced chemiluminescence detection (Clarity™ Western ECL substrate; Bio-Rad) using a ChemiDoc™ MP imaging system (Bio-Rad, Hercules, CA).

2.21 Statistics

Statistical analyses were performed using GraphPad Prism 5.0 software (San Diego, CA). Data are presented as mean ± SEM. Comparisons between 2 groups were measured using unpaired 2-tailed Student's *t* test. Comparisons of multiple groups were analyzed by 2-way ANOVA followed by Bonferroni post-tests. Significance levels were set at $p < 0.05$ (*), $p \leq 0.01$ (**), and $p \leq 0.001$ (***) (144).

3. RESULTS

3.1 DGAT1 is efficiently knocked out in the small intestine of I-DGAT1$^{-/-}$ mice

To validate DGAT1 deficiency in intestines of I-DGAT1$^{-/-}$ mice, we isolated three parts of the small intestine and measured DGAT1 expression. DGAT1 mRNA was markedly downregulated in duodenum, jejunum, and ileum of I-DGAT1$^{-/-}$ mice compared with DGAT1$^{fl/fl}$ mice, whereas no differences were observed in liver and white adipose tissue (Fig. 8A). To determine whether I-DGAT1 deficiency affects DGAT2 mRNA levels, we analyzed DGAT2 gene expression and found comparable levels to control mice in all three parts of the small intestine, liver, and white adipose tissue (Fig. 8B). Intestinal DGAT activity was significantly reduced by 70% in the intestines of I-DGAT1$^{-/-}$ mice compared to DGAT1$^{fl/fl}$ mice. Pharmacological DGAT1 inhibitor treatment confirmed that the observed residual DGAT activity was a result of intestinal DGAT2 activity (Fig. 8C).

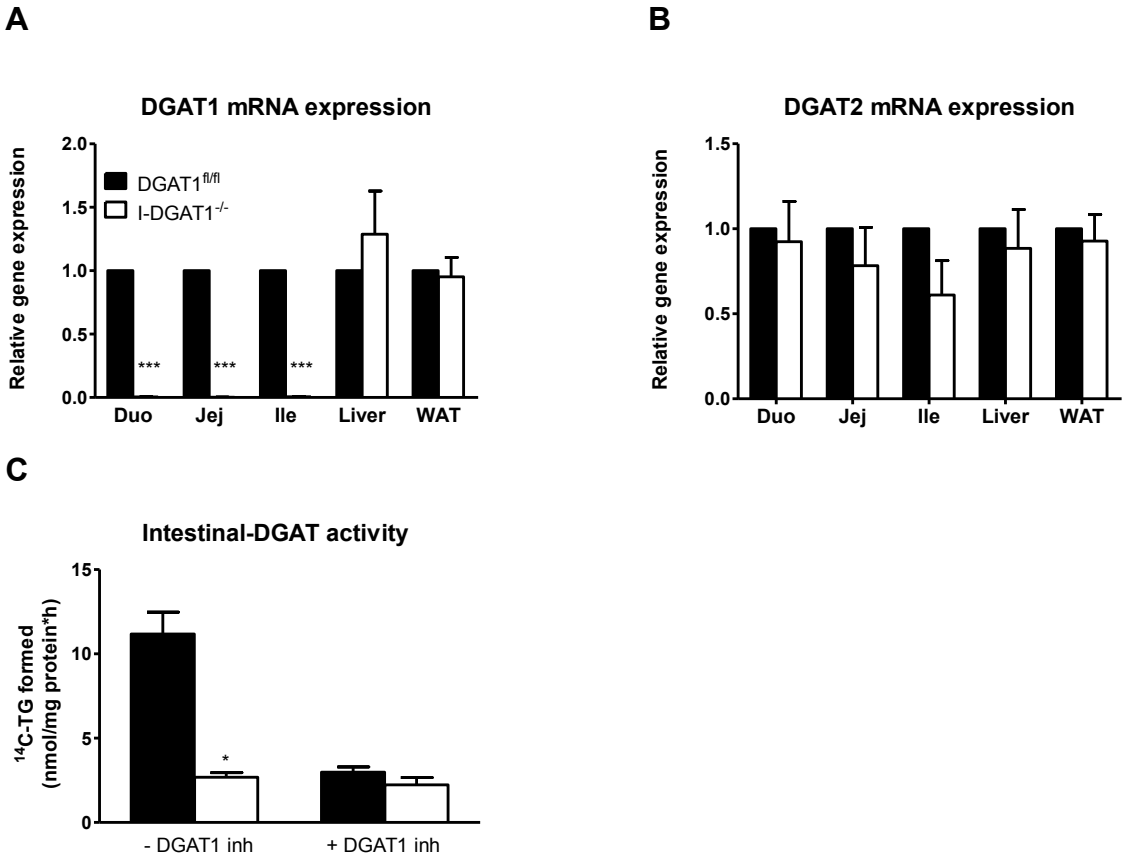

Figure 8: DGAT1 is knocked out specifically in the small intestine of I-DGAT1$^{-/-}$ mice. **(A)** DGAT1 and **(B)** DGAT2 mRNA expression was measured in the duodenum (duo), jejunum (jej), ileum (ile), liver and white

adipose tissue (WAT) of I-DGAT1$^{-/-}$ and DGAT1$^{fl/fl}$ mice. **(C)** Intestinal DGAT activity was measured in absence and presence of a DGAT1 inhibitor. Values represent mean + SEM. Student's t-test was used to compare grouped controls. *p<0.05 and ***p<0.001.

3.2 I-DGAT1 deficiency leads to decreased plasma total cholesterol and CE levels

Next, we examined body weight and plasma parameters of DGAT1$^{fl/fl}$ and I-DGAT1$^{-/-}$ mice fed a standard chow diet for 10-12 weeks. I-DGAT1$^{-/-}$ mice exhibited similar body weights (Fig. 9A) and food intake (Fig. 9B) but reduced TC and CE levels by 25% and 42 %, respectively (Fig. 9C) compared to control mice. As the chow diet in general contains only a minimal amount of cholesterol, these results gave a strong indication of altered cholesterol metabolism due to deficiency of DGAT1 in the intestines.

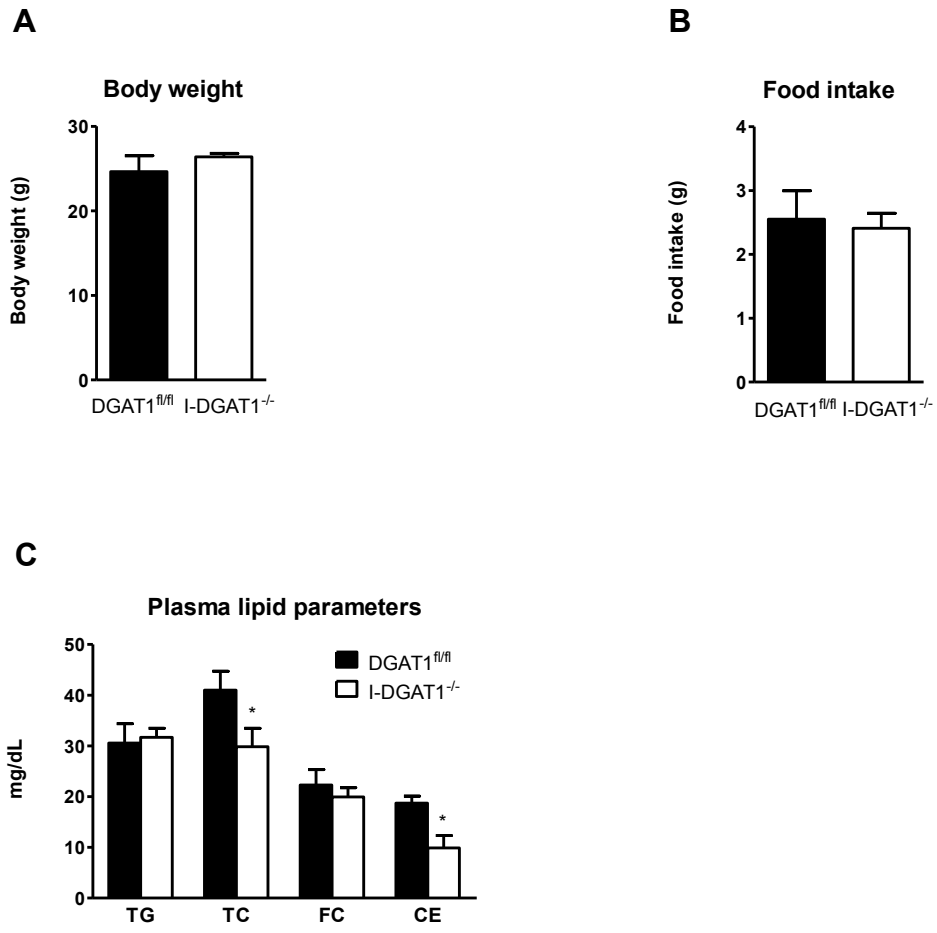

Figure 9: **Decreased plasma total cholesterol and cholesteryl ester levels in chow diet-fed male I-DGAT1$^{-/-}$ mice. (A)** Body weights, **(B)** food intake and **(C)** plasma parameters of 12-16 weeks old, 4 h fasted, male control and I-DGAT1$^{-/-}$ mice fed a standard chow diet. Values represent mean + SEM. Student's t-test was used to compare grouped controls. *p<0.05.

3.3 I-DGAT1 deficiency reduces cholesterol absorption comparable to global DGAT1 deficiency and pharmacological DGAT1 inhibition

A previous report from our group indicated reduced intestinal cholesterol uptake and absorption in global DGAT1-/- mice on an ApoE background (123). Since we observed reduced circulating cholesterol concentrations in chow diet-fed I-DGAT1$^{-/-}$ mice, we compared short-term and fractional cholesterol absorption between I-DGAT1$^{-/-}$, DGAT1$^{-/-}$, and DGAT1-Inh mice and their respective controls. Short-term cholesterol absorption was significantly decreased in I-DGAT1$^{-/-}$, DGAT1$^{-/-}$, and DGAT1-Inh mice as indicated by reduced radioactivity in intestine (58%, 78%, and 72%, respectively) and liver (50%, 82%, and 92%, respectively) (Fig. 10A, B). The radiotracer was retained considerably in the stomachs of I-DGAT1$^{-/-}$, DGAT1$^{-/-}$, and DGAT1-Inh mice compared to their respective controls (1.7-fold, 2.6-fold, and 2.6-fold, respectively) (Fig. 10C). In addition, we observed less plasma radiotracer counts in I-DGAT1$^{-/-}$ and DGAT1-Inh mice (73% and 90%, respectively) (Fig. 10D). Fractional cholesterol absorption in these mice was evaluated using the fecal dual isotope method which requires collection of fecal samples for 72 h after a single intragastric bolus of radiolabeled cholesterol and sitosterol, which acts as an internal standard. As shown in Fig. 10E, fractional cholesterol absorption was reduced in I-DGAT1$^{-/-}$, DGAT1$^{-/-}$, and DGAT1-Inh mice by 27%, 43%, and 32% respectively, compared to their respective controls (144).

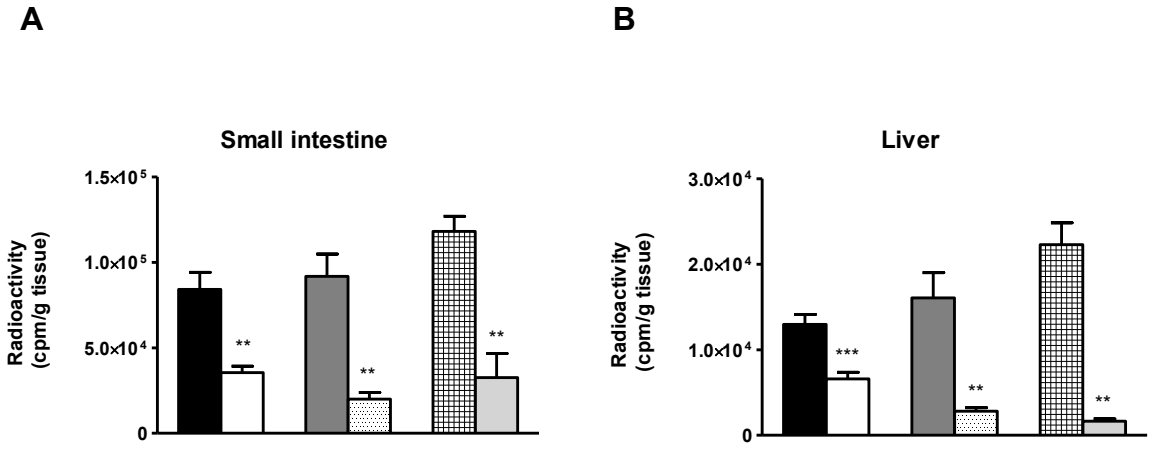

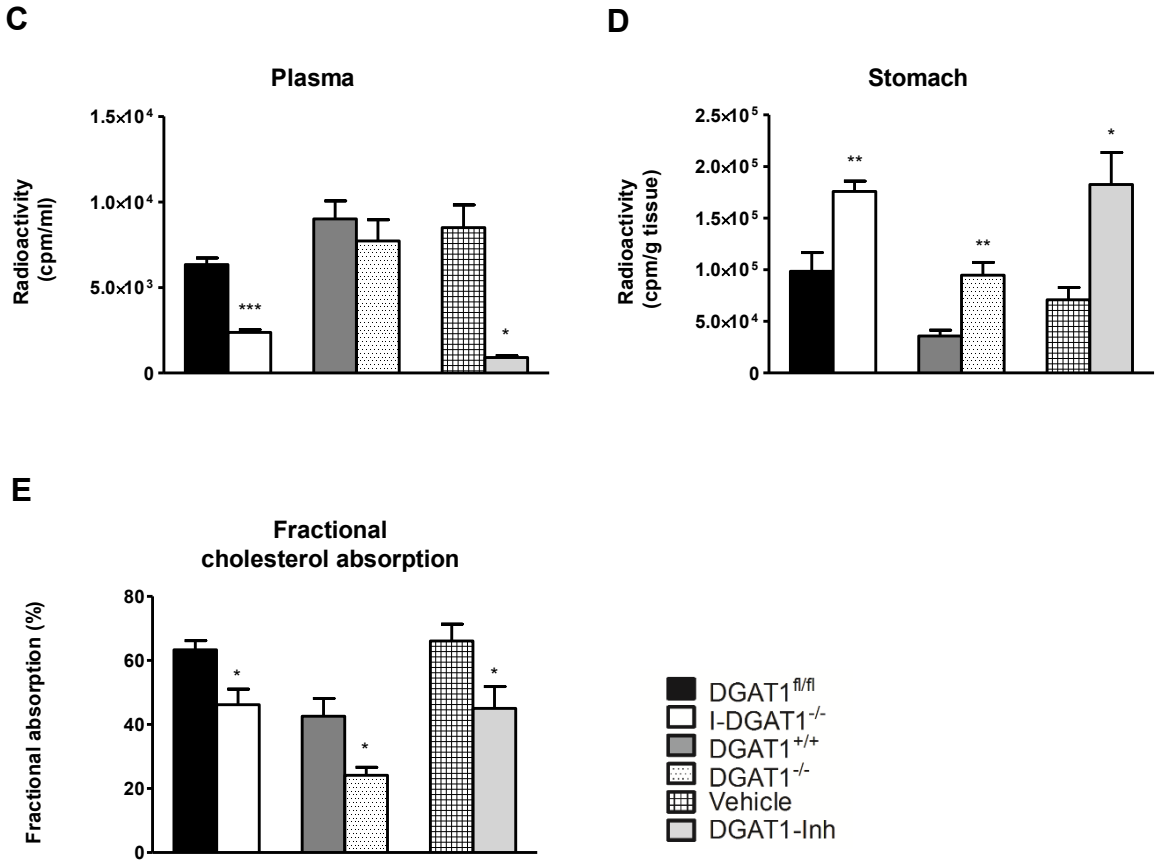

Figure 10: I-DGAT1 deficiency reduces cholesterol absorption comparable to global DGAT1 deficiency and pharmacological DGAT1 inhibition. (A-D) Mice (n=4-7) were gavaged with 200 µl corn oil containing 2 µCi [^{3}H]cholesterol and 200 µg cholesterol. Radioactivity was measured 4 h post-gavage in **(A)** duodenum, jejunum, ileum, **(B)** liver, **(C)** stomach, and **(D)** plasma by liquid scintillation counting. **(E)** Fractional cholesterol absorption was determined using the fecal dual-isotope method (n=5-10). Values represent mean + SEM. Student's t-test was used to compare grouped controls. $^*p<0.05$, $^{**}p<0.01$ and $^{***}p<0.001$ (144). Requisite permission to use this figure was obtained (Appendix).

3.4 Decreased gastric emptying due to I-DGAT1 deficiency is lipid sensing dependent

It has been consistently reported that global DGAT1 deficiency or pharmacological DGAT1 inhibition leads to reduced gastric emptying (121, 122, 125). Therefore, we investigated whether I-DGAT1 activity regulates this phenotype in mice. Indeed, when mice were gavaged with FITC-dextran in corn oil, gastric emptying was decreased by 15% and intestinal transit, as demonstrated by intestinal geometric center (IGC), was delayed significantly in I-DGAT1$^{-/-}$ compared to DGAT1$^{fl/fl}$ mice (Fig. 11A, B). Surprisingly, when gastric emptying was measured using FITC-dextran dissolved in PBS instead of corn oil, it remain unchanged between the two

groups. These results indicate that delayed gastric emptying observed in I-DGAT1$^{-/-}$ mice is dependent on lipid sensing mechanism (Fig. 11C).

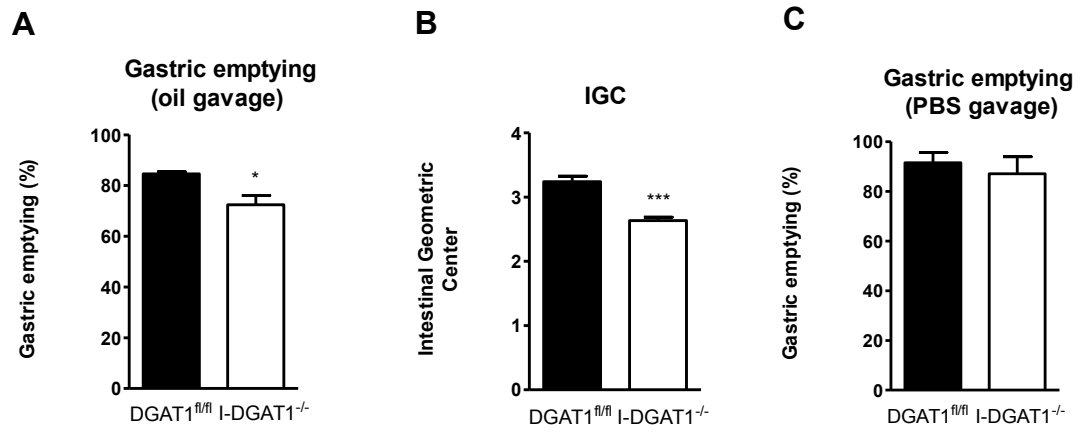

Figure 11: I-DGAT1 regulates gastric emptying in mice. Mice (n=4) were gavaged with FITC-dextran in 200 µl corn oil, and **(A)** gastric emptying and **(B)** intestinal geometric center (IGC) were determined. **(C)** gastric emptying after gavaging of FITC-dextran in 200 µl PBS was measured. Values represent mean + SEM. Student's t-test. $^{*}p<0.05$ and $^{***}p<0.001$.

3.5 I-DGAT1 deficiency reduces plasma cholesterol concentrations in mice fed with HF/HCD

Next, we compared the impact of I-DGAT1 deficiency to global DGAT1 deficiency in HF/HCD-fed mice. Over a period of 20 weeks of feeding, I-DGAT1$^{-/-}$ and DGAT1$^{-/-}$ mice exhibited resistance to body weight gain (Fig. 12A, B) and an improved metabolic profile as indicated by decreased plasma TC and CE concentrations (by 27% to 39% compared to their respective controls) (Fig. 12C, D). The observed results demonstrate that I-DGAT1 deficiency is sufficient to prevent diet-induced obesity in mice (144).

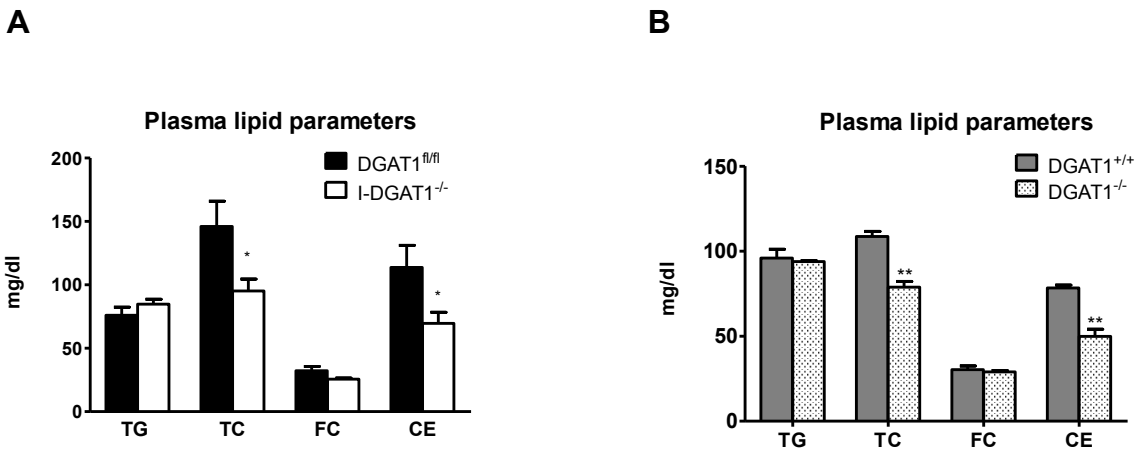

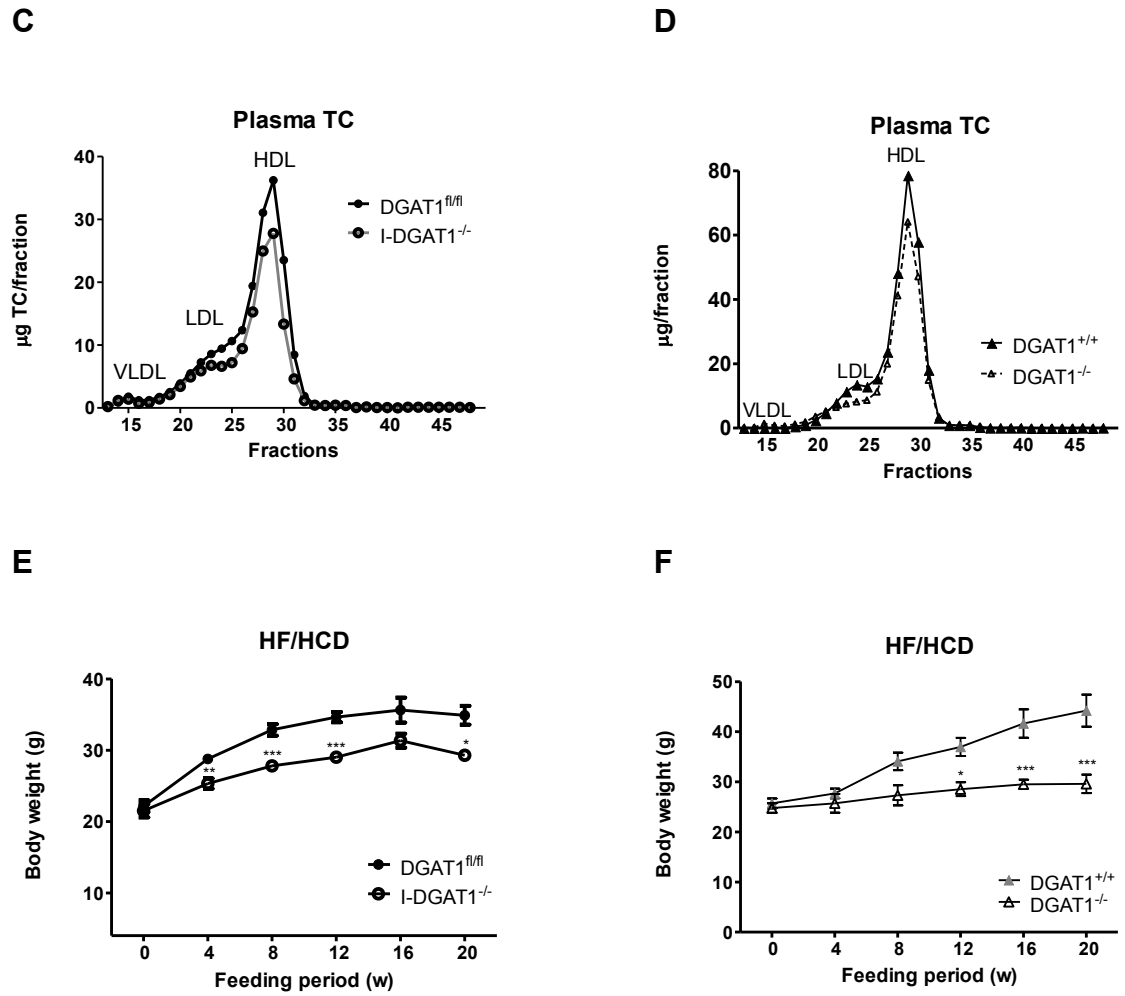

Figure 12: I-DGAT1 deficiency reduces plasma cholesterol concentrations comparable to global DGAT1 deficiency. Mice were fed HF/HCD for 20 weeks. **(A-B)** Body weights (n=3-19 until week 12, n=3-6 until week 20) of DGAT1$^{fl/fl}$, I-DGAT1$^{-/-}$, DGAT1$^{+/+}$ and DGAT1$^{-/-}$ mice. **(C-D)** Plasma TG, TC, and FC concentrations were measured spectrophotometrically. CE concentrations were determined as subtraction of FC from TC (n=5-6 for DGAT1$^{fl/fl}$ and I-DGAT1$^{-/-}$ mice and n=3 for DGAT1$^{+/+}$ and DGAT1$^{-/-}$ mice). **(E-F)** Lipoprotein profiles of TC after separation by fast performance liquid chromatography of pooled plasma (n = 5-6 for DGAT1$^{fl/fl}$ and I-DGAT1$^{-/-}$ mice and n=3 for DGAT1$^{+/+}$ and DGAT1$^{-/-}$ mice). Values represent mean ± SEM. A, B: 2-way ANOVA followed by Bonferroni post-test; C and D: Student's t-test. *p<0.05, **p<0.01 and ***p<0.001 (144). Requisite permission to use this figure was obtained (Appendix).

Plasma lipoprotein profiles after separation by fast protein liquid chromatography correspondingly revealed decreased LDL and HDL cholesterol levels in I-DGAT1$^{-/-}$ and DGAT1$^{-/-}$mice (Fig. 12E, F). Collectively, these results demonstrate that I-DGAT1 plays a critical role in the regulation of murine circulating cholesterol concentrations by altering the lipoprotein cholesterol content (144).

3.6 I-DGAT1 deficiency but not global DGAT1 deficiency in mice leads to smaller plasma HDL particle size

To determine whether decreased HDL cholesterol content in HF/HCD-fed I-DGAT1$^{-/-}$ and DGAT1$^{-/-}$mice affected HDL particle size, we ran plasma samples on a native gel followed by sudan-black staining. Though smaller HDL particle size was observed in I-DGAT1$^{-/-}$ mice (Fig. 13A), it remained unaffected in DGAT1$^{-/-}$ mice (Fig. 13B). This result excludes HDL particle size as a determining factor for the improved cholesterol profile in HF/HCD-fed I-DGAT1$^{-/-}$ and DGAT1$^{-/-}$mice.

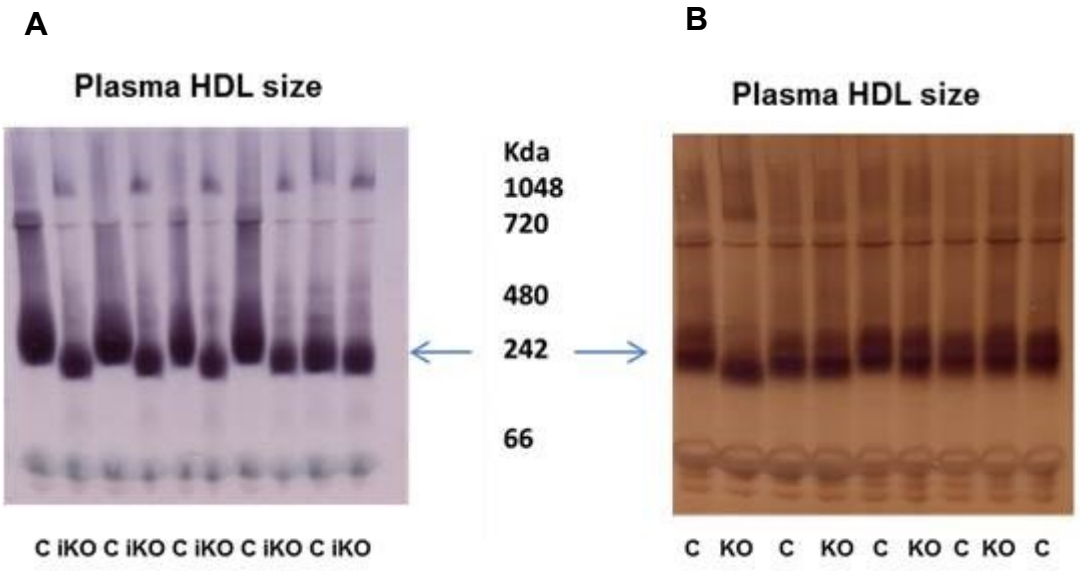

Figure 13: Plasma HDL particle size is reduced in I-DGAT1$^{-/-}$ mice but unaltered in DGAT1$^{-/-}$ mice. Plasma samples from HF/HCD-fed, **(A)** DGAT1$^{fl/fl}$, and I-DGAT1$^{-/-}$ mice (n=5), **(B)** DGAT1$^{+/+}$, and DGAT1$^{-/-}$ mice (n=4-5) were separated by gel electrophoresis on native gels followed by Sudan-black staining. Arrows indicate size of HDL particles.

3.7 DGAT1 inhibition reduces CE secretion from enterocytes

Previous reports speculated that decreased gastric emptying due to DGAT1 deficiency was critical for the improved metabolic profile in DGAT1$^{-/-}$ mice (121, 122). We performed *ex vivo* enterocyte studies to answer whether DGAT1 inhibition in enterocytes of wild-type mice affected cholesterol metabolism independent of the contribution of gastric emptying. Radiotracer cholesterol uptake in DGAT1-Inh enterocytes remained unchanged (Fig. 14A). However, compared to vehicle-treated enterocytes, cholesterol secretions specifically in FC and CE fractions were reduced in DGAT1-Inh enterocytes by 27% and 32%, respectively

(Fig. 14B, C) (144). These results strongly suggest that altered circulating cholesterol concentrations observed in I-DGAT1$^{-/-}$ were a direct consequence of DGAT1 deficiency in enterocytes of these mice.

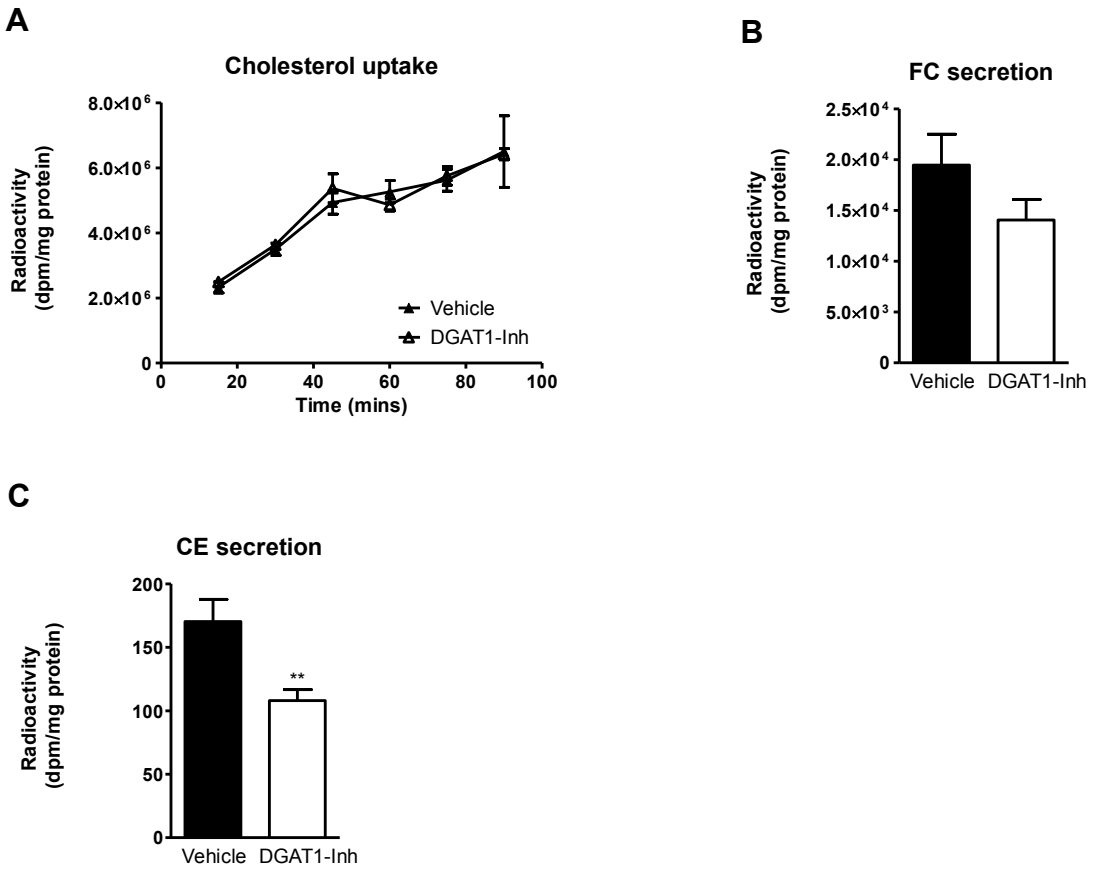

Figure 14: DGAT1 inhibition reduces enterocyte cholesteryl ester secretion. Enterocytes were isolated from overnight fasted C57BL/6 mice, treated with either vehicle or DGAT1-Inh (EC_{50} = 0.03 μM), and radiolabeled with 1 μCi [^{3}H]cholesterol/ml. **(A)** Enterocyte [^{3}H]cholesterol uptake was measured at indicated time points (n=3). **(B, C)** One hour after [^{3}H]cholesterol uptake, enterocytes were washed and chased with media containing 1.4 mM oleic acid micelles for 2 h. Lipids were isolated, subjected to TLC, and radioactivity was counted in **(B)** FC and **(C)** CE fractions. Values represent mean ± SEM. A: 2-way ANOVA followed by Bonferroni post-test; B, C: Student's t-test. $^{**}p<0.01$ (144). Requisite permission to use this figure was obtained (Appendix).

3.8 I-DGAT1 deficiency alters chylomicron composition

To evaluate whether I-DGAT1 alters post-prandial chylomicron secretion and cholesterol concentrations in chylomicrons we first treated DGAT1$^{fl/fl}$ and I-DGAT1$^{-/-}$ mice with P-407 to block lipolysis and then gavaged [^{3}H]triolein and [^{14}C]cholesterol provided in 200 μl corn oil. In I-DGAT1$^{-/-}$ mice, [^{3}H]triolein counts

were reduced by 40% 4 h post-gavage of corn oil compared to DGAT1$^{fl/fl}$ mice (Fig. 15A). Simultaneous reduction of [^{14}C]cholesterol counts by 52% was observed in I-DGAT1$^{-/-}$ mice at 4 h post fat challenge (Fig. 15B). In addition, [^{3}H]triolein and [^{14}C]cholesterol counts in the lymph were inhibited by 85% and 92%, respectively, in I-DGAT1$^{-/-}$ compared to DGAT1$^{fl/fl}$ mice (Fig. 15C, D). Based on these results we demonstrate that DGAT1 in the murine intestine regulates the amount of lipid incorporation into the chylomicrons subsequently to be released into the circulation (144).

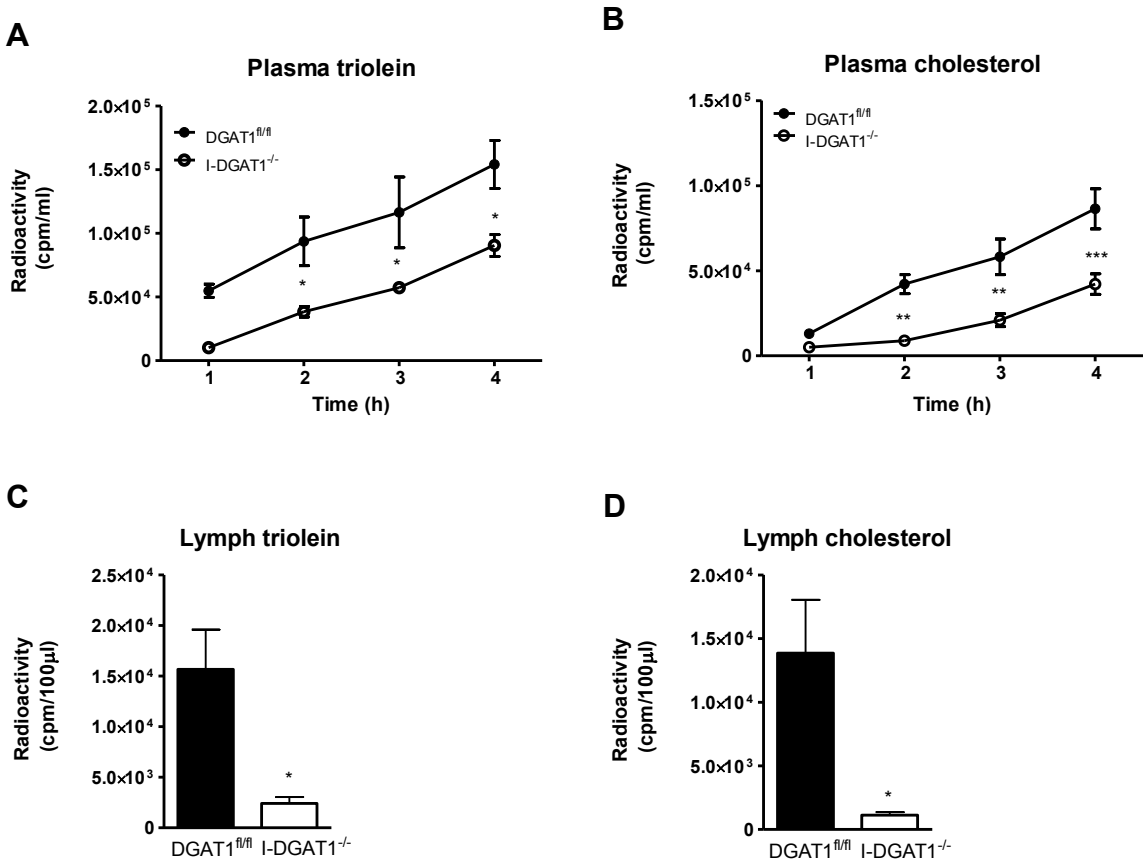

Figure 15: I-DGAT1 deficiency alters chylomicron composition. (A-D) DGAT1$^{fl/fl}$ and I-DGAT1$^{-/-}$ mice (n=4) fed HF/HCD were fasted for 4 h, injected intraperitoneally with poloxamer-407 (1 g/kg body weight, in PBS), and gavaged with 200 µl corn oil containing 1 µCi [^{3}H]triolein, 0.5 µCi [^{14}C]cholesterol, and 200 µg cholesterol. **(A, C)** [^{3}H]triolein-derived counts in **(A)** plasma and **(C)** lymph and **(B, D)** [^{14}C]cholesterol-derived counts in **(B)** plasma and (**D**) lymph were determined by liquid scintillation counting. Values represent mean ± SEM. A, B: 2-way ANOVA followed by Bonferroni post-test; C-E: Student's t-test. *p<0.05, **p<0.01 and ***p<0.001 (144). Requisite permission to use this figure was obtained (Appendix).

3.9 I-DGAT1 deficiency leads to smaller sized chylomicron particles

The core of chylomicron lipoprotein predominantly consists of TG and CE (91-96%) (93). Thus, we hypothesized that reduced lipid incorporation in chylomicrons of I-DGAT1$^{-/-}$ mice might alter their particle size. To determine the chylomicron size we isolated plasma chylomicrons and lymph from P-407-treated DGAT1$^{fl/fl}$ and I-DGAT1$^{-/-}$ mice after 90 min of fat challenge and subjected them to dynamic light scattering (DLS) and electron microscopy (EM) to estimate their size.

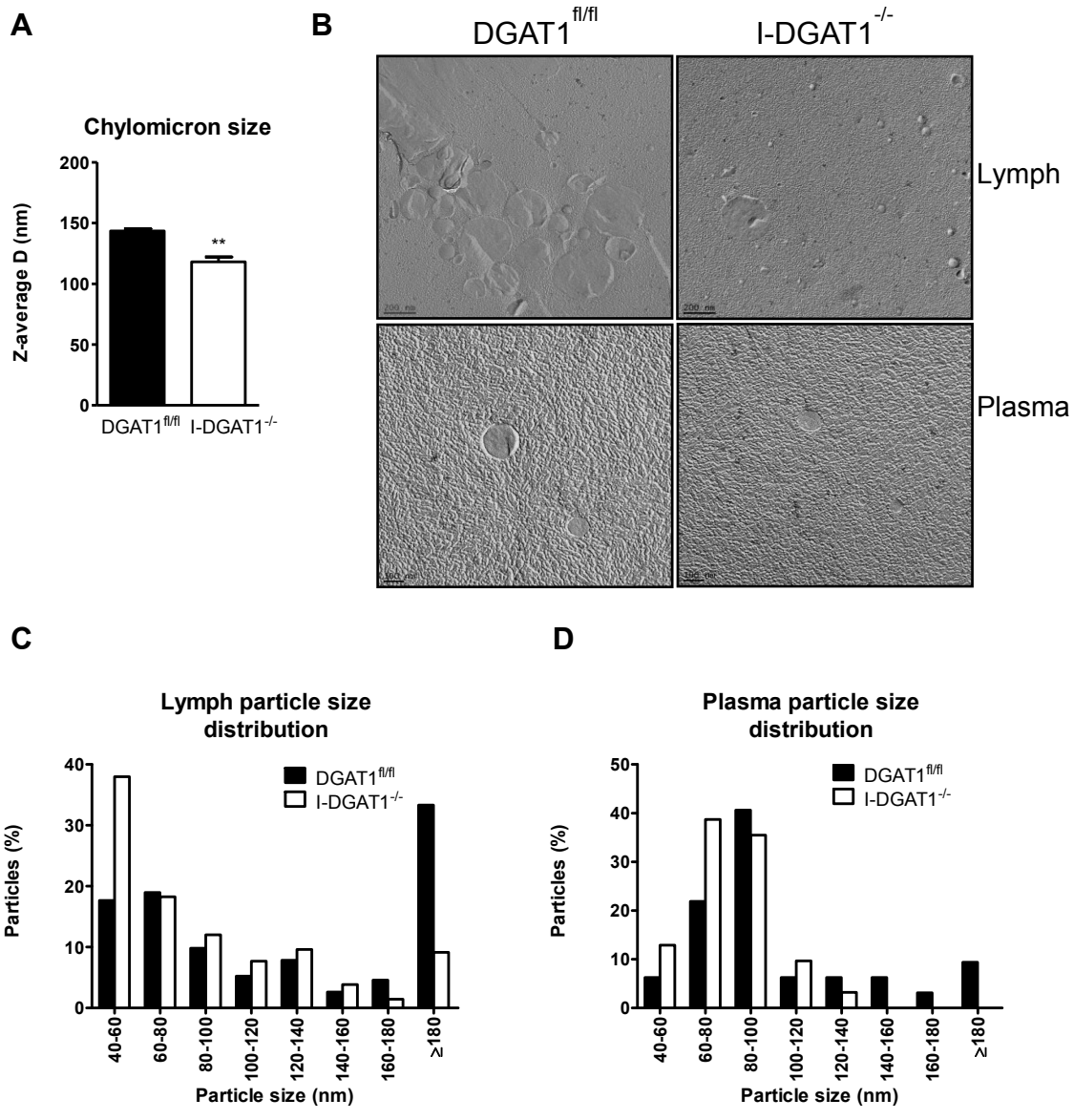

Figure 16: I-DGAT1 deficiency alters chylomicron particle size. (A-D) Plasma and lymph was collected 90 min post-gavage of 200 µl corn oil. **(A)** Postprandial plasma chylomicron size was measured by Zetasizer nano. **(B)** Electron micrographs of isolated lymph (top panel) and plasma chylomicrons (bottom panel). Distribution of particles size of **(C)** lymph and **(D)** plasma chylomicrons from 18 electron micrographs was analyzed by image J software. (A): values represent mean + SEM. Student's t-test. $^{**}p<0.01$ (144). Requisite permission to use this figure was obtained (Appendix).

Indeed, the plasma chylomicrons of I-DGAT1$^{-/-}$ mice were significantly smaller (20%) as measured by DLS (Fig. 16A). Electron micrographs of lymph (Fig. 16B, top panel) and plasma chylomicrons (Fig. 16B, bottom panel) confirmed smaller particle size in I-DGAT1$^{-/-}$ compared to DGAT1$^{fl/fl}$ mice. Semi-quantification of electron micrographs of lymph (Fig. 16C) and plasma chylomicrons (Fig. 16D) indicate a trend towards smaller particle size in I-DGAT1$^{-/-}$ compared to DGAT1$^{fl/fl}$ mice (144).

3.10 I-DGAT1 deficiency reduces intestinal and hepatic lipid accumulation

Increased tissue lipid accumulation could account for decreased circulating cholesterol concentrations observed in HF/HCD-fed I-DGAT1$^{-/-}$ mice. Thus, we measured lipid content in the intestine and liver of HF/HCD-fed I-DGAT1$^{-/-}$ mice fasted for 12 h. As shown in Fig. 17A, B, intestinal lipids, though they tended to be lower, were unchanged in I-DGAT1$^{-/-}$ mice. However, neutral lipid accumulation and specifically hepatic TG, was reduced in livers of these mice (Fig. 17C, D).

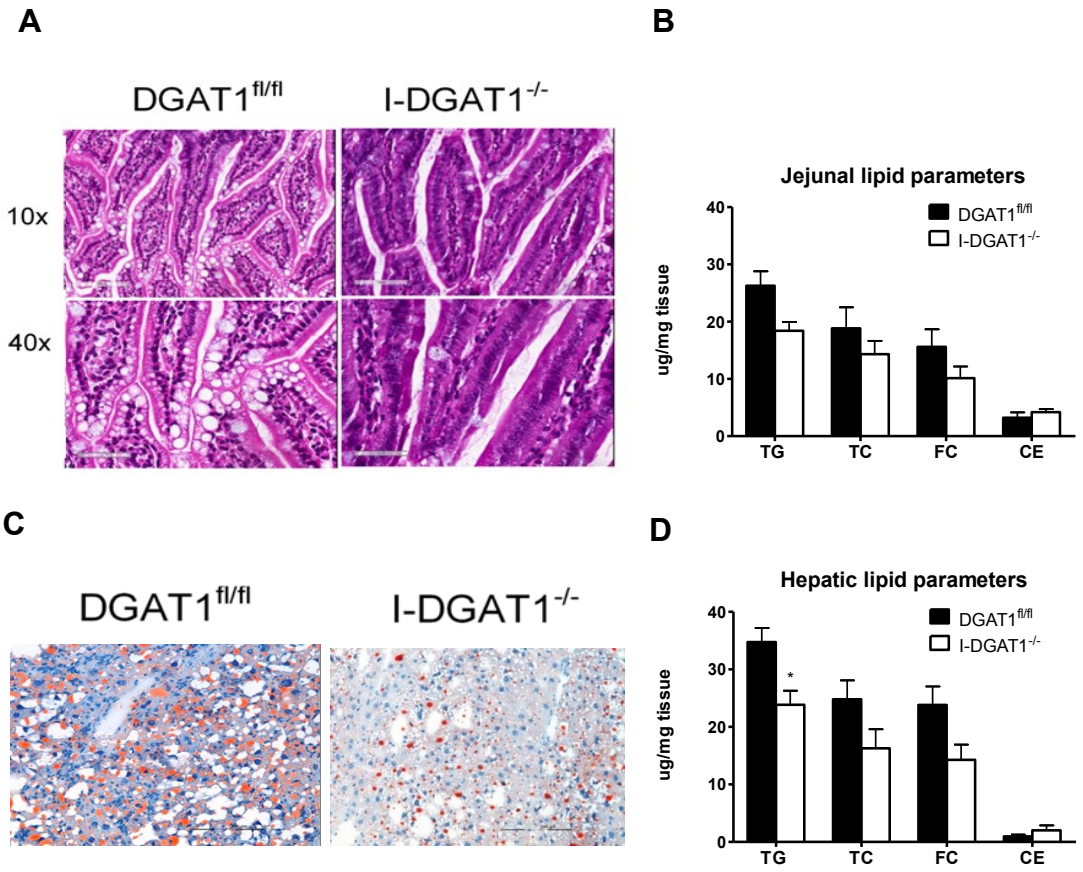

Figure 17: I-DGAT1 deficiency reduces intestinal and hepatic lipid accumulation. (**A-D**) Tissues were isolated from HF/HCD-fed, 12 h fasted, mice (n=3-4) **(A)** Representative images of hematoxylin and eosin staining of duodenal sections. Top panel: magnification, 10X; scale bar, 200 µm. Bottom panel: magnification, 40X; scale bar, 50 µm. **(B)** Jejunal lipid parameters were measured gravimeterically. **(C)** Representative images of Oil-red O stained of hepatic sections. Scale bar, 200 µm,. **(D)** Hepatic lipid parameters were measured gravimetrically. B and D: values represent mean + SEM. Student's t-test was used to compare grouped controls. $^{*}p<0.05$ (144). Requisite permission to use this figure was obtained (Appendix).

These findings were particularly interesting as previous a study has shown increased post-prandial intestinal lipid accumulation upon global DGAT1 deficiency (121). We do not underscore the possibility of transient lipid accumulation in the intestines of I-DGAT1$^{-/-}$ mice but our findings argue against chronic intestinal lipid accumulation in these mice. Furthermore, we could show that I-DGAT1 deficiency in mice mimics the phenotype of improved diet-induced hepatic lipid concentrations as observed upon global DGAT1 deficiency (144).

3.11 I-DGAT1 deficiency blunts ileal FGF15 without altering downstream target gene expression levels

Fibroblast growth factor 15 (FGF15) is a critical hormone in mice, which links intestinal and hepatic bile acid metabolism. It is synthesized in the ileum and released into the circulation from where it is transported to the liver to inhibit cholesterol 7α-hydroxylase (Cyp7a1) (155). In I-DGAT1$^{-/-}$ mice, ileal FGF15 mRNA expression levels were drastically downregulated compared to controls (Fig. 18A), however, mRNA concentrations of its downstream target, hepatic Cyp7a1, remained unaltered (Fig. 18B). These results suggested that bile acid metabolism was unaltered in I-DGAT1$^{-/-}$ mice (144).

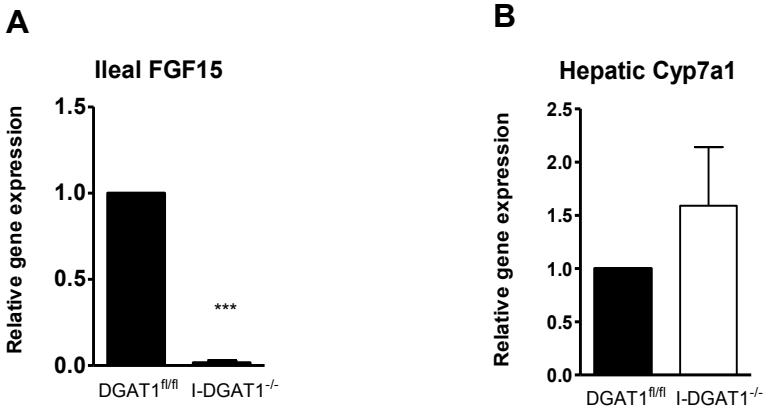

Figure 18: **Ileal FGF15 downregulation but unchanged hepatic Cyp7a1 mRNA levels in I-DGAT1$^{-/-}$ mice**. **(A)** mRNA expression levels of ileal FGF15 and, its downstream target, **(B)** hepatic Cyp7a1 were measured by real-time PCR analysis. Values represent mean + SEM. Student's t-test. ***p<0.001 (144). Requisite permission to use this figure was obtained (Appendix).

3.12 I-DGAT1 deficiency leads to increased fecal NSL and FA excretion in HF/HCD-fed mice

Reduced cholesterol absorption in mice has been shown to increase in fecal NSL (154). In accordance, we also observed increased fecal NSL and FA excretion in HF/HCD-fed DGAT1$^{fl/fl}$ and I-DGAT1$^{-/-}$ mice. Total fecal NSL and fecal cholesterol concentration was increased by 1.4-fold in I-DGAT1$^{-/-}$ mice (Fig. 19A, B). Biliary content in the fecal samples of two groups was grossly unaltered. Fecal total BA (Fig. 19C) and cholic acid (CA)-derived BA (Fig. 19D) concentrations were unchanged but slightly attenuated fecal chenodeoxycholic acid (CDCA)-derived BA (Fig. 19E) were observed in I-DGAT1$^{-/-}$ mice. Unaltered fecal BA levels were in agreement with unchanged hepatic Cyp7a1 levels in I-DGAT1$^{-/-}$ mice. Interestingly, we observed elevated fecal excretion of saturated FAs (SFA), mono-unsaturated FAs (MUFA), and polyunsaturated FAs (PUFA) in I-DGAT1$^{-/-}$ mice (Fig. 19F-H). These findings reflect that the incorporation of dietary FAs into neutral lipids is subsequently decreased due to enterocyte-DGAT1 deficiency thus leading to malabsorption of nutrient lipids and resulting in excess fecal neutral sterols and FAs excretion to the feces (144).

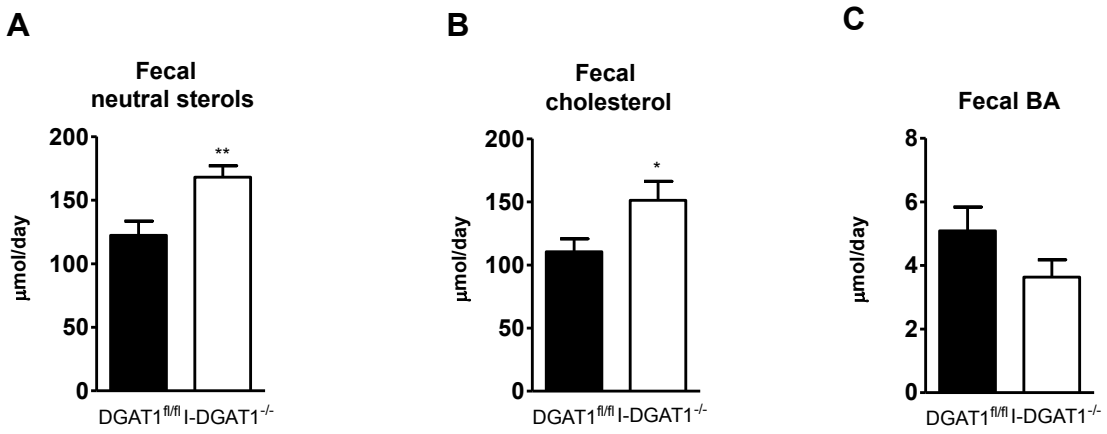

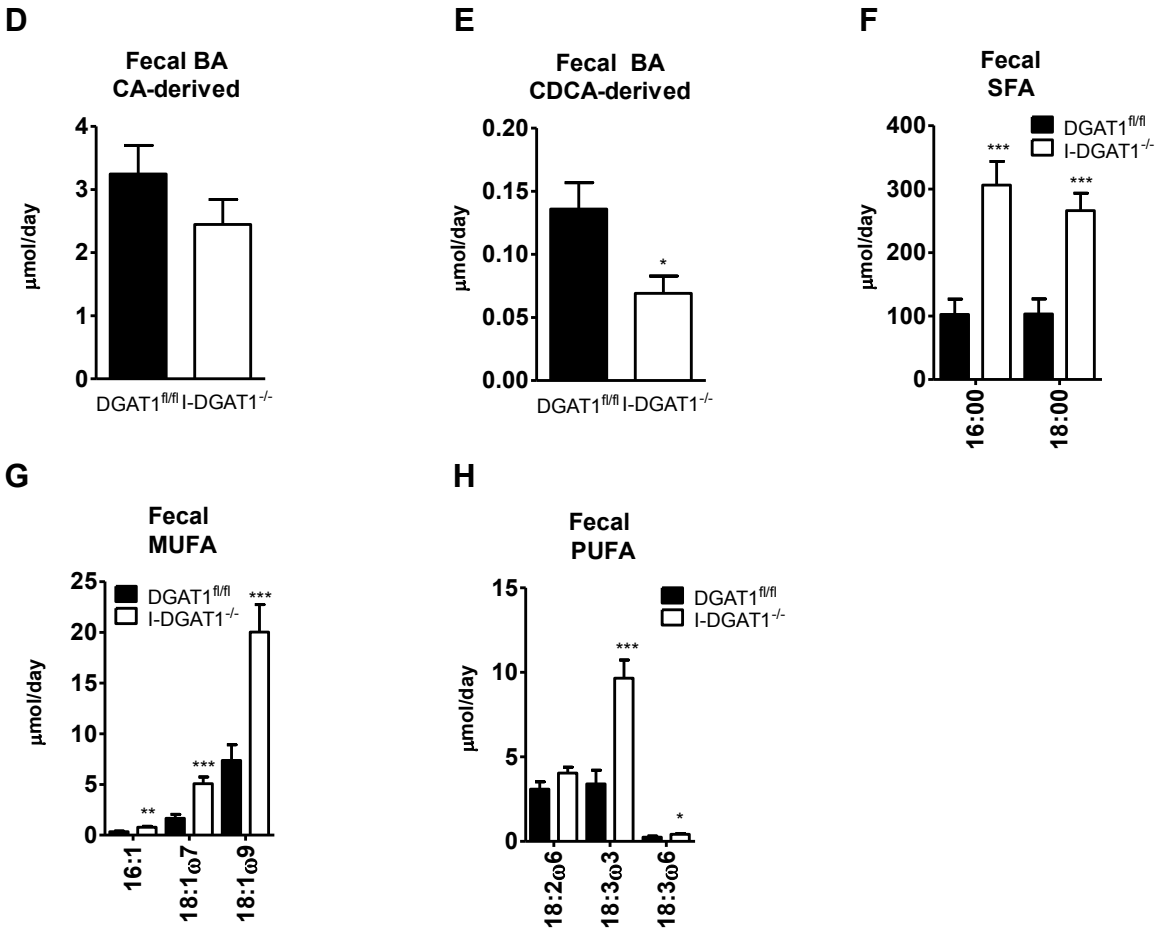

Figure. 19: I-DGAT1 deficiency leads to increased fecal neutral sterol and FA excretion in HF/HCD-fed mice. Feces of HF/HCD-fed mice (n=10-12) were collected for 72 h. Neutral sterols, bile acids (BA), and FAs (FA) were measured by gas chromatography. **(A)** Total fecal neutral sterols, **(B)** cholesterol, **(C)** total BA, **(D)** cholic acid (CA)-derived BA, and **(E)** chenodeoxycholic acid (CDCA)-derived BA, **(F)** saturated FA (SFA), **(G)** mono-unsaturated FA (MUFA), and **(H)** poly-unsaturated FA (PUFA) are indicated. Values represent mean ± SEM. Student's t-test. $^{*}p<0.05$, $^{**}p<0.01$ and $^{***}p<0.001$ (144). Requisite permission to use this figure was obtained (Appendix).

3.13 Pharmacological DGAT1 inhibition in HFD-fed mice increases fecal NLS via enhanced TICE

To determine whether chronic pharmacological DGAT1 inhibition phenocopies changes in cholesterol metabolism observed in I-DGAT1$^{-/-}$ mice we measured fecal NSL and cholesterol flux in DGAT1-Inh mice. We fed C57/B6 mice for four weeks with HFD containing either vehicle or pharmacological DGAT1 inhibitor. DGAT1-Inh mice exhibited reduced body weight gain compared to control mice (Fig. 20A) despite comparable food intake (Fig. 20B) between both groups. Similar

to I-DGAT1$^{-/-}$ mice, plasma CE concentrations were reduced in DGAT1-Inh compared to control mice (Fig. 20C).

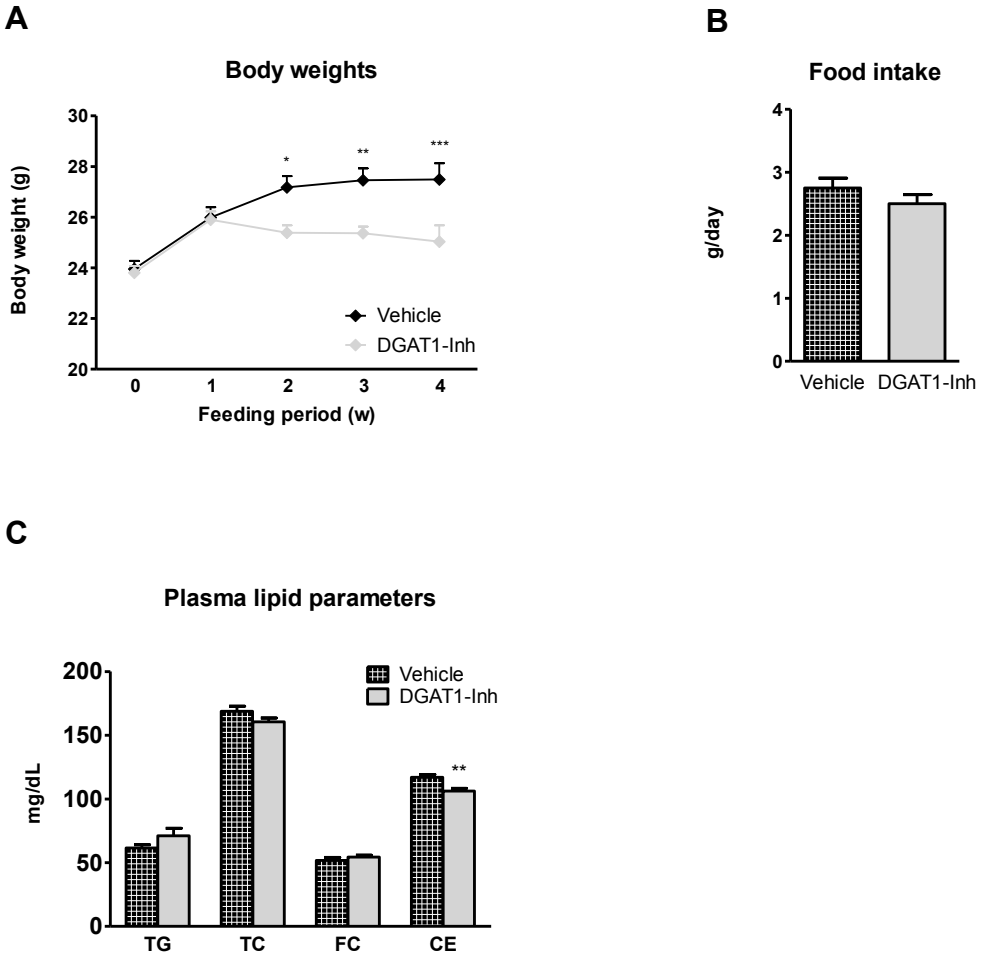

Figure. 20: Pharmacological DGAT1 inhibition in HFD-fed mice reduces body weight gain and plasma CE concentrations. Mice (n=8) were fed HFD supplemented with either vehicle or DGAT1-Inh (5 mg/kg diet) for 4 weeks, **(A)** Body weights and **(B)** food intake were measured. **(C)** Plasma lipid parameters were analyzed spectrophotometrically. Values represent mean ± SEM. A: 2-way ANOVA followed by Bonferroni post-test; B-C: Student's t-test. *p<0.05, **p<0.01, and ***p<0.001.

Similar to the observations in I-DGAT1$^{-/-}$ mice, DGAT1-Inh mice had increased fecal NSL (Fig. 21A) and augmented secretion of fecal cholesterol compared to vehicle-treated mice (Fig.21B). Fecal total BA, CA-derived BA, and CDCA-derived BA concentrations were similar between two groups (Fig. 21C-E) suggesting that increased fecal NSL was independent of BA excretion. Although fecal excretion of PUFA was unaffected (Fig. 11H), fecal SFA and MUFA concentrations were significantly increased in DGAT1-Inh compared to vehicle-treated mice (Fig. 6I, J)

indicating that nutrient malabsorption persists even upon pharmacological inhibition of DGAT1 in mice (144).

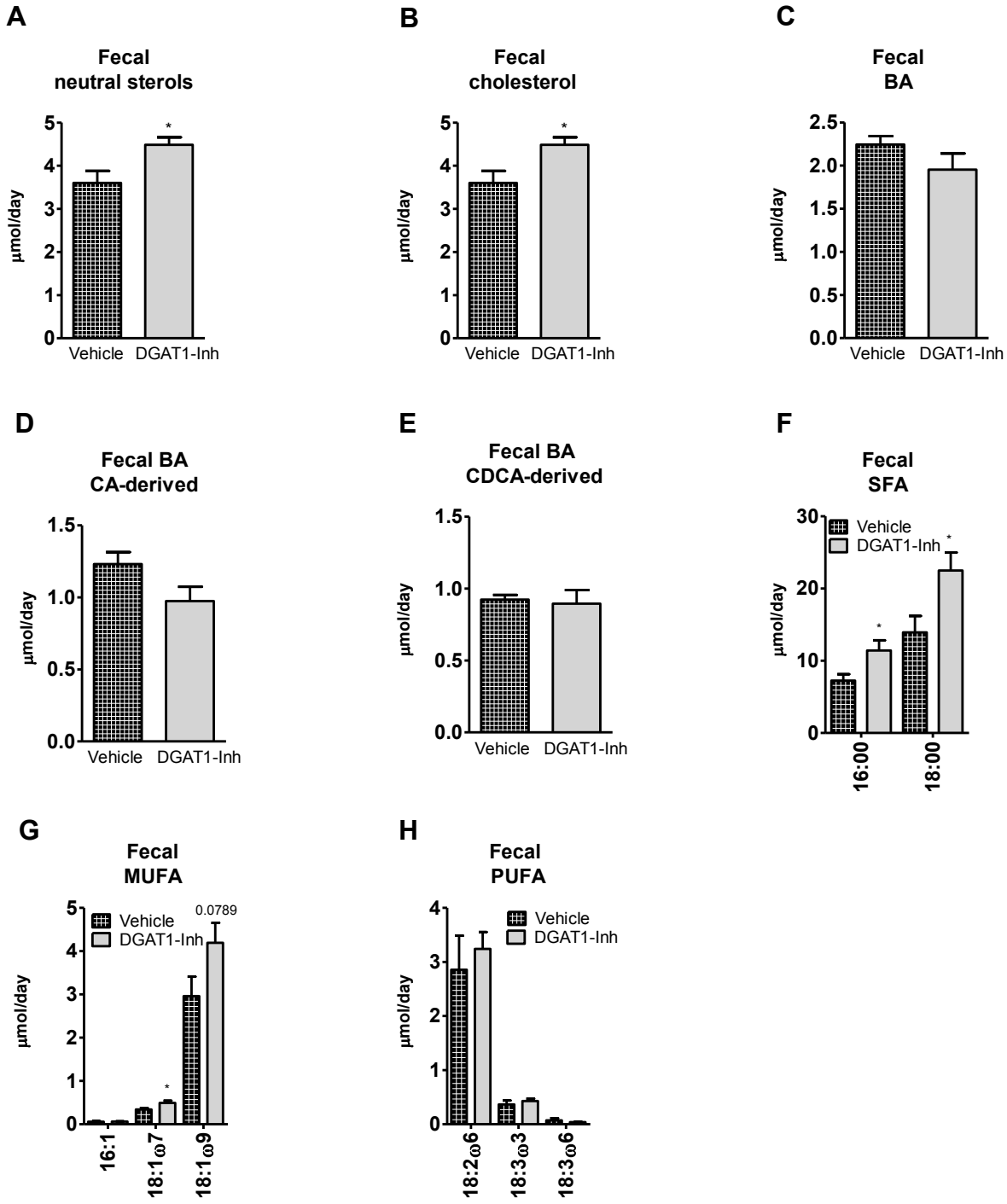

Figure 21: Pharmacological DGAT1 inhibition in HFD-fed mice increases fecal neutral sterol loss and FA excretion. Mice (n=8) were fed HFD supplemented with either vehicle or DGAT1-Inh (5mg/kg body weight) for 4 weeks. Feces were collected for 72 h and neutral sterols, bile acids (BA), and FAs (FA) were measured by gas chromatography. **(A)** Total fecal neutral sterols, **(B)** cholesterol, **(C)** total bile acids (BA), **(D)** cholic acid (CA)-derived BA, **(E)** chenodeoxycholic acid (CDCA)-derived BA, **(F)** saturated FA (SFA), **(G)**

monounsaturated FA (MUFA), and **(H)** polyunsaturated FA (PUFA) were measured. Values represent mean + SEM. Student's t-test. *p<0.05 (144). Requisite permission to use this figure was obtained (Appendix).

Bile output (Fig. 22A) and biliary cholesterol concentrations (Fig. 22B) in DGAT1-Inh mice were comparable to vehicle-treated mice. Trans-intestinal cholesterol excretion (TICE) contributes about 30% of cholesterol excretion mice (154). Unaltered bile metabolism combined with increased fecal NSL excretion reflected altered TICE in DGAT1-Inh mice which was indeed augmented by 1.7-fold (Fig. 22C) (144).

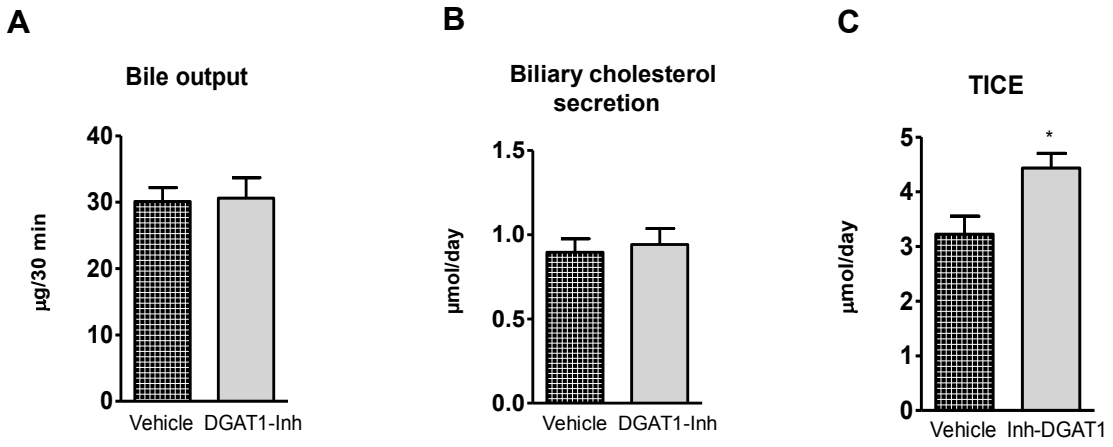

Figure 22: Pharmacological DGAT1 inhibition in HFD-fed mice increases trans-intestinal cholesterol excretion (TICE). Mice (n=8) were fed HFD supplemented with either vehicle or DGAT1-Inh (5mg/kg body weight) for 4 weeks. Bile was collected by bile duct cannulation to measure **(A)** bile output and **(B)** biliary cholesterol secretion. Values from fecal NSL and BA excretion were used to calculate **(C)** trans-intestinal cholesterol excretion (TICE) in these mice. Values represent mean + SEM. Student's t-test. *p<0.05 (144). Requisite permission to use this figure was obtained (Appendix).

3.14 I-DGAT1 deficiency does not affect mRNA and protein expression of intestinal lipid transporters

To further understand the causal mechanism leading to reduced absorption of cholesterol in the small intestine and increased fecal NSL and FA excretion of I-DGAT1$^{-/-}$ mice, we measured the expression of genes involved in lipid absorption in the proximal small intestine. Duodenal small intestinal mRNA expression in 4 h fasted mice revealed that genes involved in lipid uptake, transport, and absorption had comparable mRNA abundances in both genotypes (Fig. 23A). In addition, the

duodenal protein expression of key lipid transporters like NPC1L1, ABCG8, CD36, and SRB1 were similar in both groups tested (Fig. 23B, C). These data suggest that the reduced absorption of cholesterol in intestines and plasma of I-DGAT1$^{-/-}$ mice is independent of the intestinal expression of these genes (144).

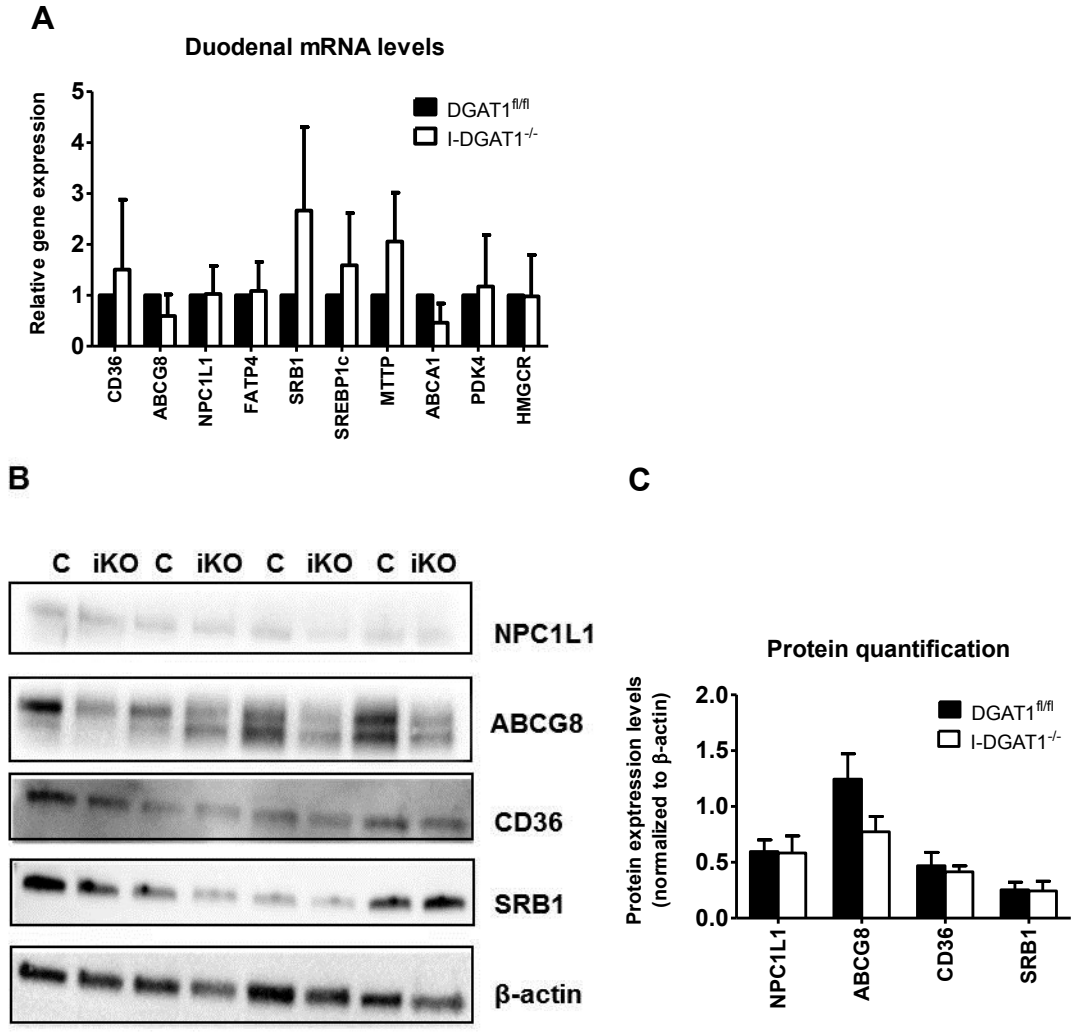

Figure 23: Unchanged mRNA and protein expression in duodena of I-DGAT1$^{-/-}$ mice. (A) Duodenal mRNA expression after 4 h fasting of mice fed HF/HCD for 20 weeks. Data represent mean values + SD (n = 3). **(B)** Duodenal lysates of HF/HCD-fed DGAT1$^{fl/fl}$ mice (denoted by C) and I-DGAT1$^{-/-}$ (denoted by iKO) were separated by SDS-PAGE. NPC1L1, ABCG8, CD36, SR-B1 and β-actin protein expression was analyzed by western blotting. The expression of β-actin served as loading control. **(C)** Quantification of protein expression. (144). Requisite permission to use this figure was obtained (Appendix).

3.15 DGAT1 deficiency in LDLR$^{-/-}$ mice reduces plasma cholesterol concentrations.

To figure out the contribution of LDLR-mediated clearance of lipoproteins to the reduction of circulating cholesterol concentrations in DGAT1$^{-/-}$ and I-DGAT1$^{-/-}$ mice, we fed LDLR$^{-/-}$ and DGAT1$^{-/-}$LDLR$^{-/-}$ mice with HF/HCD for 8 weeks. We observed reduced body weight gain (Fig. 24A) and circulating TC, FC, and CE concentrations (15%, 10% and 14%, respectively) (Fig. 24B) in DGAT1$^{-/-}$LDLR$^{-/-}$ compared to LDLR$^{-/-}$ mice. These results together with smaller chylomicron size observed in DGAT1$^{-/-}$ and I-DGAT1$^{-/-}$ mice suggest that reduced neutral lipid incorporation into chylomicrons rather than chylomicron clearance leads to decreased cholesterol concentrations observed in these mice. We also reported previously that DGAT1 deficiency on an apolipoprotein E$^{-/-}$ background results in decreased circulating cholesterol concentrations (123). Extrapolation of all these results indicate that altered chylomicron secretion rather than remnant clearance via hepatic LDLR-APOE axis drives the beneficial cholesterol phenotype observed upon DGAT1 deficiency (144).

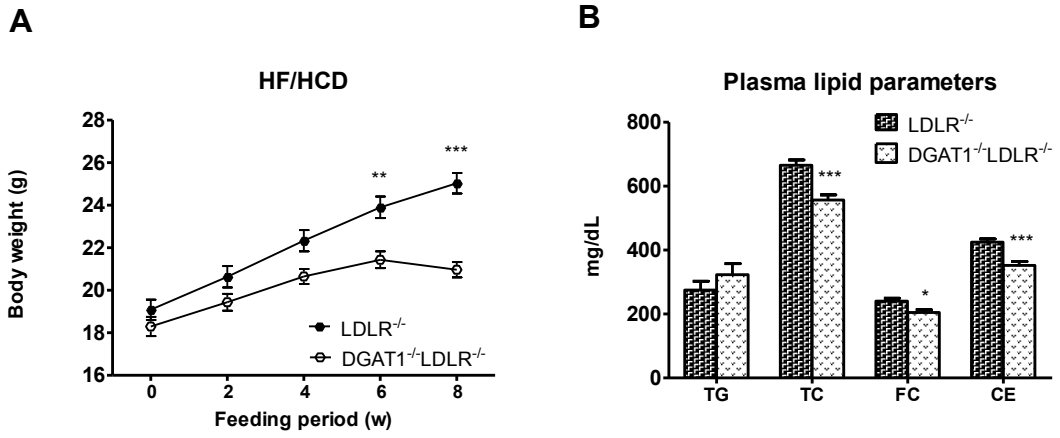

Figure 24: DGAT1 deficiency in LDLR$^{-/-}$ mice reduces plasma cholesterol concentrations. LDLR$^{-/-}$ and DGAT1$^{-/-}$LDLR$^{-/-}$ mice were fed HF/HCD for 8 weeks. **(A)** Body weights and **(B)** plasma TG, TC, and FC concentrations were measured spectrophotometrically. CE concentrations were determined as subtraction of FC from TC (n=6). Values represent mean ± SEM. A: 2-way ANOVA followed by Bonferroni post-tests; B: Student's t-test. $^{*}p<0.05$, $^{***}p<0.001$ (144). Requisite permission to use this figure was obtained (Appendix).

3.16 I-DGAT1 deficiency does not alter glucose metabolism in mice

It has been previously reported that global DGAT1 deficiency in mice improves glucose and insulin metabolism (120). Here, we aimed to determine whether resistance to obesity in I-DGAT1$^{-/-}$ mice was accompanied by increased insulin sensitivity and improved glucose homeostasis in these mice. We found that OGTT (Fig. 25A) and ITT (Fig. 25B) were comparable between HF/HCD-fed DGAT1$^{fl/fl}$ and I-DGAT1$^{-/-}$ mice. Thus, I-DGAT1 deficiency alone is not sufficient to alter glucose tolerance in mice. The reduced body weight gain observed in I-DGAT1$^{-/-}$ mice is more likely a result of altered lipid metabolism rather than glucose or insulin dys-regulation.

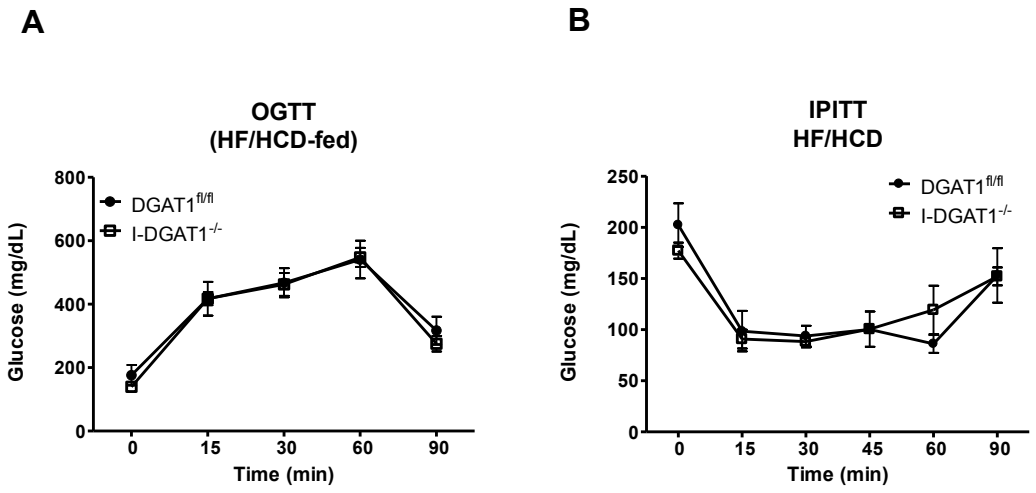

Figure 25: I-DGAT1 deficiency does not alter glucose and insulin metabolism. Mice (n=4-5) were fed HF/HCD for 20 weeks. **(A)** Oral glucose tolerance test (OGTT) and **(B)** intra-peritoneal insulin tolerance test (IPITT). Values represent mean ± SEM.

4. Discussion

Chylomicrons play a predominant role in delivering dietary fat cargo into the circulation. I-DGAT1, localized at the endoplasmic reticulum (ER) of the enterocytes, regulates the synthesis of TGs for their incorporation into chylomicrons (20, 156). In murine enterocytes, I-DGAT1 competes with other acyltransferases for the dietary FA pool to synthesize esterified TG (20, 114). DGAT1$^{-/-}$ mice are resistant to diet-induced weight gain but reversal of this phenotype is observed when DGAT1 is expressed only in the intestine (120, 138). Moreover, intestine-specific overexpression of DGAT1 does not significantly increase TG incorporation into chylomicrons as these mice secrete TG from the intestine at a comparable rate within similar sized chylomicrons compared to WT mice (114, 121). We have also previously reported that loss of DGAT1 on the APOE$^{-/-}$ background decreased plasma cholesterol concentrations and reduced intestinal cholesterol absorption (123). Using transgenic mouse models, we have then evaluated whether cholesterol concentrations and cholesterol metabolism per se is altered upon I-DGAT1 deficiency or whole-body DGAT1 inhibition in mice (144).

Chylomicron secretion per se and its cholesterol content was severely inhibited in I-DGAT1$^{-/-}$ mice. Moreover, circulating CE concentrations, which is a major cholesterol species in post-prandial chylomicrons, was consistently reduced in all our DGAT1-transgenic mouse models. Ables et al. have previously reported on reduced chylomicron secretion with reduced postprandial TG and retinyl ester (RE) excursions in I-DGAT1$^{-/-}$ mice (125), which might be the result of decreased acyl-CoA retinol acyltransferase activity due to DGAT1 deficiency (116). To our knowledge, no association has been reported between DGAT1 and ACAT activity. Together, these results demonstrate that enterocyte DGAT1 deficiency affects the intricate balance of dietary lipid esterification and thus reduced TG, RE, and CE are available for incorporation into chylomicron, subsequently altering whole body cholesterol homeostasis.

Further, reduced postprandial neutral lipid incorporation into chylomicrons in I-DGAT1$^{-/-}$ mice resulted in smaller chylomicron size, similar to the results observed in DGAT1$^{-/-}$ mice. Previous studies in other rodent models have explained that

smaller chylomicron-sized particles are cleared faster from the circulation compared to large chylomicrons due to an inverse correlation between the size of lipoprotein and surface area available for LPL to cleave TG within lipoproteins (157). We speculate that smaller chylomicron particle size and, subsequently, faster plasma clearance could account for an improved metabolic profile in HF/HCD-fed I-DGAT1$^{-/-}$ mice. Interestingly, reduction in postprandial chylomicron size is a specific characteristic of I-DGAT1 deficiency because I-ACAT2$^{-/-}$ mice have unchanged postprandial chylomicron particle size. The decrease in CE incorporation in chylomicrons was shown to be compensated mainly by TG without particle size alterations in these mice (149).

Delayed gastric emptying is a constant phenotype observed upon intestinal and global DGAT1 deficiency and inhibition in murine models and replicated in human clinical trials after pharmacological DGAT1 inhibition (122, 125, 132, 144, 158). In agreement with these studies, we observed delayed lipid sensing-dependent gastric-emptying in I-DGAT1$^{-/-}$ mice. Delayed gastric emptying is reported to result in increased cholesterol absorption in murine studies (159). However, acute and fractional cholesterol absorption was decreased in I-DGAT1$^{-/-}$, DGAT1$^{-/-}$, and DGAT1-Inh mice. These results indicate that (i) I-DGAT1 deficiency alone is capable to decrease cholesterol absorption to levels comparable to global DGAT1 deficiency or DGAT1 inhibition, and that (ii) delayed gastric emptying might be a contributing factor but not quintessential for reduced cholesterol absorption in I-DGAT1$^{-/-}$ mice. Our reasoning is strengthened by the fact that treatment of I-DGAT1$^{-/-}$ mice with the GLP-1 antagonist exendin-9 rescues the delayed gastric emptying but decrease in postprandial TG and RE excursion remain unchanged in these mice (125).

Moreover, to eliminate the likelihood of endocrinal changes resulting in altered cholesterol absorption, we utilized an *ex vivo* enterocyte isolation model and measured cholesterol absorption after DGAT1 inhibition. We observed decreased enterocyte CE secretion but comparable apical cholesterol uptake in DGAT1-Inh enterocytes. These results specify that the enterocyte cholesterol uptake machinery remains intact after DGAT1-inhibition but the secretion pathway is affected. Extrapolating our *in vivo* and *ex vivo* results we believe that decreased chylomicron secretion and decreased absorption in intestinal and global DGAT1

deficient/inhibition mouse models is a direct result of altered enterocyte cholesterol processing. Induced delay in gastric emptying is only a minor contributing factor to the observed results (144).

Decreased cholesterol absorption, correspondingly, resulted in reduced circulating plasma TC and CE concentrations in I-DGAT1$^{-/-}$ and DGAT1$^{-/-}$ mice, particularly in HDL and LDL lipoproteins. This finding is in accordance with clinical data of human volunteers treated with the same pharmacological DGAT1 inhibitor used in the present study. They exhibited significant reduction in plasma TC and LDL-C concentrations (Turnbull AV, personal communication). Moreover, decreased circulating lipid concentrations were independent of tissue lipid accumulation as we observed unchanged jejunal lipid concentrations and, surprisingly, neutral lipid accumulation in the liver was decreased in I-DGAT1$^{-/-}$ mice. In addition, HF/HCD-fed DGAT1$^{-/-}$LDLR$^{-/-}$ compared to LDLR$^{-/-}$ mice exhibited attenuated circulating TC and CE concentrations. We have also previously reported reduced plasma cholesterol levels and cholesterol absorption in DGAT1$^{-/-}$APOE$^{-/-}$ (123). To sum up these results, it can be concluded that the improved cholesterol phenotype upon DGAT1 deficiency/inhibition is a direct result of enterocyte mediated decrease in CE secretion rather than enhanced or efficient remnant clearance via the hepatic APOE-LDLR axis (144).

Based on previous reports, I-DGAT1 deficiency is speculated to be predominantly driving by the resistance to diet-induced obesity in DGAT1$^{-/-}$ mice. In accordance, we observed decreased body weight gain in HF/HCD-fed I-DGAT1$^{-/-}$, DGAT1$^{-/-}$ or DGAT1$^{-/-}$/LDLR$^{-/-}$ mice compared to their respective controls. Moreover, glucose and insulin resistance was unchanged in HF/HCD-fed I-DGAT1$^{-/-}$ mice. Our study thus confirms that I-DGAT1 deficiency alone is sufficient to prevent diet-induced weight gain in HF/HCD-fed mice (144). The resistance to diet-induced obesity might be (at least in part) due to increased fecal FA excretion upon high-fat diet as observed in our DGAT1$^{-/-}$ or DGAT1-Inh mouse models. It has been previously reported that absence of murine I-ACAT2 results in increased chylomicron TG mass and unchanged fecal fat excretion (149). In contrast, mice lacking I-MTP, the rate-limiting enzyme for chylomicron synthesis, exhibit significantly increased fecal fat output (109), comparable to our observations in I-DGAT1$^{-/-}$ and DGAT1-Inh

mice. In accordance with our data, Denison *et al*. have previously reported increased fecal FA concentrations in human subjects treated with the same DGAT1-Inh used in our study (132). Collectively, these results indicate that I-DGAT1 deficiency leads to increased fecal FA excretion since TG re-esterification by DGAT1 and incorporation into chylomicrons is crucial for channeling dietary FAs for chylomicron assembly and its failure results in excess excretion of FAs in feces (144).

Reduced cholesterol absorption is known to increase excretion of unabsorbed cholesterol in the feces (154). In agreement, we observed increased fecal NSL in I-DGAT1$^{-/-}$ mice fed HF/HCD for 20 weeks and in DGAT1-Inh mice fed HFD for 4 weeks. Altered cholesterol absorption and increased fecal NSL due to decreased NPC1L1 protein/mRNA expression, the major cholesterol transporter in enterocytes, has been previously reported (160). However, the possibility of NPC1L1 regulating the observed phenotype in I-DGAT1$^{-/-}$ mice was nullified as we observed comparable uptake of cholesterol in our *ex vivo* studies and comparable jejunal NPC1L1 protein expression in I-DGAT1$^{-/-}$ mice (144). In addition, we observed unchanged hepatic Cyp7a1 mRNA expression levels, comparable bile flow and unchanged fecal BA concentrations in our mouse models. Together, these results make the involvement of hepato-biliary pathway in maintenance of cholesterol metabolism due to DGAT1 deficiency or inhibition unlikely. Alternatively, there exists a hepato-biliary independent cholesterol excretion route where the circulating cholesterol is channeled back to the intestinal lumen via enterocytes to be subsequently excreted through feces. This pathway is described as TICE and it accounts for ~30% of total fecal NSL excreted by wild-type mice (154). Indeed, cholesterol flux measurements in DGAT1-Inh mice revealed a 1.4-fold increase in TICE. Collectively, these results demonstrate that TICE is major contributor towards the metabolically beneficial cholesterol phenotype observed in DGAT1-deficient and -inhibited mice (144).

The precise molecular mediators and basolateral transporters which facilitate TICE are still a matter of debate. To determine the mechanism/s involved in increased TICE in I-DGAT1$^{-/-}$ mice, we measured the known molecular targets associated with TICE like LXR activation and peroxisome proliferator-activated receptor δ

ligands (154, 161). However, we observed comparable mRNA and protein expression levels of number of their downstream intestinal targets such as ABCG8, NPC1L1 and SRB1 in the duodena of DGAT1$^{fl/fl}$ and I-DGAT1$^{-/-}$ mice. Furthermore, recent studies have hinted that the cholesterol destined to be secreted via TICE is transported to the intestine from the circulation through APOB-containing lipoproteins. The size of such lipoproteins is speculated to be smaller in size compared to circulating lipoproteins like VLDL and LDL (103, 162). We suggest that smaller sized APO-B48-containing chylomicrons in I-DGAT1$^{-/-}$ mice are able to exocytose the intestinal barrier to find their way back into the lumen and, eventually to be secreted into the feces. To our knowledge, smaller chylomicron particles have not yet been linked to increased TICE in mice or could explain how smaller chylomicrons could bypass the lymphatic system to be trafficked back into the intestinal lumen (144). Future studies directed towards exploring chylomicrons as a substrate for TICE should shed more light to our hypothesis.

Pharmacological DGAT1 inhibitors in humans have demonstrated consistent reduction in postprandial TG excursions to similar levels as in animal reports. Nevertheless, their progress as a viable medicinal target for hyperlipidemia and the MetS suffered an abrupt downfall due to severe gastro-intestinal side effects like vomiting and diarhhea reported during clinical trials (124, 132). Humans are suspected to be more sensitive to DGAT1 inhibition because, unlike murine models, human gut has very low expression of DGAT2 enzyme (133, 134). It is important to note that we observed no diarrheal phenotype in I-DGAT1$^{-/-}$, DGAT1$^{-/-}$ or DGAT1-Inh mice, suggesting species-specific variations in the sensitivity to DGAT1 inhibition. Altered endocrinal factors due to DGAT1 inhibition for example elevated GLP-1 levels might also trigger exaggerated reactions of gastric disturbances in humans compared than mice (132, 144). In addition, other pharmaceutical inhibitors that modulate chylomicron metabolism such as ACAT2 and MTP inhibitors were similarly doomed (163, 164). Thus, we underscore the importance of the intricate balance and interdependancy between incorporation of TG and other neutral lipids into chylomicrons. In accordance, we argue that modulation of this intricate neutral lipid balance due to I-DGAT1 deficiency concomitantly decreases the proportion of other neutral lipids like CE and RE into

chylomicron and thereby decrease the postprandial cargo size (144). Further elucidation and knowledge of this critical phenomenon might pave the way for better tolerable pharmacological inhibitors targeting gut lipid metabolism.

Conclusion

We conclude that deficiency or inhibition of DGAT1 affects cholesterol metabolism in mice due to reduced cholesterol absorption, smaller chylomicron size, and increased TICE as shown in Fig. 26. These effects are likely independent of cholesterol uptake by the intestine but mediated through altered dietary FA metabolism in the intestine (144).

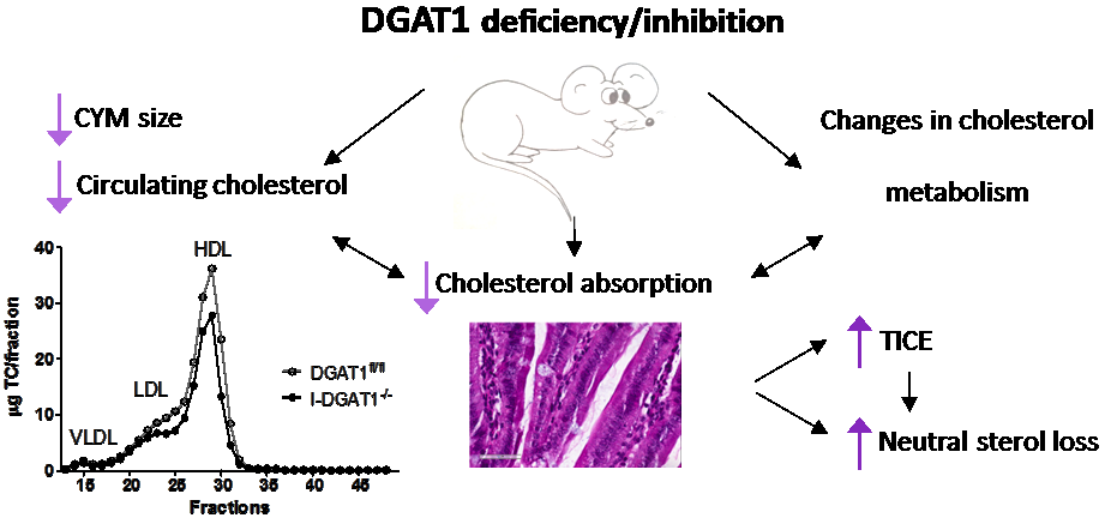

Figure 26: Cartoon depicting the potential mechanism leading to the altered cholesterol homeostasis upon DGAT1 deficiency or inhibition. Deficiency or inhibition of DGAT1 affects cholesterol metabolism in mice due to reduced cholesterol absorption, decreased circulating cholesterol concentrations, smaller chylomicron size, and increased TICE (144). Requisite permission to use this figure was obtained (Appendix).

Chapter II

Contribution of DGATs in maintenance of thermogenesis

1. Introduction

1.1. Role of brown adipose tissue in lipid metabolism

Cardiovascular diseases are a growing epidemic of modern society resulting in large number of morbidities and mortalities world-wide (3). In general, these diseases are the manifestation of various disturbed metabolic parameters which converge to result in major cardiovascular events. Hyperlipidemia is a key factor often associated with insulin resistance, obesity, T2DM and atherosclerosis. As introduced in section 1.1, hyperlipidemia thus is a major contributor to the MetS. Moreover, statins - the choice of drug to reduce LDL-C levels in the setting of acute coronary syndrome – is effective in preventing major cardiovascular event in 10% of population with pre-existing occlusive vascular disease (14, 165). Elevated plasma TG itself is reported as an independent risk factor for cardiac disorders (7). Though fibrates are used in the clinics to reduce hypertriglyceridemia by stimulating increased TG clearance by peripheral organs, the simultaneous reduction of atherogenic lipoproteins has been a challenge (7).

Unlike white adipose tissue (WAT) which stores excessive calories in the form of TGs, brown adipose tissue (BAT) also plays critical towards the energy utilization owing to its multilocular morphological structure, abundant with mitochondria (166) BAT is highly vascularized and innervated by sympathetic nerves, which are activated under the control of beta-adrenergic receptors (β-ARs). These characteristics together make BAT as the major center of non-shivering thermogenesis (NST) regulated by a brown adipocyte-specific protein called uncoupling protein 1 (UCP1) (167). Along with the well-defined depots, brown-like adipocytes are also present in other tissues like WAT and skeletal muscle (SM). These cells known as beige or brite cells are recruited under stimulatory conditions such as sustained cold exposure or through β3-adrenergic receptor (β3-AR) agonists (168). Increasing energy expenditure (EE) by stimulating NST has been the target as an alternate line of treatment for obesity and related MetS components. Stimulating NST can trigger increased utilization of free FAs from the depots of WAT to the more energy consuming tissues such as BAT or beige adipocytes by efficiently redistributing fuels such as glucose and non-esterified FAs away from metabolically critical organs like heart, SM or liver. The overall

improved metabolism might lead to insulin sensitivity and is targeted by pharmacological approaches as summarized in Fig. 27 (169).

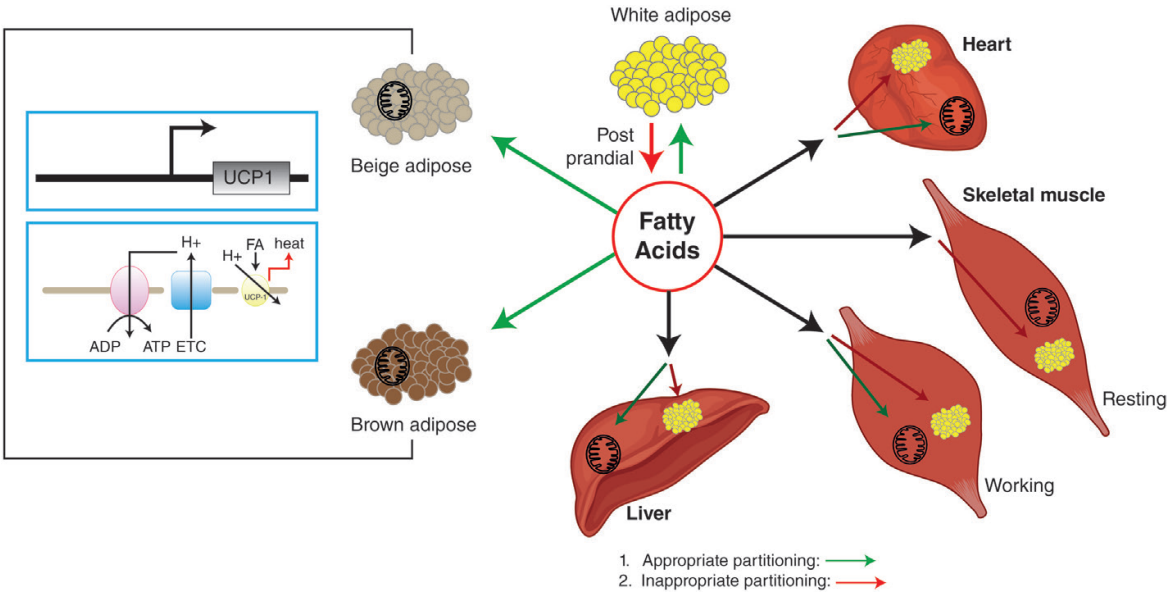

Figure 27: White adipose tissue stores excess energy as triglycerides that can be mobilized by lipolysis to generate FFA for use by other tissues. BAT is the central player in regulating non-shivering thermogenesis, majorly by the action of uncoupling protein 1 (UCP1). Beige adipocytes also possess similar uncoupling capacity like brown adipocytes. These beige adipocytes are usually present on WAT depots and have been a prospective pharmacological target to maintain postprandial energy imbalance. Access peripheral tissue lipid accumulation can be decreased in the metabolically critical organs like liver, skeletal muscles and heart if appropriate partitioning of FAs from WAT (energy storage tissue) into BAT (energy consuming tissue) can be achieved (169). Requisite permission to use this figure was obtained (Appendix).

In rodents and non-human primates, the role of BAT has long been established as a key regulator of non-shivering thermogenesis more importantly during cold exposure (167, 169, 170). Human studies in the early 1970's, however, indicated very small depots of BAT, which was inversely proportional to the age (170). Thus, in adult humans, BAT was considered to be insignificant. The field was lightened with interest in the 1980's, when the imaging reports using stable isotope-labeled glucose in humans revealed substantial amount of active BAT depots around supraclavicular and neck regions (171-174). The interest was further spurred with the findings that glucose and FA uptake were significantly higher in the BAT after cold exposure (172, 175) . Moreover, it was found to be the site of EE and maintenance of non-shivering thermogenesis. Hence, BAT was suggested to be a

therapeutic target for the treatment MetS disorders such as insulin resistance, obesity, and CVDs (166, 174)Activation of BAT in humans by repeated cold-sensitization resulted in elevated BAT activity and an improved metabolic profile (176, 177)

1.1.1 Intravascular processing of TRLs

Lipoprotein transport is a highly regulated process, which is coordinated by a concerted action of transporters and mediators. Disturbances in the lipoprotein regulation results in increased fat accumulation and metabolic imbalance. In addition to intestinal chylomicrons (see section Chapter I, 1.2.3), hepatic VLDL are the major TRLs which transport hydrophobic lipids to peripheral organs for catabolic needs (17). Postprandial chylomicrons are released into the bloodstream via the lymphatic system. During the intra-prandial period, liver-synthesized VLDL particles are expelled in the circulation to be transported to peripheral organs to maintain their nutrient needs. In the bloodstream, these lipoproteins are catabolized predominantly by LPL though hepatic and endothelial lipases also play a minor role (178, 179). LPL bound to heparan sulphate proteoglycans (HSPGs) is present on vascular endothelial cells to facilitate the release of FAs from the circulating lipoproteins. GPI-anchored HDL-binding protein 1 (GPIHBP1) regulates LPL transcytosis from peripheral tissue to the endothelial wall, where it also binds to LPL (180, 181). The transporters internalizing the FAs generated by LPL action on TRLs are still debatable, however, the role of FATPs, CD36, and FABPs are reported to co-ordinate FA uptake into the heart, adipose tissue, liver and muscle (182). Various apoproteins such as APOCII and APOAV, which bind to the TRLs, also enhance LPL-mediated TG hydrolysis, whereas APOCIII and angiopoeitin-like proteins 3 and 4 decrease the LPL activity (183-186). Deficiency of lipase maturation factor 1 in mice led to severely decreased lipase activity since it is an important posttranslational mediator of LPL (187). Humans with lack of function mutations of GPIHBP1, LPL, apoCII and apoAV show severe hypertriglyceridemia, indicating the importance of these proteins in TRL metabolism (188-191).

Once FAs are taken up by peripheral tissues, the resultant atherogenic TRL remnants consist of increased amount of APOE while APOA5, LPL and the dense TG core are still present. These remnants are destined to be taken up by the liver

through APOE binding to the LDL receptor and also partly by binding to LDL receptor-related protein1 (LRP1) (192, 193). Certain factors like HSPGs or syndecan-1 regulate hepatic remnant uptake, however, their deficiencies in mice do not lead pronounced hypertriglyceridemia (194). Thus, they might be essential but not critical for TG remnant metabolism (195). Thus, at normal housing temperature in mouse models, hepatic TRL remnant uptake in mice is the only pathway leading to clearance of remnant particles.

Mice exposed to cold temperatures have increased blood supply to BAT and eventually increased transport of heat from BAT to peripheral organs (167). Injection of dual-radiolabeled TLR-like particles, indicating either TG or the particle core, into cold-exposed mice resulted in a 10-fold increase in releasable and non-releasable label uptake in BAT when compared to mice housed at 22°C (196). These results indicate that apart from hepatocytes and macrophages, BAT also possesses the capacity to take up TRL particles. The authors described that distribution of both labels upon cold exposure was similar in all tissues including liver. Moreover, fasting TG levels and even the postprandial TG peak was also reduced in cold-exposed mice, although lipoprotein production by the intestine or liver remained unchanged. The decrease in plasma TG concentrations was attributed to the increased mobilization of LPL to the luminal side of the BAT to catalyze the increased release and uptake of FAs from circulating lipoproteins as increased expression of LPL and CD36 was observed. The authors proposed two possibilities through which a complete TRL can be taken up by the BAT. The first scenario proposed that sustained cold exposure results in the generation of increased LPL, which interacts with various factors like CD36, caveolin, and HSPGs to internalize whole TRL. This idea is supported by the observation that heparin injection in cold-exposed mice prevents an increased FA uptake by the BAT indicating that TRLs enter as whole particle rather than released FAs. The second possibility involves tissue remodeling, where (similar to liver) the endothelial layer of BAT consists of pores which upon stimulatory or energy-demanding conditions results in uptake of whole particles into the BAT (195). The speculation of holoparticle uptake is interesting from a therapeutic point of view as the triggering of BAT with β-ARs or cold exposure might help in remnant particle clearance, which is presently known to be only under hepatic control. The

difference in TRL uptake during normal housing conditions or at 4°C in mice is summarized in Fig. 28.

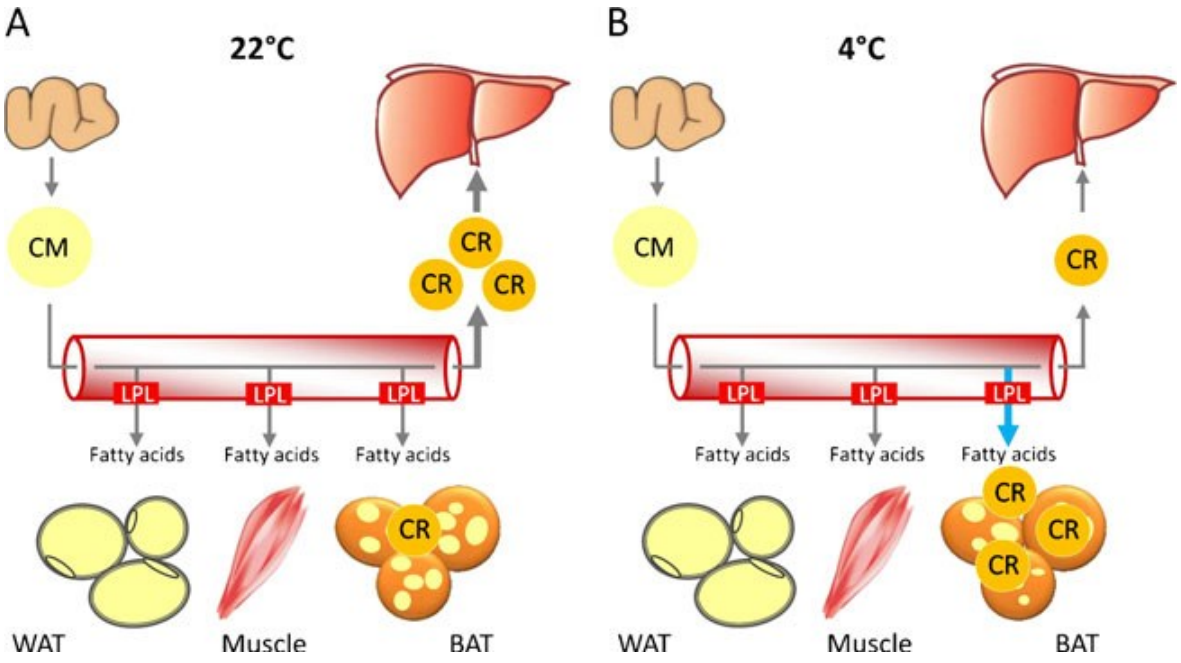

Figure 28: Chylomicron remnant uptake in mice during normal housing conditions and cold exposure. Under normal physiological conditions, the chylomicrons released into the circulation are catabolized by LPL present on the vascular endothelial cells to generate FAs for peripheral tissues like WAT, muscle, and BAT. Chylomicron remnants (CRs) are taken up mainly by the liver. However, at 4°C, the metabolic program is triggered in BAT to take up released FAs and CRs for necessitate for the increased energy demand (195). Requisite permission to use this figure was obtained (Appendix).

The prospect that cold exposure shifts the processing of lipoproteins from the liver to the BAT seems highly fascinating. However, a recent study by Khedoe *et al*, reported that although there was a significant increase in TRL-derived FA uptake by the BAT under cold conditions, the uptake of holoparticles was only slightly increased (197). In addition, injection of ex vivo labeled VLDL particles into mice after β3-AR activation by CL316243 revealed that the liver takes up most of the remnant particles (166). These observations indicate that differences in lipoprotein processing and lipid content might be responsible for the target uptake of lipoproteins by the BAT.

1.1.2 Lipid fuel utilization in brown adipose tissue

Unlike WAT, which stores energy in form of neutral lipids, the metabolically active BAT utilizes glucose and FAs as the major lipid sources to maintain thermoregulation. Studies in humans using positron emission tomography-computed tomography (PET-CT) imaging revealed that BAT glucose uptake under stimulatory conditions like cold exposure is even higher than the uptake by SM through insulin-mediated pathway. In addition, glucose uptake in the BAT increases several folds under cold exposure compared to room temperature with positive correlation of EE (198, 199). Gene expression analysis showed that the glucose transporter GLUT4 was significantly up-regulated in BAT of cold-exposed humans. This finding correlated with murine studies showing increased expression of GLUT1 and GLUT4 in BAT of cold-exposed mice compared to other tissues such as SMs, WAT, and heart (200). These reports clearly indicate the importance of BAT as the metabolic sink crucial for the maintenance of insulin sensitivity.

Glucose taken up by BAT has two known fates: (i) it can either undergo glycolysis which results in ATP generation or (ii) it triggers de novo lipogenesis. Interestingly, glucose in cold-exposed murine BAT is more susceptible to be used for energy-releasing pathways than for de novo lipogenesis (166, 201). However, insulin is not the only mediator of glucose uptake in BAT. Insulin-independent pathways like the hedgehog-pathway are involved in BAT glucose homeostasis. The activation of AMP-activated protein kinase (AMPK) via smoothened proteins, a member of the hedgehog signaling pathway, increases glucose uptake in BAT and SM (202). In addition, thyroid hormone can alter glucose levels in BAT thus regulating thermoregulation. The hormone undergoes structural transformation from the less potent Thyroxine to highly catalytic form (3, 3', 5-triiodothryonine) under the action of deiodinases 1 and 2 (DIO1 and DIO2). Deficiency of either of these enzymes results in decreased lipid generation and hydrolysis in BAT and defective adaptive thermoregulation despite increased UCP1 gene expression (203, 204). $DIO2^{-/-}$ mice fed with high-fat diet also exhibit decreased body weight gain, insulin sensitivity, and energy expenditure (205). Thus, BAT utilizes insulin-dependent and -independent pathways to maintain whole body glucose homeostasis.

FAs, which are cleaved by LPL from circulating lipoproteins, are internalized by BAT due to its metabolic demand. These FAs are first incorporated into lipid droplets by the action of various enzymes like DGATs. This TG pool is further hydrolyzed sequentially by the lipases ATGL, HSL, and MGL to generate FAs, which can be utilized as acetyl-CoA by mitochondria for β-oxidation in the citric acid cycle, which triggers the electron transport chain and activates uncoupling potential of UCP1 to generate heat instead of ATP (166). It is tempting to speculate that internalized FAs from the TRLs can be used for β-oxidation to release heat instead of first converting to TG stores, however, based on the available scientific evidence it is highly unlikely. Global ATGL-/- mice get severely hypothermic at cold temperatures and are unable to maintain their thermoregulation. These mice have increased lipid stores in adipose tissue, nevertheless they exhibit decreased energy expenditure and UCP1 gene expression in BAT (206). Thus, ATGL-dependent TG hydrolysis is an important regulator for thermogenesis potential of BAT, thus preventing any unstipulated oxidation and excess heat generation by BAT.

Lipolysis in the BAT is also triggered by increased norepinephrine stimulation pathway. BAT is a highly innervated tissue with brown adipocytes within close access to the sympathetic nervous system. Thus, the increased release of norepinephrine under stimulatory conditions like increased metabolic demand results in its binding to the β3-AR, which is located at the outer membrane of the brown adipocyte. This cascade activates adenylyl cyclase, which facilitates enhanced catalytic activity of protein kinase A (PKA) via increased production of cyclic AMP (cAMP). The resulting signaling events increase phosphorylation of the enzymes critical for lipolysis like ATGL, HSL, and MGL, thereby increasing the release of FAs pumped into the β-oxidation cycle (166). In addition, the adrenergic stimulated increase in cAMP activates co-activator cAMP response element-binding protein (CREB) leading to increased gene levels of peroxisome proliferator-activated receptor γ coactivator 1α (PGC1α) and UCP1, further fueling β-oxidation (166, 207). The third way, in which activation of PKA fuels thermogenesis, is by enhancing the p38 activity resulting in activation of the mitogen-activated protein kinase (MAPK) pathway, which in turn is positively correlated with increased gene expression of PGC1α and UCP1 (208). The

complex signaling pathway regulating the lipid fuel utilization in the BAT is briefly summarized in Fig. 29.

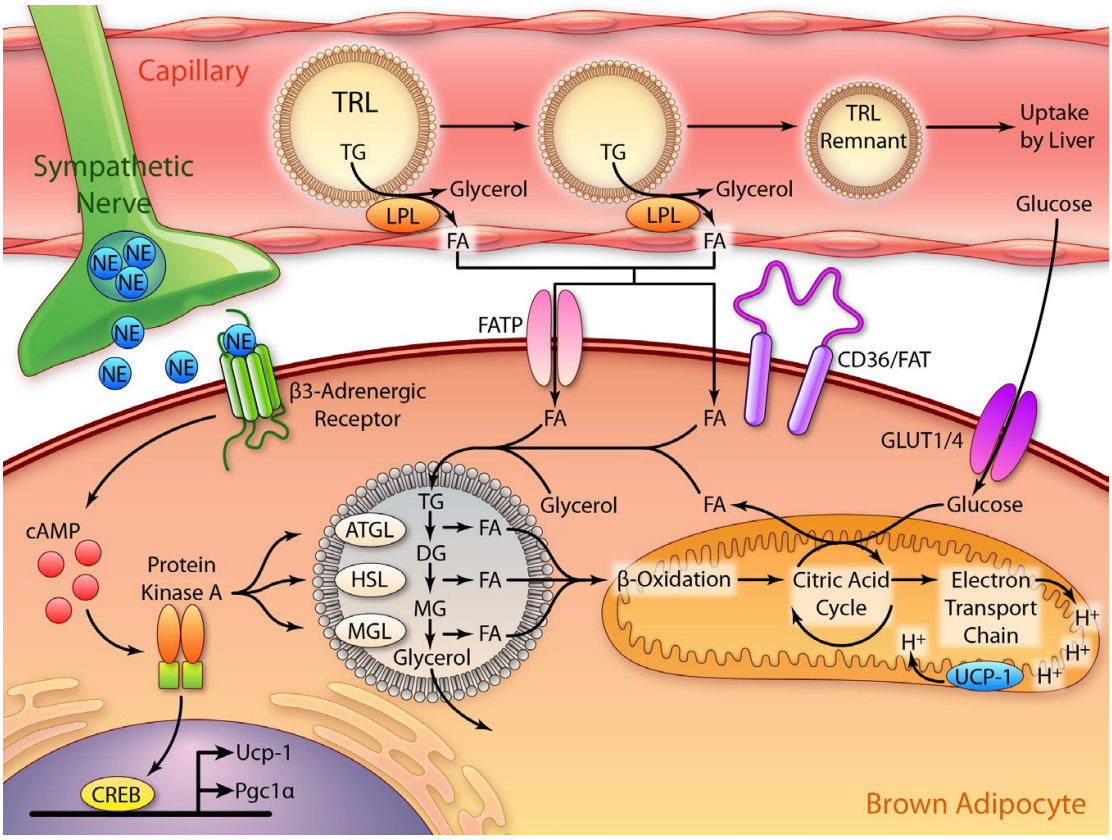

Figure 29: Lipid fuel utilization in activated brown adipose tissue. Under stimulatory conditions like cold exposure, norepinephrine (NE) secreted from the sympathetic nervous system stimulates binding to the β3-adrenergic receptor on brown and brown-like adipocytes. The resultant cascade activates adenylyl cyclase to produce cyclic adenosine monophosphate (cAMP) which can activate protein kinase A (PKA). PKA phosphorylation results in increased activity of cAMP response element-binding protein (CREB) resulting in increased transcription of uncoupling protein-1 (*Ucp-1)* and peroxisome proliferator-activated receptor-gamma co-activator (*Pgc-1*α). In addition, phosphorylation of PKA mediates increased activity of lipolytic enzymes that catabolize intracellular lipid droplets resulting in release of FAs (FA) that act as a fuel for mitochodrial β-oxidation. Acetyl-CoA acts as a substrate for the citric acid cycle where intermediates suffice generation of the electrons to maintain the electron transport chain. UCP-1, a characteristic proton transporter, shifts the reaction from ATP production to an uncoupling reaction resulting in heat production. The continuous flux of FAs into the mitochondria depletes TG stores in the BAT, which are continuously replenished by enhanced uptake of FAs cleaved by LPL-mediated processing of circulating TG-rich lipoproteins (TRLs). The uptake of FAs is facilitated by cluster of differentiation 36 (CD36) and FA transport proteins (FATP) and converted to TGs by several enzymes including diglyceride-acyl transferase (DGAT) enzymes. Furthermore, glucose enters BAT by the action of glucose transporter (GLUT) 1 and 4 and used for, among others, de novo lipogenesis. ATGL, adipose triglyceride lipase; DAG, diacylglycerol; HSL, hormone-sensitive lipase; MAG, monoacylglycerol; MGL, monoglyceride lipase (166). Requisite permission to use this figure was obtained (Appendix).

1.2. Lipogenesis in brown adipose tissue

The substrate utilization in the BAT is largely dependent on the extent of stimulation by either cold exposure or by β3-AR agonist treatment (9). Moreover, the level of contribution of each of the different substrates like circulating glucose, lipids or intracellular TG stores in the overall maintenance of thermogenesis is still debatable (209). It is speculated that FAs taken up in the BAT from circulating lipids or generated via de novo lipogenesis are first esterified within TGs before being hydrolyzed by lipolytic enzymes for heat production in the mitochondria. In addition, BAT is a major site for lipogenesis under non-shivering thermogenic conditions with almost 33% of total lipogenesis being carried out in BAT (210). Smaller chain FAs that contain 16 or less carbon atoms are generated by FA synthase (FAS) and their elongation is carried out by very long-chain FA elongases (ELOVL). ELOVL3 and ELOVL6 are highly expressed in the BAT upon cold stimulation (211, 212). Nevertheless, the newly synthesized FAs are not readily oxidized but are incorporated into the TG pool to be subsequently utilized upon thermogenic stimulation (209). Glucose uptake in BAT also results in synthesis of pyruvate, which can act as substrate for the citric acid cycle. Its contribution to the overall electron transport chain cycle in BAT mitochondria upon cold exposure, however, is minimal (167). Thus, exogenous as well as endogenous FAs are first incorporated into the intracellular TG pool which contributes to the majority of FAs to be fueled for β- oxidation (209).

The only dedicated step in the synthesis of TGs is carried out the by the DGAT enzymes. DGAT1 and DGAT2 are shown to catalyze the final step to convert DG to TG (45). The contribution of these enzymes in maintenance of thermogenesis is predominantly given by the fact that all FAs in BAT are first incorporated into TGs. It is also reported that DGAT enzymes are responsible for nearly all TG synthesis in murine adipocytes (213). However, the extent of the individual contribution of these two enzymes in synthesis of TG in BAT, specifically under cold exposure, is still a matter of debate. It is also still unclear whether under stimulatory conditions, TG synthesized in BAT via one of the two DGAT enzymes is sufficient to maintain whole body thermogenesis.

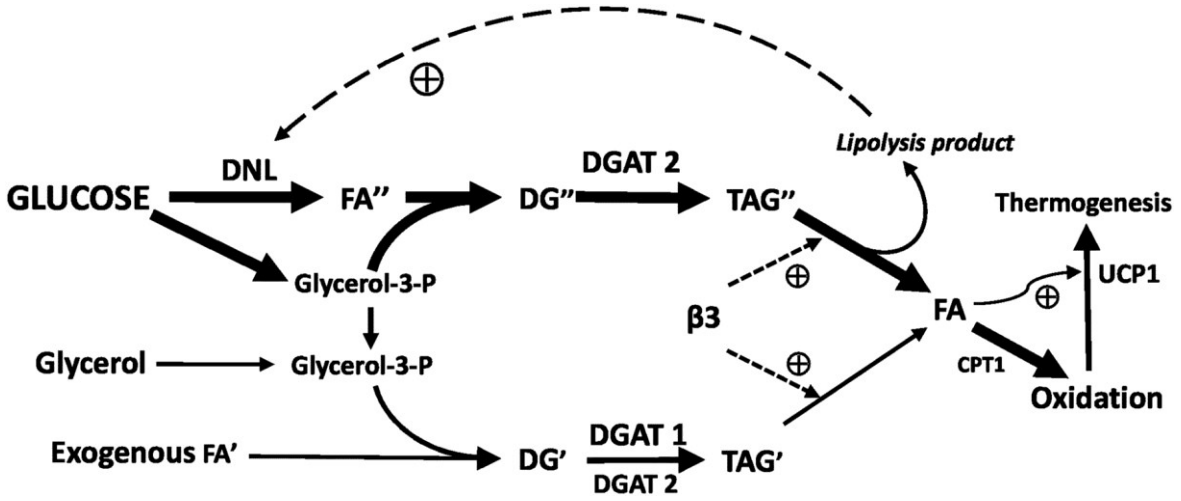

Figure 30: Hypothetical model that links DGAT1 and DGAT2 to adrenergic stimulated thermoregulation in brown adipocytes. Different pools of TG are generated by DGAT1 and DGAT2 where DGAT2 mediated TG'' synthesis prefers endogenous FAs (FA'') derived from glucose and de novo lipogenesis (DNL). DGAT1, on the other hand, utilizes dietary lipids derived from exogenous FAs' to biosynthesize TG'. Under stimulatory conditions such as β3 agonist treatment, FAs released from both TG pools are utilized for oxidation by the action of uncoupling protein-1 (UCP-1) (214). Requisite permission to use this figure was obtained (Appendix).

In ex vivo studies, single deletion of DGAT1 or DGAT2 had a marginal effect on the TG concentrations in murine embryonic fibroblast-derived adipocytes. The dual deletion, however, resulted in nearly absent levels of LDs without affecting adipogenesis, which indicates that either of these enzymes can compensate for TG synthesis and maintain adipocyte number (213). These data are consistent with results that DGAT1$^{-/-}$ mice and pharmacological DGAT2-inhibitor treated mice have unchanged TG concentrations on chow diet (113, 215). Both DGATs are expressed in the BAT of rodents and their expression is increased upon adaptive thermogenesis in rats (113, 209). A recent report suggests that in primary murine adipocytes under adrenergic stimulation DGAT2 prefers endogenous FAs derived after de novo lipogenesis whereas DGAT1 might for important to biosynthesis of TG from the lipoprotein-derived FAs as shown in Fig. 30. The authors also suggest the existence of two different pools of TGs generated by the action of either DGAT1 or DGAT2 (214). It still remains unanswered, whether a similar scenario exists in vivo and whether under extreme thermogenic stimulations like acute and chronic cold exposure either of the two TG pools can sustain thermoregulation.

1.3. Aim of the study

The primary objective of this study was to explore the contribution of DGAT enzymes in the maintenance of thermoregulation upon acute and chronic cold exposure. It is known that circulating lipoproteins like chylomicrons play a significant role towards fuel replenishment in the BAT during high energy demand conditions. However, whether the alterations in the chylomicron metabolism affect BAT regulation is still unclear. Using genetically modified murine models and pharmacological inhibitor/s we investigated the following objectives:

Specific aim 1:

To determine whether reduced circulating cholesterol concentrations and smaller chylomicron size observed in I-DGAT1-/- mice affects thermoregulation upon acute and/or chronic cold exposure.

Specific aim 2:

To determine the extent of the individual contribution of DGAT1 and DGAT2 in the synthesis of TG in BAT specifically under cold exposure.

2. Materials and Methods

2.1 Animals and diets

C57BL/6 mice purchased from Jackson Laboratory (Bar Harbor, ME) were used for all pharmacological inhibition experiments performed in this study. Age-matched female mice between 3-4 months of age were used for all experiments unless indicated otherwise. For the description of I-DGAT1$^{-/-}$ (125) mice, diets used in this study, animal housing conditions, and ethical considerations, please refer to Chapter I, section 2.2.

2.2 Acute and adaptive thermogenesis measurement

Twelve-week old mice were placed in individual cages for 2 weeks and fed either chow diet or HF/HCD. For adaptive thermogenesis measurements, mice were acquainted to 4°C housing temperature for 2 weeks. On the day of the experiment, food was removed at 10 a.m. which was considered as 0 h time point. At indicated time points, core body temperature was recorded with a rectal probe connected to a digital thermometer (BAT-12 Microprobe-Thermometer; Physitemp Instruments, Inc., Clifton, NJ) and blood glucose concentrations were determined using glucometer (AccuCheck-active; Roche Diagnostics, Palo Alto, CA). Thereafter, mice were euthanized and blood and tissues were collected. Cut-off temperature for all thermogenic experiments was set at 30°C and experiment was terminated when average core body temperature of either group of mice reached around 30°C.

2.3 Acute and adaptive thermogenesis measurement upon pharmacological DGATs inhibition

C57BL/6 mice were used for the experiments. The pharmacological DGAT1 inhibitor used in this study is described in Chapter I, section 2.3. DGAT2 inhibitor (PF-06424439) was purchased from Sigma-Aldrich, St. Louis, MO. Inhibitors were dissolved in vehicle (0.5% (w:v) of hydroxypropylmethylcellulose (Sigma-Aldrich, St. Louis, MO) in 0.1% (v:v) Tween 80) before use. The dosage and regimen for the inhibitors treatment was performed based on previous reports (125, 215).

Briefly, mice were fed with HF/HCD for 2 weeks and segregated into three groups: Vehicle, DGAT1-inhibitor treated (DGAT1-Inh) or DGAT1+DGAT2-inhibitor treated (DGAT1/2-Inh) mice. Three days before start of the experiment, DGAT1/2-Inh mice were administered two daily doses of DGAT2 inhibitor (10 mg/kg BW BID, total of five doses) and a single daily dose of DGAT1 inhibitor (5 mg/kg BW). DGAT1-Inh mice group received DGAT1-inhibitor (5 mg/kg BW) once every morning and the remaining two doses consisted of vehicle only. The vehicle mice group received a total of five doses of vehicle only. Acute and adaptive thermogenesis measurements were performed as described above.

2.4 Post-prandial lipoprotein uptake in cold-exposed brown adipose tissue

Dual-radiotracer substrate was prepared by mixing 200 µl corn oil with 1 µCi [^{3}H]triolein, 0.5 µCi [^{14}C]cholesterol and 200 µg FC. Mice were fed HF/HCD for 2 weeks before the start of the experiment. To measure radiotracer uptake in BAT, mice were housed at 4°C, fasted for 4 h, and then gavaged with the substrate. Four hours post gavage, mice were sacrificed, BAT was collected and dissolved in 1 ml of 1M NaOH at 65°C. Radioactive counts were measured by liquid scintillation counting.

2.5 Cell culture, differentiation, lipid staining, and quantification

In vitro experiments were performed as described previously (216). All reagents were purchased from Carl Roth, Karlsruhe, Germany, unless specified otherwise. Briefly, immortalized brown adipogenic cells (iBACs) were grown in DMEM containing 10% FBS, 50 µg/ml streptomycin, 50 units/ml penicillin, and 20 mM HEPES. Cells were induced, considered as day 0, with a mixture of 0.5 mM 3-isobutyl-1-methylxanthine, 0.5 µM dexamethasone, 20 nM insulin, 1 nM triiodthyronine, and 125 µM indomethacin. On day 2, induction medium was replaced with maintenance medium containing 20 nM insulin and 1 nM triiodthyronine, and cells were maintained in this medium until harvest on day 7. To determine the role DGATs on neutral lipid synthesis in fully differentiated cells, iBACs were treated with vehicle (DMSO), DGAT1-Inh (1 µM), DGAT2-Inh (3 µM) or DGAT1/DGAT2-inh from day 7 until day 9, at which point cells were collected,

fixed, rinsed in PBS, and stained with oil red O. Cellular TG content was estimated in iBACs using Infinity Triglyceride Reagent (Life Technologies, Vienna, Austria). Results were normalized to protein concentrations measured using BCA reagent (Pierce, Dayton, UK).

In a separate experiment, cells were treated with either vehicle, DGAT1-Inh, DGAT2-Inh or DGAT1/2-Inh starting on day 0, and then every 48 h until day 7. At the end of the experiment, images were taken with a CCD camera (CoolSNAP-HQ, Roper Scientific Corp., Martinsried, Germany) to estimate the inhibitory effects of DGAT enzymes on iBACs differentiation.

2.6 Blood biochemical analyses

Please refer to Chapter I, section 2.3.

2.7 Western blotting analysis

Western blotting analysis was performed as described in section 2.20. For detection of UCP1 protein, I used anti-UCP1 (1:1000) (Calbiochem, Vienna, Austria) and monoclonal anti-mouse ß-actin (1:5000, Santa Cruz Biotechnology, Heidelberg, Germany as a loading control.

2.8 RNA isolation and quantitative real-time PCR

Real-time PCR analysis was performed as described in section 2.1.3. The primers used for this study are shown in Table 8.

Table 10: Primers for real time PCR

Gene	Forward primer (5`-3`)	Reverse primer (5`-3`)
UCP1	ACTGCCACACCTCCAGTCATT	CTTTGCCTCACTCAGGATTGG
PGC-1A	CCCTGCCATTGTTAAGACC	TGCTGCTGTTCTTGTTTTC
CD36	GCAGGTCTATCTACGCTGTG	GGTTGTCTGGATTCTGGAGG
DIO2	AGAGTGGAGGCGCATGCT	GGCATCTAGGAGGAAGCTGTTC
LPL	ACATTCCCGTTACCGTCCATC	GGACCCCTGAAGACACAG
PPAR-G	CTGTCCACACTATGAAGAC	AGGTTCTTCATGAGGCCTGT
PRDM-16	TGCTAAGCCTTCACCGTTCT	GAAGTTGAACGGGTGGTGAG

CIDEA	TGACATTCATGGGATTGCAGAC	CATGGTTTGAAACTCGAAAAGGG
PPAR-A	TTCACAAGTGCCTGTCTGTC	GGCCTTGACCTTGT?CATGT
HSL	GCTGGTGACACTCGCAGAAG	TGGCTGGTGTCTCTGTGTCC
ATGL	GCCACTCACATCTACGGAGC	GACAGCCACGGATGGTCTTC
MGL	CGGACTTCCAAGTTTTTGTCAGA	GCAGCCACTAGGATGGAGATG
CPT-1B	TTCAACACTACACGCATCCC	GCCCTCATAGAGCCAGACC

3. Results

3.1 UCP1 expression is reduced in brown adipose tissue of 16 h fasted I-DGAT1$^{-/-}$ mice

We observed reduced circulating cholesterol concentrations and smaller chylomicron size in I-DGAT1$^{-/-}$ mice. Therefore, we questioned whether altered lipid metabolism in I-DGAT1$^{-/-}$ mice affects thermogenesis. First, we measured the regulation of thermogenic genes in BAT of 16 h fasted I-DGAT1$^{-/-}$ and control mice. mRNA expression of UCP1, a master regulator of mitochondrial uncoupling in BAT (29), was significantly downregulated in I-DGAT1$^{-/-}$ mice by 70% compared to DGAT1$^{fl/fl}$ mice (Fig. 31A). Reduction in UCP1 was in line with down-regulation of other thermogenic and lipolytic genes (Fig. 31A). Moreover, protein expression of UCP1 was also decreased in BAT of I-DGAT1$^{-/-}$ mice (Fig. 31B, C). These results indicate that I-DGAT1-/- affects fasting thermogenesis in mice, at least in part, by decreasing mitochondrial uncoupling via UCP1 expression in BAT.

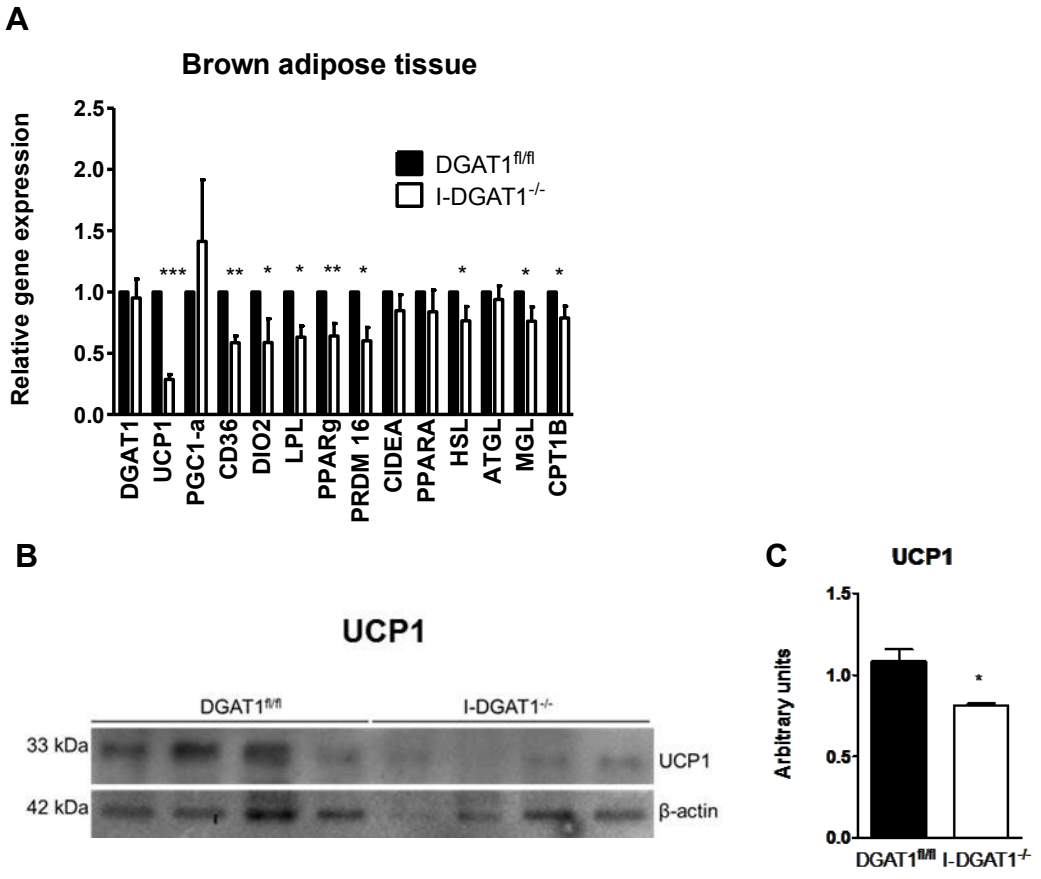

Figure 31: I-DGAT1-/- reduces expression of genes involved in mitochondrial uncoupling in brown adipose tissue of 16 h-fasted mice. Mice (n=4) were fasted for 16 h. **(A)** mRNA expression of thermogenic genes in brown adipose tissue (BAT). **(B)** BAT lysates were separated by SDS-PAGE and UCP1 protein expression was analyzed by western blotting. The expression of β-actin served as loading control. (C) Quantification of UCP1 protein expression. Values represent mean + SEM. $^{*}p<0.05$, $^{**}p<0.01$, $^{***}p<0.001$, Student's t-test.

3.2 Comparable acute thermogenesis in chow diet-fed I-DGAT1$^{-/-}$ mice

Next, we measured whether acute thermogenesis upon cold exposure is altered in I-DGAT1$^{-/-}$ mice. We exposed chow diet-fed DGAT1$^{fl/fl}$ and I-DGAT1$^{-/-}$ mice to 4°C with *ad libitum* excess to food and water. We observed comparable thermogenesis between the two groups tested as indicated by unchanged body temperature (Fig. 32A) and body weight (Fig. 32B).

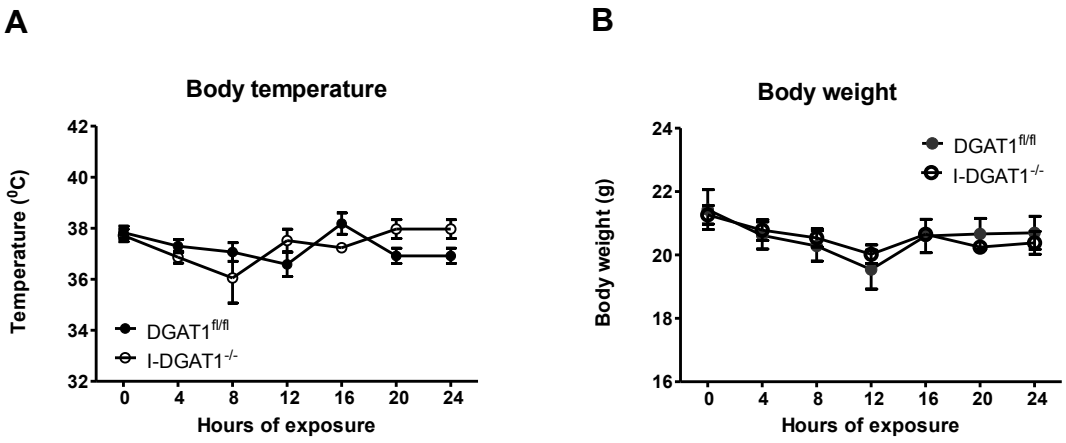

Figure 32: Unchanged acute thermogenesis in I-DGAT1$^{-/-}$ mice. Mice (n=6) were exposed to 4°C with ad libitum excess to food and water. **(A)** Body temperature and **(B)** body weights of mice over a period of 24 h during exposure. Values represent mean + SEM.

As we observed reduced UCP1 expression in I-DGAT1$^{-/-}$ mice under fasted condition, we determined whether acute thermogenesis in I-DGAT1$^{-/-}$ mice is altered upon nutrient starvation. Chow diet-fed DGAT1$^{fl/fl}$ and I-DGAT1$^{-/-}$ mice were exposed to 4°C without access to food. Unlike under cold exposure with *ad libitum* excess to food, I-DGAT1$^{-/-}$ mice under starvation were unable to sustain their body temperature and body weight for more than 6h after cold exposure. However, these results were phenocopied also in controls (Fig. 33A, B).

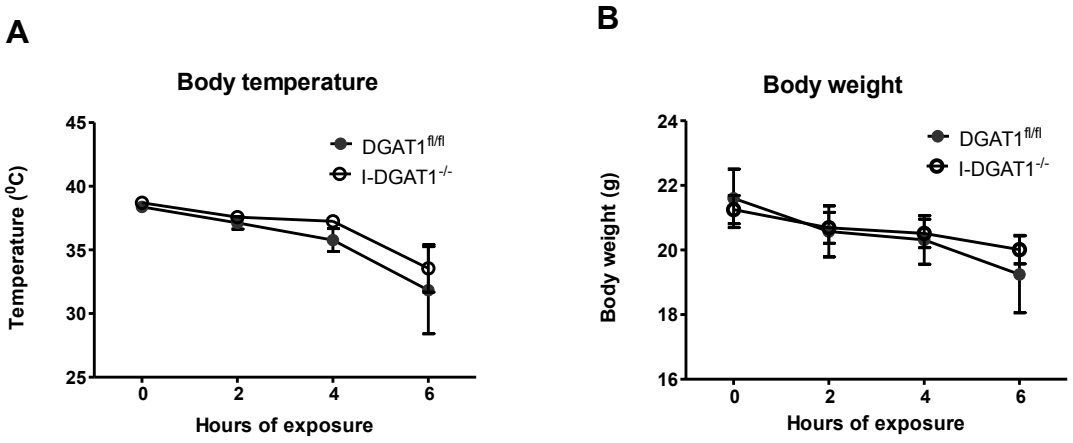

Figure 33: Comparable acute thermogenesis in I-DGAT1$^{-/-}$ and DGAT1$^{fl/fl}$ mice under nutrient-starved condition. Mice (n=4) were exposed to 4°C under nutrient-starved condition, **(A)** body temperature and **(B)** body weights of mice over period for 6h after exposure. Values represent mean + SEM.

3.3 HF/HCD-fed I-DGAT1$^{-/-}$ mice have exhibit improved acute thermogenesis

Since I-DGAT1$^{-/-}$ mice demonstrated the strongest reduction in circulating cholesterol levels after being challenged with dietary fat and cholesterol (Fig. 12A), we measured acute thermogenesis in HF/HCD-fed I-DGAT1$^{-/-}$ and DGAT1$^{fl/fl}$ mice under nutrient-starved condition. We observed that I-DGAT1$^{-/-}$ mice could sustain higher core body temperature compared to DGAT1$^{fl/fl}$ mice (Fig. 34A). This result was particularly surprising as reduced UCP1 expression was observed in 16 h-fasted I-DGAT1$^{-/-}$ mice (Fig. 31A, B) and cold exposure is a higher energy demanding scenario than fasting. Increased mobilization of FAs from adipose lipid stores or enhanced glucose uptake could explain better thermogenic profile in I-DGAT1$^{-/-}$ mice. We believe latter to be more likely as we observed comparable reduction of body weight between two groups (Fig. 34B). Blood glucose concentrations were reduced in I-DGAT1$^{-/-}$ compared to DGAT1$^{fl/fl}$ mice (Fig. 34C) which hinted to the possibility that I-DGAT1$^{-/-}$ mice could better mobilize blood glucose to maintain body heat during cold exposure.

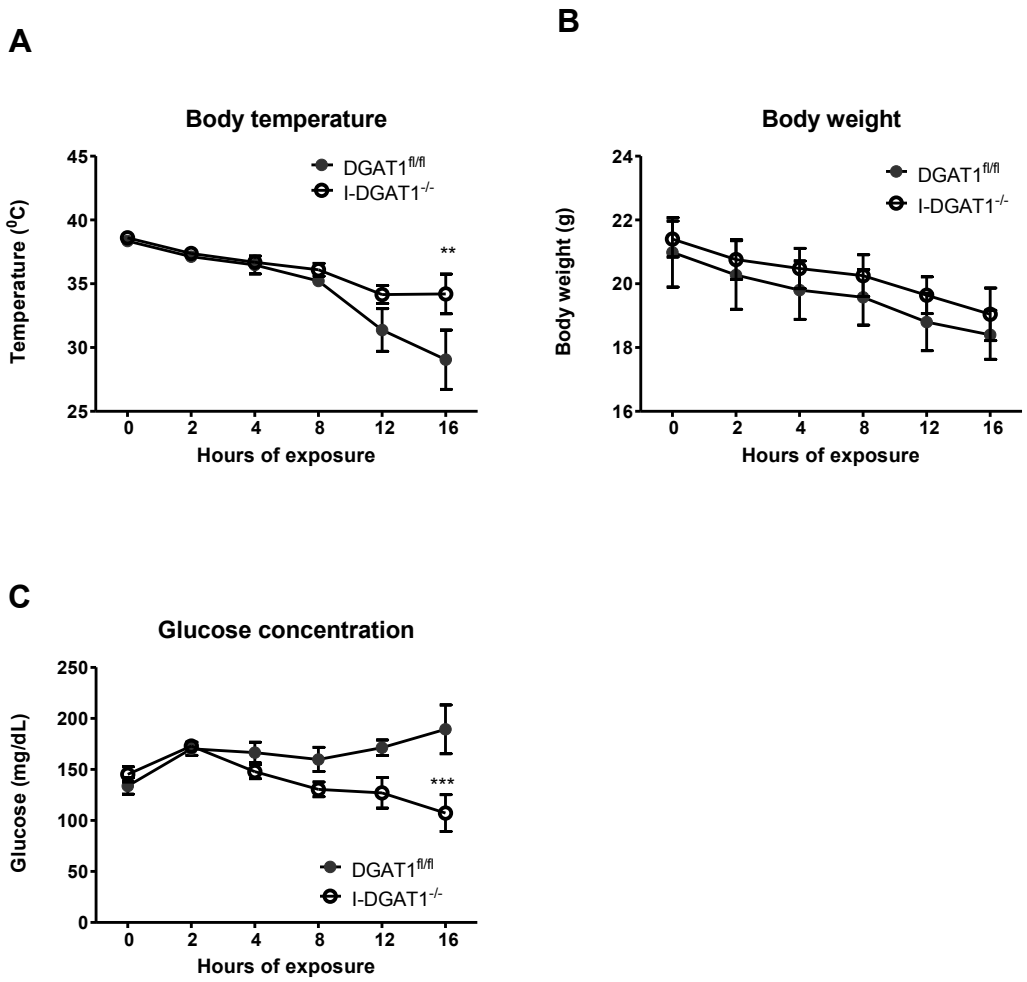

Figure 34: Improved acute thermogenesis in HF/HCD-fed I-DGAT1$^{-/-}$. Mice (n=4-5) were fed with HF/HCD for 8 weeks and exposed to 4°C under nutrient-starved condition. **(A)** Body temperature, **(B)** body weights and **(C)** blood glucose concentrations were measured over the course of the experiment. Values represent mean + SEM. 2-way ANOVA followed by Bonferroni post-test; $^{**}p<0.01$, $^{***}p<0.001$.

3.4 HF/HCD-fed I-DGAT1$^{-/-}$ mice have increased chylomicron uptake upon cold exposure

BAT under exposure has been reported to mediate uptake of FAs derived via classical LPL-mediated lipolysis of circulating lipoproteins or via 'holoparticle' uptake of circulating TRLs (196). We have observed smaller chylomicron particles in HF/HCD-fed I-DGAT1$^{-/-}$ mice (Fig. 16). Therefore, to determine postprandial lipid uptake in BAT, DGAT1$^{fl/fl}$ and I-DGAT1$^{-/-}$ (HF/HCD-fed) mice were treated with P-407 to inhibit peripheral lipolysis. Then, we gavaged the mice with [^{3}H]triolein and [^{14}C]cholesterol and measured radiotracer counts in BAT. Indeed, the counts of

[^{3}H] and [^{14}C], indicative of newly formed chylomicrons, were found to be considerably higher in I-DGAT1$^{-/-}$ mice (Fig. 35). This result indicates that I-DGAT1-/- results in better mobilization of nutrient lipids in BAT upon cold exposure probably via increased whole particle chylomicron uptake in BAT of I-DGAT1$^{-/-}$ mice.

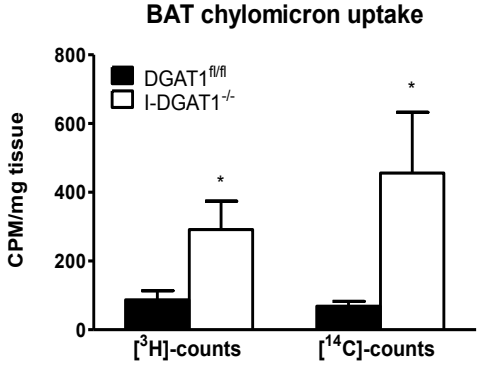

Figure 35: Increased chylomicron uptake in HF/HCD-fed I-DGAT1$^{-/-}$ mice compared to DGAT1$^{fl/fl}$ mice. Mice (n=4-5) were fed with HF/HCD for 4 weeks, exposed to 4°C and treated with P-407 before gavaging 200 µl corn oil containing 1 µCi [^{3}H]triolein, 0.5 µCi [^{14}C]cholesterol, and 200 µg cholesterol. [^{3}H]triolein- and [^{14}C]cholesterol-derived counts in BAT were determined by liquid scintillation counting. Values represent mean + SEM. Student's t-test. *p<0.05.

3.5 HF/HCD-fed I-DGAT1$^{-/-}$ mice have unaltered adaptive thermogenesis

During acute thermogenesis, mice are able to maintain body temperature via heat generated through shivering as well as BAT-mediated thermogenesis. During adaptive thermogenesis, mice completely rely on BAT-mediated mitochondrial uncoupling to maintain their body temperature (167). Thus, we determined whether I-DGAT1-/- in mice affects adaptive thermogenesis. Mice were fed with HF/HCD and adapted to 4°C housing temperature for 2 weeks to maximize their thermogenic potential before being challenged by nutrient starvation. We observed comparable body temperature (Fig. 36A) and body weight reduction (Fig. 36B) between DGAT1$^{fl/fl}$ and I-DGAT1$^{-/-}$ mice throughout the period of cold exposure. These results suggest that although I-DGAT1$^{-/-}$ mice have an improved metabolic profile during acute thermogenesis, over the period of prolonged cold exposure, both control and I-DGAT1$^{-/-}$ mice adapt similarly to maintain core body temperature.

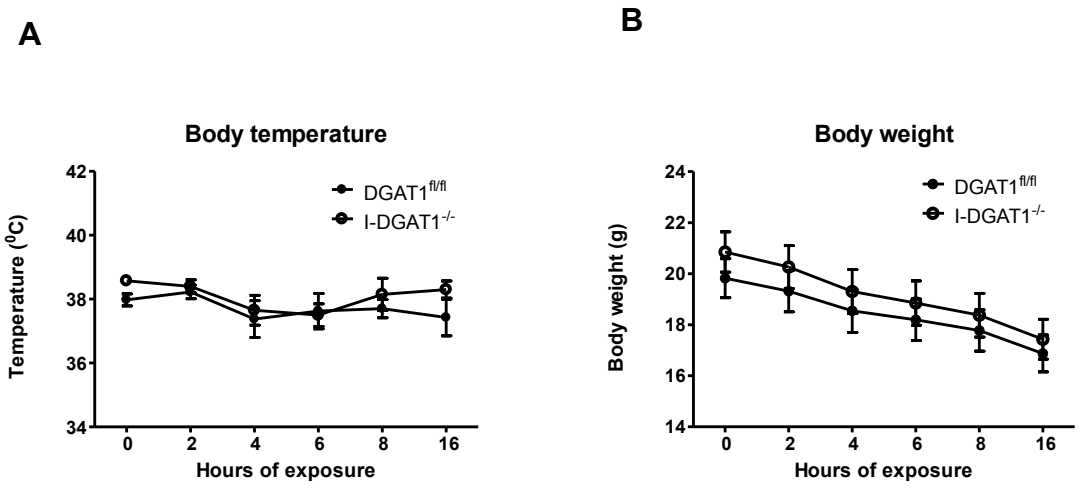

Figure 36: Comparable adaptive thermogenesis in HF/HCD-fed I-DGAT1$^{-/-}$ and DGAT1$^{fl/fl}$ mice. Mice (n=4) were fed with HF/HCD and adapted to 4°C temperature for 2 weeks before being challenged with cold exposure under nutrient starvation. **(A)** Body temperature and **(B)** body weights were measured during the course of nutrient starvation at 4°C. Values represent mean + SEM. 2-way ANOVA followed by Bonferroni post-test.

3.6 Pharmacological-DGAT1 inhibition in mice does not affect adaptive thermogenesis

Global DGAT1 deficiency/inhibition in mice results in pleiotropic effects including improved insulin and leptin sensitivity and increased energy expenditure (20). We next evaluated whether whole body DGAT1 is critical for maintaining adaptive thermogenesis. Therefore, we measured adaptive thermogenesis in C57BL/6 mice fed with HF/HCD supplemented with either vehicle or pharmacological DGAT1-inhibitor. They were adapted to 4°C housing temperature for 2 weeks after which food was removed to evaluate the thermogenic capacity of BAT to maintain body temperature. Nevertheless, adaptive thermogenesis was comparable between vehicle and DGAT1-inh mice. Body temperature (Fig. 37A) and body weight reduction (Fig. 37B) was similar between both groups. Together, the results clarify that intestinal or whole body DGAT1 does not play a predominant role in murine adaptive thermogenesis.

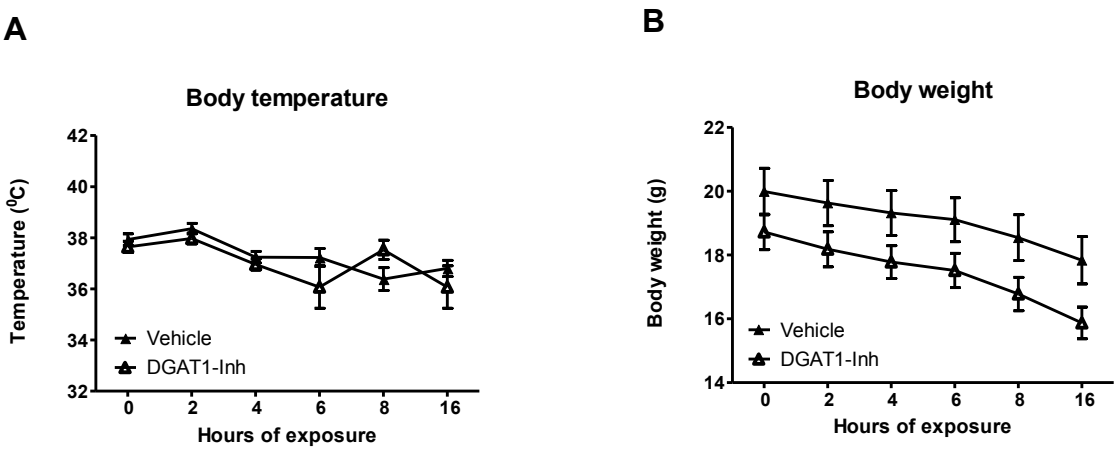

Figure 37: Unchanged adaptive thermogenesis in HF/HCD-fed DGAT1-Inh mice compared to vehicle mice. Mice (n=5-6) were fed with HF/HCD and adapted to 4°C housing temperature for 2 weeks after which they were challenged by nutrient starvation under cold exposure. **(A)** Body temperature and **(B)** body weights were measured during nutrient starvation at 4°C housing temperature. Values represent mean + SEM. 2-way ANOVA followed by Bonferroni post-test.

3.7 DGAT enzymes are quintessential for acute and adaptive thermogenesis in mice

It is tempting to speculate that the FAs taken up by BAT after LPL-mediated lipolysis of TRLs or those generated via de novo lipogenesis are directly utilized for oxidation without first being incorporated into the TG pool. DGAT enzymes catalyze the only dedicated step in TG biosynthesis (45). Since we did not observe significant changes in thermogenic potential upon DGAT1 inhibition, we determined whether dual-DGAT (DGAT1 and DGAT2) inhibition abolishes thermogenesis upon cold exposure. To evaluate this possibility, first we measured acute thermogenesis upon dual-DGAT1 and DGAT2 inhibition (DGAT1/2-Inh) in HF/HCD-fed mice and compared them to vehicle-treated and DGAT1-Inh mice. As shown in Fig. 38A, DGAT1/2-Inh mice exhibited decrease in body temperature as early as 2 h after cold exposure and were severely hypothermic after 4 h at 4°C. Decreased body temperature coincided with attenuated plasma TG, TC, FC, and CE concentrations in DGAT1/2-Inh mice (Fig. 38B).

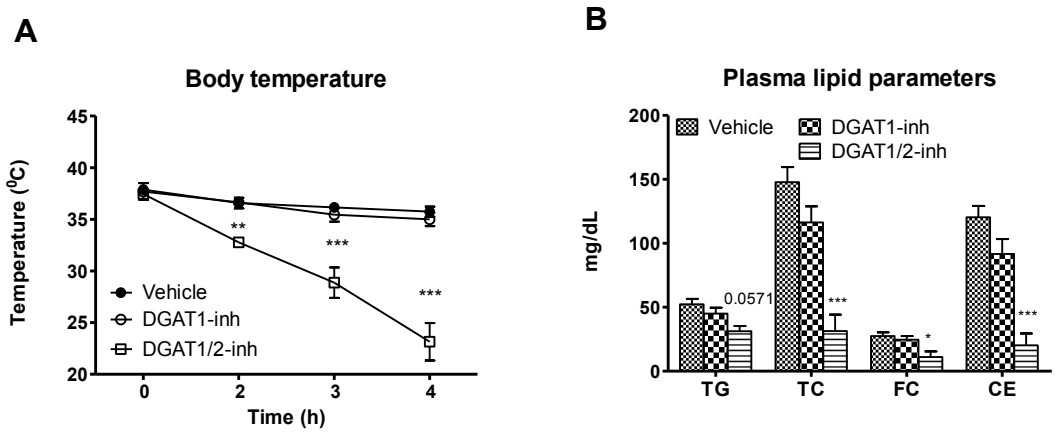

Figure 38: Reduced acute thermogenesis in HF/HCD-fed DGAT1/2-Inh mice. HF/HCD-fed mice (n=4) were treated with either vehicle, DGAT1-Inh or DGAT1/2-Inh. **(A)** Body temperature and **(B)** plasma parameters were measured during nutrient starvation at 4°C. Values represent mean + SEM. A: 2-way ANOVA followed by Bonferroni post-test; B: Student's t-test. *p<0.05, **p<0.01, ***p<0.001.

Next, we measured adaptive thermogenesis in these mice by initiating the vehicle or pharmacological DGAT inhibition treatment after adapting HF/HCD-fed mice to 4°C housing temperature for 2 weeks. DGAT1/2-Inh mice started losing core body temperature after 8 h of nutrient starvation and were severely hypothermic after 16 h, whereas body temperature was unchanged in vehicle-treated or DGAT1-Inh mice (Fig. 39A). As observed during acute thermogenesis measurements, plasma lipid parameters were significantly reduced in DGAT1/2-Inh mice compared to vehicle mice (Fig 39B). These results strongly elucidate that re-esterification of TGs in mice is quintessential to maintain thermogenesis upon cold exposure and that DGAT2 is able to compensate for reduced TG synthesis due to DGAT1 inhibition in mice.

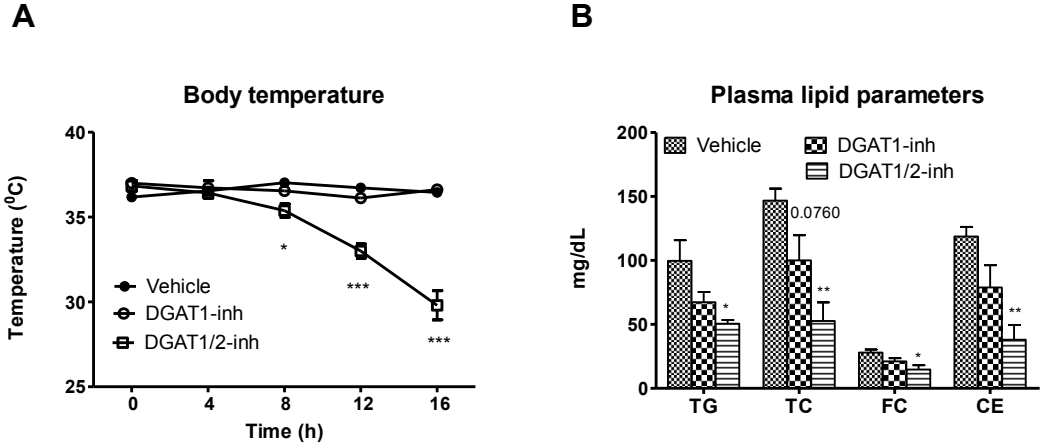

Figure 39: Reduced adaptive thermogenesis in HF/HCD-fed DGAT1/2-Inh mice. HF/HCD-fed mice (n=4) were adapted to 4°C housing temperature for 2 weeks and treated with either vehicle, DGAT1-Inh or DGAT1/2-Inh. **(A)** Body temperature and **(B)** plasma parameters were measured during nutrient starvation at 4°C housing temperature. Values represent mean + SEM. A: 2-way ANOVA followed by Bonferroni post-test; B: Student's t-test. *p<0.05, **p<0.01, ***p<0.001.

3.8 DGAT1/2 inhibition reduces adipocyte differentiation capacity and neutral lipid content of iBACs

To further assess the contribution of DGATs to biogenesis of BAT, we first measured the differentiation capacity of iBACS, an immortalized brown adipogenic cell line, iBACs, after pharmacological inhibition of DGAT1, DGAT2 or a combination of both inhibitors. We observed that dual-inhibition of DGAT1 and DGAT2 severely impaired the differentiation capacity of iBACs as early as 2 days after initiation of the treatment, whereas the differentiation capacity was only slightly reduced by individual inhibition of DGAT1 and largely unchanged by inhibition of DGAT2 (Fig 40). At the day 7 of the treatment, adipocyte differentiation was reduced by 90% in DGAT1/2-Inh-treated cells compared to vehicle. The data suggesting that the presence of a single DGAT enzyme can compensate to maintain sufficient adipocyte differentiation are in line with a previously published report of unchanged MEF-derived adipocytes differentiation after single deletion of DGAT1 or DGAT2 (ref). However, the same report suggests comparable MEF-derived adipocytes differentiation after dual-deletion of DGAT enzymes (ref), which is contradicting to our results observed in iBACs.

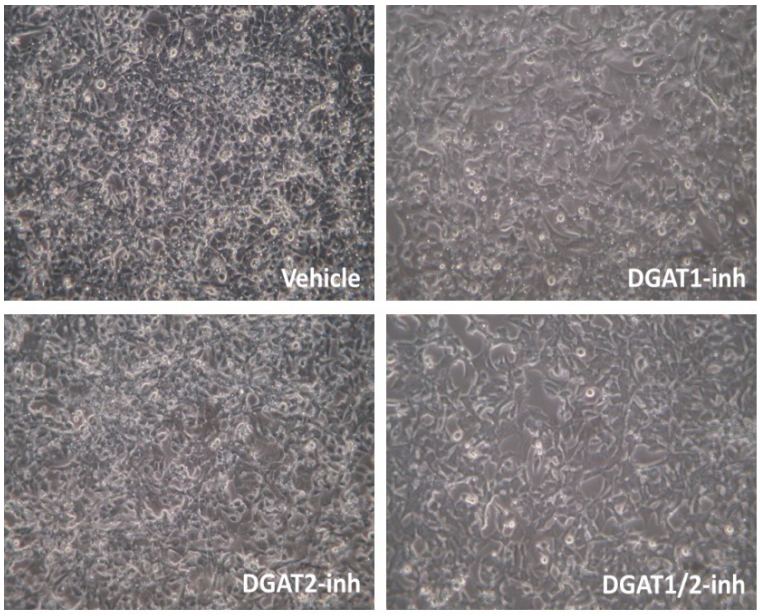

Figure 40: DGAT1/2-inhibition severely impairs iBACs differentiation. iBACs were cultured and at day 0 of differentiation, cells were treated with either vehicle, 1 μM DGAT1-Inh, 3 μM DGAT2-Inh or combination of both. Images indicate day 2 of differentiation after initiation of the treatment. Magnification, 200x.

Next, we measured the contribution of DGATs to neutral lipid synthesis in fully differentiated iBACs. In a separate set of experiments, differentiated iBACs were treated either with vehicle, DGAT1-Inh, DGAT2-Inh or DGAT1/2-Inh for two days followed by ORO staining. As shown in Fig 45A and B, neutral lipid synthesis and cellular TG content was considerably lower in DGAT1/2-Inh-treated iBACs compared to vehicle-treated controls. Surprisingly, neutral lipid content was also significantly reduced in DGAT1-Inh treated iBACs but remained unchanged in DGAT2-Inh treated iBACs (Fig. 41A, B). Together, these data partially explain the findings obtained after *in vivo* pharmacological inhibition of DGAT1 and dual-inhibition of DGAT1 and DGAT2 indicating that complete but not partial reduction of neutral lipid synthesis in BAT results in defective thermogenesis in mice upon cold exposure.

A

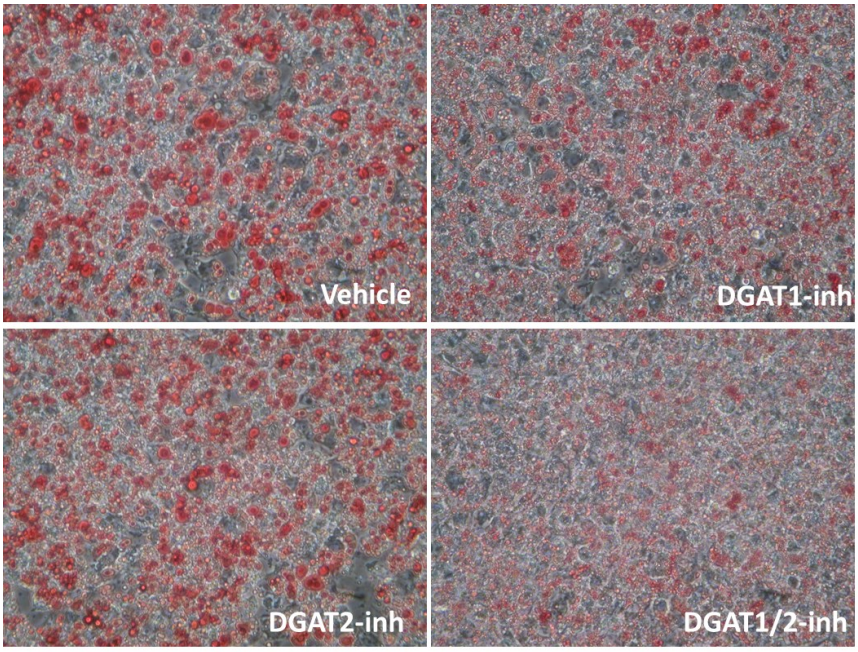

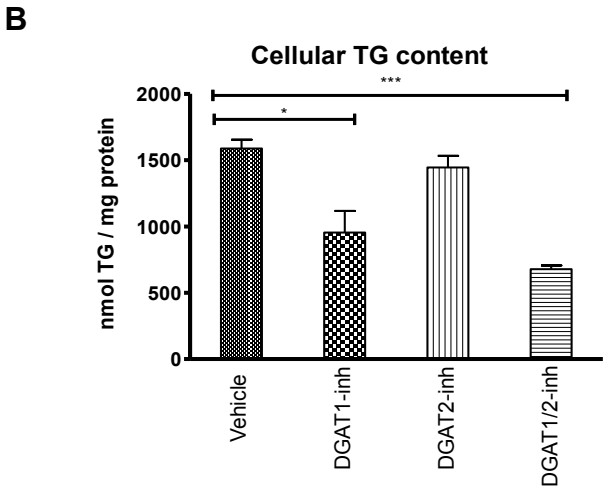

Figure 41: DGAT1/2-inhibition severely impairs neutral lipid synthesis in iBACs. Differentiated iBACs were treated with either vehicle, 1 µM DGAT1 (DGAT1-Inh), 3 µM DGAT2 (DGAT2-Inh) or a combination of both DGAT inhibitors (DGAT1/2-Inh). (A) Representative images of ORO stainings of cells at day 2 of treatment. Magnification, 400x; (B) Cellular TG content was measured spectrophotometrically (n=3). Values represent mean + SEM. B: Student's t-test. *$p<0.05$ and ***$p<0.001$.

4. Discussion

Obesity is a result of constantly imbalanced energy supply and expenditure. It is commonly associated with impaired glucose, lipid and lipoprotein metabolism ultimately resulting in the development of metabolic diseases (195). Whereas white fat stores excess energy in the form of TG, BAT oxidizes lipids and glucose and dissipates the energy as heat (166). Thus, TG metabolism in BAT could play a role in obesity considering its potential to tilt the energy balance from storage to expenditure. Here we report that *in vivo* dual-inhibition of DGAT1/DGAT2 severely impairs the thermogenic capacity of BAT and DGAT enzymes are quintessential in maintaining TG synthesis in BAT.

Harris *et al.* have previously described that adipocytes derived from DGAT1/DGAT2-double knockout MEFs, though lacking LDs, were able to differentiate (213). However, in our study, DGAT1/2-treated iBACs could not maintain their differentiation potential beyond day 2 of induction. The discrepancy can be explained due to the difference of induction media used in the two studies. In the former study, isolated cells were induced to differentiate into WAT-like adipocytes whereas in our study, iBACS were targeted to be differentiated into brown adipocytes. It is likely that due to higher mitochondrial content, iBACs have increased TG substrate requirement and thus fail to differentiate in the absence of TG synthesis due to DGAT1/2 inhibition. Our *in vitro* results ascertained that DGAT1 and DGAT2 are able to compensate for each other to maintain cellular TG synthesis. This finding is in agreement with *in vivo* observations where, DGAT1-Inh and I-DGAT1$^{-/-}$ mice exhibited comparable adaptive thermogenesis upon cold exposure.

Upon BAT activation, intracellular lipolysis depletes intracellular TG stores that subsequently need to be replenished via de novo lipogenesis and the uptake of FAs from the circulation. Chylomicrons and VLDL, upon catabolism by LPL, aid the replenishment of FAs for TG synthesis in BAT (195). However, whether altered lipoprotein metabolism affects BAT thermogenesis is still underexplored. We observed increased uptake of chylomicron-derived lipids in the BAT of cold exposed I-DGAT1-/- mice. We posit that smaller chylomicron-sized particles are

cleared faster from the circulation compared to large chylomicrons due to an inverse correlation between size of lipoprotein and surface area available for LPL to cleave TRLs (157). The precise mechanism/s via by which BAT acquires FAs from TRL derived FA from the plasma upon LPL-mediated lipolysis, via holoparticle uptake of TRL, or a combination of both is a matter of debate (166). In an elegant study, Bartelt *et al.* have shown an increased uptake of lipoprotein particles, which were double-labeled with nonreleasable core lipid, [^{3}H]-cholesterol ethers and [^{14}C]-triolein in the BAT of cold-exposed mice (196). The authors proposed the theory of holoparticle uptake by BAT of mice to maintain thermogenesis upon cold exposure and speculated that this was a consequence of remodeling of the endothelial permeability. Our results of increased triolein and cholesterol-derived counts in BAT and improved acute thermogenesis in I-DGAT1-/- mice further strengthen the possibility of holoparticle uptake in BAT and, in addition, indicate that smaller holoparticles are more efficiently taken up by BAT. However, when Khedoe *et al.* injected TRL-like particles into cold-exposed mice, they observed a rather selective increase in uptake of TG by BAT, whereas the uptake of holoparticles was only minimally increased (197). The discrepancy was attributed to difference in particle size, the methodology of particle preparation, and classes of surface apolipoproteins present on particles used in these two studies (166). In our point of view, future studies designed to compare thermogenesis in mouse models known to have altered TRL size and composition might help to better characterize the phenomenon of holoparticle uptake in BAT, for example in multidrug resistance protein 2-/- mice or in essential FA-deficient mice (102, 217)

We observed improved acute thermogenesis in HF/HCD-fed I-DGAT1$^{-/-}$ mice but adaptive thermogenesis was comparable between DGAT1$^{fl/fl}$ and I-DGAT1$^{-/-}$ mice. A plausible explanation is that the improved metabolic profile in I-DGAT1$^{-/-}$ mice might aid them to better adapt to acute challenges of energy demand by increasing the mobilization of glucose away from circulation to the BAT for heat generation. This mobilization is more critical during acute cold exposure, where shivering and non-shivering thermogenesis contribute in synergy to maintain thermoregulation (167). It is likely that once BAT takes over adaptive thermogenesis, the lipid mobilization might not be that important and thus both

DGAT1$^{fl/fl}$ and I-DGAT1$^{-/-}$ mice exhibited comparable core body temperature and body weight reduction.

It might be argued that TRL-derived FA in BAT, instead of first being incorporated into intracellular TG rich-lipid droplets, can directly be utilized for mitochondrial β-oxidation via UCP1-mediated thermogenesis, especially during high energy demand conditions like cold exposure. As we observed blunted acute as well as adaptive thermogenesis in DGAT1/2-Inh mice, it is likely that DGAT-mediated TG synthesis in BAT is essential for maintaining oxidation and UCP-1 activation. These results are in line with previous report where diminished intracellular lipolysis in ATGL$^{-/-}$ and adipose-specific ATGL$^{-/-}$ mice led to defective thermogenesis (218, 219) . In addition, by inhibiting intracellular lipolysis using nicotinic acid injections in rats, Labbé *et al*. have recently demonstrated that the intracellular TG pools predominantly contribute to acute as well as adaptive thermogenesis (209). Collectively, these results show that internalized FAs are first esterified into TGs, upon which intracellular lipolysis liberates FAs for mitochondrial β-oxidation. Thus DGAT enzymes are major mediators of BAT centric thermoregulation.

Conclusion

Our present study confirms that TG biosynthesis is a critical check-point for BAT-mediated non-shivering thermogenesis and that DGAT enzymes play a predominant role in maintaining thermoregulation. Furthermore, intracellular TG stores, glucose and de novo lipogenesis help to sustain non-shivering thermogenesis only for a limited amount of time. For sufficient adaptive thermogenesis a constant replenishment of TG biosynthesis is fundamental.

References

1. Ford ES. The metabolic syndrome and mortality from cardiovascular disease and all-causes: findings from the National Health and Nutrition Examination Survey II Mortality Study. Atherosclerosis. 2004 Apr;173(2):309-14. PubMed PMID: 15064107.

2. Alberti KG, Zimmet PZ. Definition, diagnosis and classification of diabetes mellitus and its complications. Part 1: diagnosis and classification of diabetes mellitus provisional report of a WHO consultation. Diabet Med. 1998 Jul;15(7):539-53. PubMed PMID: 9686693.

3. Srikanthan K, Feyh A, Visweshwar H, Shapiro JI, Sodhi K. Systematic Review of Metabolic Syndrome Biomarkers: A Panel for Early Detection, Management, and Risk Stratification in the West Virginian Population. Int J Med Sci. 2016;13(1):25-38. PubMed PMID: 26816492. Pubmed Central PMCID: PMC4716817.

4. Bhandari R, Kelley GA, Hartley TA, Rockett IR. Metabolic syndrome is associated with increased breast cancer risk: a systematic review with meta-analysis. Int J Breast Cancer. 2014;2014:189384. PubMed PMID: 25653879. Pubmed Central PMCID: PMC4295135.

5. Grundy SM, Brewer HB, Jr., Cleeman JI, Smith SC, Jr., Lenfant C, American Heart A, et al. Definition of metabolic syndrome: Report of the National Heart, Lung, and Blood Institute/American Heart Association conference on scientific issues related to definition. Circulation. 2004 Jan 27;109(3):433-8. PubMed PMID: 14744958.

6. Dash S, Xiao C, Morgantini C, Lewis GF. New Insights into the Regulation of Chylomicron Production. Annu Rev Nutr. 2015;35:265-94. PubMed PMID: 25974693.

7. Do R, Willer CJ, Schmidt EM, Sengupta S, Gao C, Peloso GM, et al. Common variants associated with plasma triglycerides and risk for coronary artery disease. Nat Genet. 2013 Nov;45(11):1345-52. PubMed PMID: 24097064. Pubmed Central PMCID: PMC3904346.

8. Therond P. Catabolism of lipoproteins and metabolic syndrome. Curr Opin Clin Nutr Metab Care. 2009 Jul;12(4):366-71. PubMed PMID: 19474714.

9. Eckel RH, Grundy SM, Zimmet PZ. The metabolic syndrome. Lancet. 2005 Apr 16-22;365(9468):1415-28. PubMed PMID: 15836891.

10. Shulman GI. Ectopic fat in insulin resistance, dyslipidemia, and cardiometabolic disease. N Engl J Med. 2014 Sep 18;371(12):1131-41. PubMed PMID: 25229917.

11. Han TS, Lean ME. A clinical perspective of obesity, metabolic syndrome and cardiovascular disease. JRSM Cardiovasc Dis. 2016 Jan-Dec;5:2048004016633371. PubMed PMID: 26998259. Pubmed Central PMCID: PMC4780070.

12. Tsatsoulis A, Mantzaris MD, Bellou S, Andrikoula M. Insulin resistance: an adaptive mechanism becomes maladaptive in the current environment - an evolutionary perspective. Metabolism. 2013 May;62(5):622-33. PubMed PMID: 23260798.

13. Appel LJ, Brands MW, Daniels SR, Karanja N, Elmer PJ, Sacks FM, et al. Dietary approaches to prevent and treat hypertension: a scientific statement from the American Heart Association. Hypertension. 2006 Feb;47(2):296-308. PubMed PMID: 16434724.

14. Kaur J. A comprehensive review on metabolic syndrome. Cardiology research and practice. 2014;2014:943162. PubMed PMID: 24711954. Pubmed Central PMCID: 3966331.

15. Israili ZH, Lyoussi B, Hernandez-Hernandez R, Velasco M. Metabolic syndrome: treatment of hypertensive patients. American journal of therapeutics. 2007 Jul-Aug;14(4):386-402. PubMed PMID: 17667215.

16. Ostadal P. Statins as first-line therapy for acute coronary syndrome? Experimental and clinical cardiology. 2012 Winter;17(4):227-36. PubMed PMID: 23592942. Pubmed Central PMCID: 3627281.

17. Williams KJ. Molecular processes that handle -- and mishandle -- dietary lipids. J Clin Invest. 2008 Oct;118(10):3247-59. PubMed PMID: 18830418. Pubmed Central PMCID: PMC2556568.

18. Shiau YF, Boyle JT, Umstetter C, Koldovsky O. Apical distribution of fatty acid esterification capacity along the villus-crypt unit of rat jejunum. Gastroenterology. 1980 Jul;79(1):47-53. PubMed PMID: 7380223.

19. Swaminathan R, King RF, Holmfield J, Siwek RA, Baker M, Wales JK. Thermic effect of feeding carbohydrate, fat, protein and mixed meal in lean and obese subjects. Am J Clin Nutr. 1985 Aug;42(2):177-81. PubMed PMID: 4025189.

20. Yen CL, Nelson DW, Yen MI. Intestinal triacylglycerol synthesis in fat absorption and systemic energy metabolism. J Lipid Res. 2015 Mar;56(3):489-501. PubMed PMID: 25231105. Pubmed Central PMCID: PMC4340298.

21. Niot I, Poirier H, Tran TT, Besnard P. Intestinal absorption of long-chain fatty acids: evidence and uncertainties. Prog Lipid Res. 2009 Mar;48(2):101-15. PubMed PMID: 19280719.

22. Grevengoed TJ, Klett EL, Coleman RA. Acyl-CoA metabolism and partitioning. Annu Rev Nutr. 2014;34:1-30. PubMed PMID: 24819326.

23. Shim J, Moulson CL, Newberry EP, Lin MH, Xie Y, Kennedy SM, et al. Fatty acid transport protein 4 is dispensable for intestinal lipid absorption in mice. J Lipid Res. 2009 Mar;50(3):491-500. PubMed PMID: 18843142. Pubmed Central PMCID: PMC2638106.

24. Pepino MY, Kuda O, Samovski D, Abumrad NA. Structure-function of CD36 and importance of fatty acid signal transduction in fat metabolism. Annu Rev Nutr. 2014;34:281-303. PubMed PMID: 24850384. Pubmed Central PMCID: PMC4329921.

25. Nassir F, Wilson B, Han X, Gross RW, Abumrad NA. CD36 is important for fatty acid and cholesterol uptake by the proximal but not distal intestine. J Biol Chem. 2007 Jul 06;282(27):19493-501. PubMed PMID: 17507371.

26. Xu S, Jay A, Brunaldi K, Huang N, Hamilton JA. CD36 enhances fatty acid uptake by increasing the rate of intracellular esterification but not transport across the plasma membrane. Biochemistry. 2013 Oct 15;52(41):7254-61. PubMed PMID: 24090054.

27. Masuda D, Hirano K, Oku H, Sandoval JC, Kawase R, Yuasa-Kawase M, et al. Chylomicron remnants are increased in the postprandial state in CD36 deficiency. J Lipid Res. 2009 May;50(5):999-1011. PubMed PMID: 18753675. Pubmed Central PMCID: PMC2666186.

28. Sundaresan S, Shahid R, Riehl TE, Chandra R, Nassir F, Stenson WF, et al. CD36-dependent signaling mediates fatty acid-induced gut release of secretin and cholecystokinin. FASEB J. 2013 Mar;27(3):1191-202. PubMed PMID: 23233532. Pubmed Central PMCID: PMC3574291.

29. Pan X, Hussain MM. Gut triglyceride production. Biochim Biophys Acta. 2012 May;1821(5):727-35. PubMed PMID: 21989069. Pubmed Central PMCID: PMC3319358.

30. Ring A, Le Lay S, Pohl J, Verkade P, Stremmel W. Caveolin-1 is required for fatty acid translocase (FAT/CD36) localization and function at the plasma membrane of mouse embryonic fibroblasts. Biochim Biophys Acta. 2006 Apr;1761(4):416-23. PubMed PMID: 16702023.

31. Siddiqi S, Sheth A, Patel F, Barnes M, Mansbach CM, 2nd. Intestinal caveolin-1 is important for dietary fatty acid absorption. Biochim Biophys Acta. 2013 Aug;1831(8):1311-21. PubMed PMID: 23665238. Pubmed Central PMCID: PMC3751415.

32. Stremmel W, Lotz G, Strohmeyer G, Berk PD. Identification, isolation, and partial characterization of a fatty acid binding protein from rat jejunal microvillous membranes. J Clin Invest. 1985 Mar;75(3):1068-76. PubMed PMID: 3884664. Pubmed Central PMCID: 423666.

33. Berk PD, Wada H, Horio Y, Potter BJ, Sorrentino D, Zhou SL, et al. Plasma membrane fatty acid-binding protein and mitochondrial glutamic-oxaloacetic

transaminase of rat liver are related. Proc Natl Acad Sci U S A. 1990 May;87(9):3484-8. PubMed PMID: 2185471. Pubmed Central PMCID: 53925.

34. Stump DD, Zhou SL, Berk PD. Comparison of plasma membrane FABP and mitochondrial isoform of aspartate aminotransferase from rat liver. Am J Physiol. 1993 Nov;265(5 Pt 1):G894-902. PubMed PMID: 8238519.

35. Storch J, Corsico B. The emerging functions and mechanisms of mammalian fatty acid-binding proteins. Annu Rev Nutr. 2008;28:73-95. PubMed PMID: 18435590.

36. Storch J, McDermott L. Structural and functional analysis of fatty acid-binding proteins. J Lipid Res. 2009 Apr;50 Suppl:S126-31. PubMed PMID: 19017610. Pubmed Central PMCID: 2674722.

37. Agren JJ, Valve R, Vidgren H, Laakso M, Uusitupa M. Postprandial lipemic response is modified by the polymorphism at codon 54 of the fatty acid-binding protein 2 gene. Arteriosclerosis, thrombosis, and vascular biology. 1998 Oct;18(10):1606-10. PubMed PMID: 9763533.

38. Baier LJ, Sacchettini JC, Knowler WC, Eads J, Paolisso G, Tataranni PA, et al. An amino acid substitution in the human intestinal fatty acid binding protein is associated with increased fatty acid binding, increased fat oxidation, and insulin resistance. J Clin Invest. 1995 Mar;95(3):1281-7. PubMed PMID: 7883976. Pubmed Central PMCID: 441467.

39. Hegele RA, Harris SB, Hanley AJ, Sadikian S, Connelly PW, Zinman B. Genetic variation of intestinal fatty acid-binding protein associated with variation in body mass in aboriginal Canadians. The Journal of clinical endocrinology and metabolism. 1996 Dec;81(12):4334-7. PubMed PMID: 8954037.

40. Gajda AM, Zhou YX, Agellon LB, Fried SK, Kodukula S, Fortson W, et al. Direct comparison of mice null for liver or intestinal fatty acid-binding proteins reveals highly divergent phenotypic responses to high fat feeding. J Biol Chem. 2013 Oct 18;288(42):30330-44. PubMed PMID: 23990461. Pubmed Central PMCID: PMC3798498.

41. Neeli I, Siddiqi SA, Siddiqi S, Mahan J, Lagakos WS, Binas B, et al. Liver fatty acid-binding protein initiates budding of pre-chylomicron transport vesicles from intestinal endoplasmic reticulum. J Biol Chem. 2007 Jun 22;282(25):17974-84. PubMed PMID: 17449472.

42. Vassileva G, Huwyler L, Poirier K, Agellon LB, Toth MJ. The intestinal fatty acid binding protein is not essential for dietary fat absorption in mice. FASEB J. 2000 Oct;14(13):2040-6. PubMed PMID: 11023988.

43. Newberry EP, Xie Y, Kennedy S, Han X, Buhman KK, Luo J, et al. Decreased hepatic triglyceride accumulation and altered fatty acid uptake in mice with deletion of the liver fatty acid-binding protein gene. J Biol Chem. 2003 Dec 19;278(51):51664-72. PubMed PMID: 14534295.

44. Meller N, Morgan ME, Wong WP, Altemus JB, Sehayek E. Targeting of Acyl-CoA synthetase 5 decreases jejunal fatty acid activation with no effect on dietary long-chain fatty acid absorption. Lipids Health Dis. 2013 Jun 14;12:88. PubMed PMID: 23767941. Pubmed Central PMCID: PMC3699395.

45. Yen CL, Stone SJ, Koliwad S, Harris C, Farese RV, Jr. Thematic review series: glycerolipids. DGAT enzymes and triacylglycerol biosynthesis. J Lipid Res. 2008 Nov;49(11):2283-301. PubMed PMID: 18757836. Pubmed Central PMCID: PMC3837458.

46. Ellis JM, Frahm JL, Li LO, Coleman RA. Acyl-coenzyme A synthetases in metabolic control. Curr Opin Lipidol. 2010 Jun;21(3):212-7. PubMed PMID: 20480548. Pubmed Central PMCID: PMC4040134.

47. Coleman RA, Lewin TM, Van Horn CG, Gonzalez-Baro MR. Do long-chain acyl-CoA synthetases regulate fatty acid entry into synthetic versus degradative pathways? J Nutr. 2002 Aug;132(8):2123-6. PubMed PMID: 12163649.

48. Johnston JM, Rao GA. Intestinal absorption of fat. Protoplasma. 1967;63(1):40-4. PubMed PMID: 6037223.

49. Innis SM. Dietary triacylglycerol structure and its role in infant nutrition. Adv Nutr. 2011 May;2(3):275-83. PubMed PMID: 22332059. Pubmed Central PMCID: PMC3090172.

50. Davis HR, Jr., Tershakovec AM, Tomassini JE, Musliner T. Intestinal sterol transporters and cholesterol absorption inhibition. Curr Opin Lipidol. 2011 Dec;22(6):467-78. PubMed PMID: 22101558.

51. Wang LJ, Song BL. Niemann-Pick C1-Like 1 and cholesterol uptake. Biochim Biophys Acta. 2012 Jul;1821(7):964-72. PubMed PMID: 22480541.

52. Li PS, Fu ZY, Zhang YY, Zhang JH, Xu CQ, Ma YT, et al. The clathrin adaptor Numb regulates intestinal cholesterol absorption through dynamic interaction with NPC1L1. Nat Med. 2014 Jan;20(1):80-6. PubMed PMID: 24336247.

53. Altmann SW, Davis HR, Jr., Zhu LJ, Yao X, Hoos LM, Tetzloff G, et al. Niemann-Pick C1 Like 1 protein is critical for intestinal cholesterol absorption. Science. 2004 Feb 20;303(5661):1201-4. PubMed PMID: 14976318.

54. Berge KE, Tian H, Graf GA, Yu L, Grishin NV, Schultz J, et al. Accumulation of dietary cholesterol in sitosterolemia caused by mutations in adjacent ABC transporters. Science. 2000 Dec 01;290(5497):1771-5. PubMed PMID: 11099417.

55. Hazard SE, Patel SB. Sterolins ABCG5 and ABCG8: regulators of whole body dietary sterols. Pflugers Archiv : European journal of physiology. 2007 Feb;453(5):745-52. PubMed PMID: 16440216. Pubmed Central PMCID: 1785388.

56. Lee MH, Lu K, Hazard S, Yu H, Shulenin S, Hidaka H, et al. Identification of a gene, ABCG5, important in the regulation of dietary cholesterol absorption. Nat Genet. 2001 Jan;27(1):79-83. PubMed PMID: 11138003. Pubmed Central PMCID: PMC1350991.

57. Lu K, Lee MH, Hazard S, Brooks-Wilson A, Hidaka H, Kojima H, et al. Two genes that map to the STSL locus cause sitosterolemia: genomic structure and spectrum of mutations involving sterolin-1 and sterolin-2, encoded by ABCG5 and ABCG8, respectively. American journal of human genetics. 2001 Aug;69(2):278-90. PubMed PMID: 11452359. Pubmed Central PMCID: 1201544.

58. Yu L, Hammer RE, Li-Hawkins J, Von Bergmann K, Lutjohann D, Cohen JC, et al. Disruption of Abcg5 and Abcg8 in mice reveals their crucial role in biliary

cholesterol secretion. Proc Natl Acad Sci U S A. 2002 Dec 10;99(25):16237-42. PubMed PMID: 12444248. Pubmed Central PMCID: PMC138595.

59. Plosch T, Bloks VW, Terasawa Y, Berdy S, Siegler K, Van Der Sluijs F, et al. Sitosterolemia in ABC-transporter G5-deficient mice is aggravated on activation of the liver-X receptor. Gastroenterology. 2004 Jan;126(1):290-300. PubMed PMID: 14699507.

60. Klett EL, Lu K, Kosters A, Vink E, Lee MH, Altenburg M, et al. A mouse model of sitosterolemia: absence of Abcg8/sterolin-2 results in failure to secrete biliary cholesterol. BMC Med. 2004 Mar 24;2:5. PubMed PMID: 15040800. Pubmed Central PMCID: PMC394351.

61. Bietrix F, Yan D, Nauze M, Rolland C, Bertrand-Michel J, Comera C, et al. Accelerated lipid absorption in mice overexpressing intestinal SR-BI. J Biol Chem. 2006 Mar 17;281(11):7214-9. PubMed PMID: 16421100. Pubmed Central PMCID: PMC2034750.

62. Cai L, Eckhardt ER, Shi W, Zhao Z, Nasser M, de Villiers WJ, et al. Scavenger receptor class B type I reduces cholesterol absorption in cultured enterocyte CaCo-2 cells. J Lipid Res. 2004 Feb;45(2):253-62. PubMed PMID: 14617739.

63. Mardones P, Quinones V, Amigo L, Moreno M, Miquel JF, Schwarz M, et al. Hepatic cholesterol and bile acid metabolism and intestinal cholesterol absorption in scavenger receptor class B type I-deficient mice. J Lipid Res. 2001 Feb;42(2):170-80. PubMed PMID: 11181745.

64. Wang DQ, Carey MC. Susceptibility to murine cholesterol gallstone formation is not affected by partial disruption of the HDL receptor SR-BI. Biochim Biophys Acta. 2002 Jul 11;1583(2):141-50. PubMed PMID: 12117558.

65. Agellon LB, Toth MJ, Thomson AB. Intracellular lipid binding proteins of the small intestine. Mol Cell Biochem. 2002 Oct;239(1-2):79-82. PubMed PMID: 12479571.

66. van Bennekum A, Werder M, Thuahnai ST, Han CH, Duong P, Williams DL, et al. Class B scavenger receptor-mediated intestinal absorption of dietary beta-

carotene and cholesterol. Biochemistry. 2005 Mar 22;44(11):4517-25. PubMed PMID: 15766282.

67. Nauli AM, Nassir F, Zheng S, Yang Q, Lo CM, Vonlehmden SB, et al. CD36 is important for chylomicron formation and secretion and may mediate cholesterol uptake in the proximal intestine. Gastroenterology. 2006 Oct;131(4):1197-207. PubMed PMID: 17030189. Pubmed Central PMCID: PMC1994908.

68. Iqbal J, Hussain MM. Evidence for multiple complementary pathways for efficient cholesterol absorption in mice. J Lipid Res. 2005 Jul;46(7):1491-501. PubMed PMID: 15834127.

69. Iqbal J, Anwar K, Hussain MM. Multiple, independently regulated pathways of cholesterol transport across the intestinal epithelial cells. J Biol Chem. 2003 Aug 22;278(34):31610-20. PubMed PMID: 12775725.

70. Repa JJ, Turley SD, Lobaccaro JA, Medina J, Li L, Lustig K, et al. Regulation of absorption and ABC1-mediated efflux of cholesterol by RXR heterodimers. Science. 2000 Sep 01;289(5484):1524-9. PubMed PMID: 10968783.

71. During A, Harrison EH. Mechanisms of provitamin A (carotenoid) and vitamin A (retinol) transport into and out of intestinal Caco-2 cells. J Lipid Res. 2007 Oct;48(10):2283-94. PubMed PMID: 17644776.

72. Iqbal J, Parks JS, Hussain MM. Lipid absorption defects in intestine-specific microsomal triglyceride transfer protein and ATP-binding cassette transporter A1-deficient mice. J Biol Chem. 2013 Oct 18;288(42):30432-44. PubMed PMID: 24019513. Pubmed Central PMCID: PMC3798507.

73. Hussain MM. Intestinal lipid absorption and lipoprotein formation. Curr Opin Lipidol. 2014 Jun;25(3):200-6. PubMed PMID: 24751933. Pubmed Central PMCID: PMC4265799.

74. Brunham LR, Kruit JK, Iqbal J, Fievet C, Timmins JM, Pape TD, et al. Intestinal ABCA1 directly contributes to HDL biogenesis in vivo. J Clin Invest. 2006 Apr;116(4):1052-62. PubMed PMID: 16543947. Pubmed Central PMCID: PMC1401485.

75. Shelness GS, Ledford AS. Evolution and mechanism of apolipoprotein B-containing lipoprotein assembly. Curr Opin Lipidol. 2005 Jun;16(3):325-32. PubMed PMID: 15891394.

76. Chateau D, Pauquai T, Delers F, Rousset M, Chambaz J, Demignot S. Lipid micelles stimulate the secretion of triglyceride-enriched apolipoprotein B48-containing lipoproteins by Caco-2 cells. J Cell Physiol. 2005 Mar;202(3):767-76. PubMed PMID: 15389567.

77. Jiang ZG, Liu Y, Hussain MM, Atkinson D, McKnight CJ. Reconstituting initial events during the assembly of apolipoprotein B-containing lipoproteins in a cell-free system. J Mol Biol. 2008 Nov 28;383(5):1181-94. PubMed PMID: 18804479. Pubmed Central PMCID: PMC2637522.

78. Luchoomun J, Hussain MM. Assembly and secretion of chylomicrons by differentiated Caco-2 cells. Nascent triglycerides and preformed phospholipids are preferentially used for lipoprotein assembly. J Biol Chem. 1999 Jul 09;274(28):19565-72. PubMed PMID: 10391890.

79. Pan X, Munshi MK, Iqbal J, Queiroz J, Sirwi AA, Shah S, et al. Circadian regulation of intestinal lipid absorption by apolipoprotein AIV involves forkhead transcription factors A2 and O1 and microsomal triglyceride transfer protein. J Biol Chem. 2013 Jul 12;288(28):20464-76. PubMed PMID: 23729668. Pubmed Central PMCID: PMC3711312.

80. Mansbach CM, 2nd, Gorelick F. Development and physiological regulation of intestinal lipid absorption. II. Dietary lipid absorption, complex lipid synthesis, and the intracellular packaging and secretion of chylomicrons. Am J Physiol Gastrointest Liver Physiol. 2007 Oct;293(4):G645-50. PubMed PMID: 17627968.

81. Siddiqi SA, Gorelick FS, Mahan JT, Mansbach CM, 2nd. COPII proteins are required for Golgi fusion but not for endoplasmic reticulum budding of the pre-chylomicron transport vesicle. J Cell Sci. 2003 Jan 15;116(Pt 2):415-27. PubMed PMID: 12482926.

82. Black DD. Development and physiological regulation of intestinal lipid absorption. I. Development of intestinal lipid absorption: cellular events in

chylomicron assembly and secretion. Am J Physiol Gastrointest Liver Physiol. 2007 Sep;293(3):G519-24. PubMed PMID: 17495031.

83. Siddiqi S, Saleem U, Abumrad NA, Davidson NO, Storch J, Siddiqi SA, et al. A novel multiprotein complex is required to generate the prechylomicron transport vesicle from intestinal ER. J Lipid Res. 2010 Jul;51(7):1918-28. PubMed PMID: 20237389. Pubmed Central PMCID: PMC2882727.

84. Mansbach CM, Siddiqi SA. The biogenesis of chylomicrons. Annu Rev Physiol. 2010;72:315-33. PubMed PMID: 20148678. Pubmed Central PMCID: PMC4861230.

85. Wong DM, Webb JP, Malinowski PM, Xu E, Macri J, Adeli K. Proteomic profiling of intestinal prechylomicron transport vesicle (PCTV)-associated proteins in an animal model of insulin resistance (94 char). Journal of proteomics. 2010 May 07;73(7):1291-305. PubMed PMID: 20117256.

86. Wong DM, Webb JP, Malinowski PM, Macri J, Adeli K. Proteomic profiling of the prechylomicron transport vesicle involved in the assembly and secretion of apoB-48-containing chylomicrons in the intestinal enterocytes. Proteomics. 2009 Jul;9(14):3698-711. PubMed PMID: 19639588.

87. Siddiqi SA, Mahan J, Siddiqi S, Gorelick FS, Mansbach CM, 2nd. Vesicle-associated membrane protein 7 is expressed in intestinal ER. J Cell Sci. 2006 Mar 01;119(Pt 5):943-50. PubMed PMID: 16495485. Pubmed Central PMCID: PMC2828367.

88. Mangat R, Su J, Scott PG, Russell JC, Vine DF, Proctor SD. Chylomicron and apoB48 metabolism in the JCR:LA corpulent rat, a model for the metabolic syndrome. Biochem Soc Trans. 2007 Jun;35(Pt 3):477-81. PubMed PMID: 17511632.

89. Kumar NS, Mansbach CM, 2nd. Prechylomicron transport vesicle: isolation and partial characterization. Am J Physiol. 1999 Feb;276(2 Pt 1):G378-86. PubMed PMID: 9950811.

90. Nevin P, Koelsch D, Mansbach CM, 2nd. Intestinal triacylglycerol storage pool size changes under differing physiological conditions. J Lipid Res. 1995 Nov;36(11):2405-12. PubMed PMID: 8656078.

91. Thiam AR, Farese RV, Jr., Walther TC. The biophysics and cell biology of lipid droplets. Nat Rev Mol Cell Biol. 2013 Dec;14(12):775-86. PubMed PMID: 24220094. Pubmed Central PMCID: PMC4526153.

92. Wilfling F, Haas JT, Walther TC, Farese RV, Jr. Lipid droplet biogenesis. Curr Opin Cell Biol. 2014 Aug;29:39-45. PubMed PMID: 24736091. Pubmed Central PMCID: PMC4526149.

93. Demignot S, Beilstein F, Morel E. Triglyceride-rich lipoproteins and cytosolic lipid droplets in enterocytes: key players in intestinal physiology and metabolic disorders. Biochimie. 2014 Jan;96:48-55. PubMed PMID: 23871915.

94. Hashemi HF, Goodman JM. The life cycle of lipid droplets. Curr Opin Cell Biol. 2015 Apr;33:119-24. PubMed PMID: 25703629. Pubmed Central PMCID: 4380764.

95. Zechner R, Zimmermann R, Eichmann TO, Kohlwein SD, Haemmerle G, Lass A, et al. FAT SIGNALS--lipases and lipolysis in lipid metabolism and signaling. Cell Metab. 2012 Mar 07;15(3):279-91. PubMed PMID: 22405066. Pubmed Central PMCID: PMC3314979.

96. Zhang LJ, Wang C, Yuan Y, Wang H, Wu J, Liu F, et al. Cideb facilitates the lipidation of chylomicrons in the small intestine. J Lipid Res. 2014 Jul;55(7):1279-87. PubMed PMID: 24831470. Pubmed Central PMCID: PMC4076075.

97. Lambert JE, Parks EJ. Postprandial metabolism of meal triglyceride in humans. Biochim Biophys Acta. 2012 May;1821(5):721-6. PubMed PMID: 22281699. Pubmed Central PMCID: PMC3588585.

98. Lewis GF, Rader DJ. New insights into the regulation of HDL metabolism and reverse cholesterol transport. Circ Res. 2005 Jun 24;96(12):1221-32. PubMed PMID: 15976321.

99. Temel RE, Brown JM. A new framework for reverse cholesterol transport: non-biliary contributions to reverse cholesterol transport. World J Gastroenterol. 2010 Dec 21;16(47):5946-52. PubMed PMID: 21157970. Pubmed Central PMCID: PMC3007104.

100. Jakulj L, van Dijk TH, de Boer JF, Kootte RS, Schonewille M, Paalvast Y, et al. Transintestinal Cholesterol Transport Is Active in Mice and Humans and Controls Ezetimibe-Induced Fecal Neutral Sterol Excretion. Cell Metab. 2016 Dec 13;24(6):783-94. PubMed PMID: 27818259.

101. Temel RE, Tang W, Ma Y, Rudel LL, Willingham MC, Ioannou YA, et al. Hepatic Niemann-Pick C1-like 1 regulates biliary cholesterol concentration and is a target of ezetimibe. J Clin Invest. 2007 Jul;117(7):1968-78. PubMed PMID: 17571164. Pubmed Central PMCID: PMC1888567.

102. Voshol PJ, Havinga R, Wolters H, Ottenhoff R, Princen HM, Oude Elferink RP, et al. Reduced plasma cholesterol and increased fecal sterol loss in multidrug resistance gene 2 P-glycoprotein-deficient mice. Gastroenterology. 1998 May;114(5):1024-34. PubMed PMID: 9558293.

103. Temel RE, Brown JM. A new model of reverse cholesterol transport: enTICEing strategies to stimulate intestinal cholesterol excretion. Trends in pharmacological sciences. 2015 Jul;36(7):440-51. PubMed PMID: 25930707. Pubmed Central PMCID: 4485953.

104. Brown JM, Bell TA, 3rd, Alger HM, Sawyer JK, Smith TL, Kelley K, et al. Targeted depletion of hepatic ACAT2-driven cholesterol esterification reveals a non-biliary route for fecal neutral sterol loss. J Biol Chem. 2008 Apr 18;283(16):10522-34. PubMed PMID: 18281279. Pubmed Central PMCID: 2447638.

105. Le May C, Berger JM, Lespine A, Pillot B, Prieur X, Letessier E, et al. Transintestinal cholesterol excretion is an active metabolic process modulated by PCSK9 and statin involving ABCB1. Arteriosclerosis, thrombosis, and vascular biology. 2013 Jul;33(7):1484-93. PubMed PMID: 23559630.

106. Groen A, Kunne C, Jongsma G, van den Oever K, Mok KS, Petruzzelli M, et al. Abcg5/8 independent biliary cholesterol excretion in Atp8b1-deficient mice. Gastroenterology. 2008 Jun;134(7):2091-100. PubMed PMID: 18466903.

107. Wiersma H, Gatti A, Nijstad N, Oude Elferink RP, Kuipers F, Tietge UJ. Scavenger receptor class B type I mediates biliary cholesterol secretion independent of ATP-binding cassette transporter g5/g8 in mice. Hepatology. 2009 Oct;50(4):1263-72. PubMed PMID: 19637290.

108. Young SG, Cham CM, Pitas RE, Burri BJ, Connolly A, Flynn L, et al. A genetic model for absent chylomicron formation: mice producing apolipoprotein B in the liver, but not in the intestine. J Clin Invest. 1995 Dec;96(6):2932-46. PubMed PMID: 8675665. Pubmed Central PMCID: 186005.

109. Xie Y, Newberry EP, Young SG, Robine S, Hamilton RL, Wong JS, et al. Compensatory increase in hepatic lipogenesis in mice with conditional intestine-specific Mttp deficiency. J Biol Chem. 2006 Feb 17;281(7):4075-86. PubMed PMID: 16354657.

110. Weiss SB, Kennedy EP, Kiyasu JY. The enzymatic synthesis of triglycerides. J Biol Chem. 1960 Jan;235:40-4. PubMed PMID: 13843753.

111. Chang CC, Huh HY, Cadigan KM, Chang TY. Molecular cloning and functional expression of human acyl-coenzyme A:cholesterol acyltransferase cDNA in mutant Chinese hamster ovary cells. J Biol Chem. 1993 Oct 05;268(28):20747-55. PubMed PMID: 8407899.

112. Cases S, Stone SJ, Zhou P, Yen E, Tow B, Lardizabal KD, et al. Cloning of DGAT2, a second mammalian diacylglycerol acyltransferase, and related family members. J Biol Chem. 2001 Oct 19;276(42):38870-6. PubMed PMID: 11481335.

113. Cases S, Smith SJ, Zheng YW, Myers HM, Lear SR, Sande E, et al. Identification of a gene encoding an acyl CoA:diacylglycerol acyltransferase, a key enzyme in triacylglycerol synthesis. Proc Natl Acad Sci U S A. 1998 Oct 27;95(22):13018-23. PubMed PMID: 9789033. Pubmed Central PMCID: PMC23692.

114. D'Aquila T, Hung YH, Carreiro A, Buhman KK. Recent discoveries on absorption of dietary fat: Presence, synthesis, and metabolism of cytoplasmic lipid droplets within enterocytes. Biochim Biophys Acta. 2016 Aug;1861(8 Pt A):730-47. PubMed PMID: 27108063.

115. Grigor MR, Bell RM. Separate monoacylglycerol and diacylglycerol acyltransferases function in intestinal triacylglycerol synthesis. Biochim Biophys Acta. 1982 Sep 14;712(3):464-72. PubMed PMID: 6289909.

116. Shih MY, Kane MA, Zhou P, Yen CL, Streeper RS, Napoli JL, et al. Retinol Esterification by DGAT1 Is Essential for Retinoid Homeostasis in Murine Skin. J Biol Chem. 2009 Feb 13;284(7):4292-9. PubMed PMID: 19028692. Pubmed Central PMCID: 2640966.

117. Stone SJ, Levin MC, Zhou P, Han J, Walther TC, Farese RV, Jr. The endoplasmic reticulum enzyme DGAT2 is found in mitochondria-associated membranes and has a mitochondrial targeting signal that promotes its association with mitochondria. J Biol Chem. 2009 Feb 20;284(8):5352-61. PubMed PMID: 19049983. Pubmed Central PMCID: 2643492.

118. Wilfling F, Wang H, Haas JT, Krahmer N, Gould TJ, Uchida A, et al. Triacylglycerol synthesis enzymes mediate lipid droplet growth by relocalizing from the ER to lipid droplets. Developmental cell. 2013 Feb 25;24(4):384-99. PubMed PMID: 23415954. Pubmed Central PMCID: 3727400.

119. Chen HC, Smith SJ, Tow B, Elias PM, Farese RV, Jr. Leptin modulates the effects of acyl CoA:diacylglycerol acyltransferase deficiency on murine fur and sebaceous glands. J Clin Invest. 2002 Jan;109(2):175-81. PubMed PMID: 11805129. Pubmed Central PMCID: PMC150839.

120. Chen HC, Smith SJ, Ladha Z, Jensen DR, Ferreira LD, Pulawa LK, et al. Increased insulin and leptin sensitivity in mice lacking acyl CoA:diacylglycerol acyltransferase 1. J Clin Invest. 2002 Apr;109(8):1049-55. PubMed PMID: 11956242. Pubmed Central PMCID: PMC150948.

121. Buhman KK, Smith SJ, Stone SJ, Repa JJ, Wong JS, Knapp FF, Jr., et al. DGAT1 is not essential for intestinal triacylglycerol absorption or chylomicron synthesis. J Biol Chem. 2002 Jul 12;277(28):25474-9. PubMed PMID: 11959864.

122. Okawa M, Fujii K, Ohbuchi K, Okumoto M, Aragane K, Sato H, et al. Role of MGAT2 and DGAT1 in the release of gut peptides after triglyceride ingestion. Biochem Biophys Res Commun. 2009 Dec 18;390(3):377-81. PubMed PMID: 19732742.

123. Chandak PG, Obrowsky S, Radovic B, Doddapattar P, Aflaki E, Kratzer A, et al. Lack of acyl-CoA:diacylglycerol acyltransferase 1 reduces intestinal cholesterol absorption and attenuates atherosclerosis in apolipoprotein E knockout mice. Biochim Biophys Acta. 2011 Dec;1811(12):1011-20. PubMed PMID: 21924378. Pubmed Central PMCID: PMC3223411.

124. DeVita RJ, Pinto S. Current status of the research and development of diacylglycerol O-acyltransferase 1 (DGAT1) inhibitors. J Med Chem. 2013 Dec 27;56(24):9820-5. PubMed PMID: 23919406.

125. Ables GP, Yang KJ, Vogel S, Hernandez-Ono A, Yu S, Yuen JJ, et al. Intestinal DGAT1 deficiency reduces postprandial triglyceride and retinyl ester excursions by inhibiting chylomicron secretion and delaying gastric emptying. J Lipid Res. 2012 Nov;53(11):2364-79. PubMed PMID: 22911105. Pubmed Central PMCID: PMC3466005.

126. Cao J, Zhou Y, Peng H, Huang X, Stahler S, Suri V, et al. Targeting Acyl-CoA:diacylglycerol acyltransferase 1 (DGAT1) with small molecule inhibitors for the treatment of metabolic diseases. J Biol Chem. 2011 Dec 02;286(48):41838-51. PubMed PMID: 21990351. Pubmed Central PMCID: PMC3308890.

127. Schober G, Arnold M, Birtles S, Buckett LK, Pacheco-Lopez G, Turnbull AV, et al. Diacylglycerol acyltransferase-1 inhibition enhances intestinal fatty acid oxidation and reduces energy intake in rats. J Lipid Res. 2013 May;54(5):1369-84. PubMed PMID: 23449193. Pubmed Central PMCID: PMC3622331.

128. Dow RL, Li JC, Pence MP, Gibbs EM, LaPerle JL, Litchfield J, et al. Discovery of PF-04620110, a Potent, Selective, and Orally Bioavailable Inhibitor of

DGAT-1. ACS Med Chem Lett. 2011 May 12;2(5):407-12. PubMed PMID: 24900321. Pubmed Central PMCID: PMC4018057.

129. Yamamoto T, Yamaguchi H, Miki H, Kitamura S, Nakada Y, Aicher TD, et al. A novel coenzyme A:diacylglycerol acyltransferase 1 inhibitor stimulates lipid metabolism in muscle and lowers weight in animal models of obesity. Eur J Pharmacol. 2011 Jan 15;650(2-3):663-72. PubMed PMID: 21034741.

130. Zhao G, Souers AJ, Voorbach M, Falls HD, Droz B, Brodjian S, et al. Validation of diacyl glycerolacyltransferase I as a novel target for the treatment of obesity and dyslipidemia using a potent and selective small molecule inhibitor. J Med Chem. 2008 Feb 14;51(3):380-3. PubMed PMID: 18183944.

131. Cheng D, Iqbal J, Devenny J, Chu CH, Chen L, Dong J, et al. Acylation of acylglycerols by acyl coenzyme A:diacylglycerol acyltransferase 1 (DGAT1). Functional importance of DGAT1 in the intestinal fat absorption. J Biol Chem. 2008 Oct 31;283(44):29802-11. PubMed PMID: 18768481. Pubmed Central PMCID: PMC2662058.

132. Denison H, Nilsson C, Lofgren L, Himmelmann A, Martensson G, Knutsson M, et al. Diacylglycerol acyltransferase 1 inhibition with AZD7687 alters lipid handling and hormone secretion in the gut with intolerable side effects: a randomized clinical trial. Diabetes Obes Metab. 2014 Apr;16(4):334-43. PubMed PMID: 24118885.

133. Haas JT, Winter HS, Lim E, Kirby A, Blumenstiel B, DeFelice M, et al. DGAT1 mutation is linked to a congenital diarrheal disorder. J Clin Invest. 2012 Dec;122(12):4680-4. PubMed PMID: 23114594. Pubmed Central PMCID: PMC3533555.

134. Gluchowski NL, Chitraju C, Picoraro JA, Mejhert N, Pinto S, Xin W, et al. Identification and characterization of a novel DGAT1 missense mutation associated with congenital diarrhea. J Lipid Res. 2017 Apr 03. PubMed PMID: 28373485.

135. Meyers CD, Tremblay K, Amer A, Chen J, Jiang L, Gaudet D. Effect of the DGAT1 inhibitor pradigastat on triglyceride and apoB48 levels in patients with

familial chylomicronemia syndrome. Lipids Health Dis. 2015 Feb 18;14:8. PubMed PMID: 25889044. Pubmed Central PMCID: PMC4337059.

136. Stone SJ, Myers HM, Watkins SM, Brown BE, Feingold KR, Elias PM, et al. Lipopenia and skin barrier abnormalities in DGAT2-deficient mice. J Biol Chem. 2004 Mar 19;279(12):11767-76. PubMed PMID: 14668353.

137. Wakimoto K, Chiba H, Michibata H, Seishima M, Kawasaki S, Okubo K, et al. A novel diacylglycerol acyltransferase (DGAT2) is decreased in human psoriatic skin and increased in diabetic mice. Biochem Biophys Res Commun. 2003 Oct 17;310(2):296-302. PubMed PMID: 14521909.

138. Lee B, Fast AM, Zhu J, Cheng JX, Buhman KK. Intestine-specific expression of acyl CoA:diacylglycerol acyltransferase 1 reverses resistance to diet-induced hepatic steatosis and obesity in Dgat1-/- mice. J Lipid Res. 2010 Jul;51(7):1770-80. PubMed PMID: 20147738.

139. Cao J, Hawkins E, Brozinick J, Liu X, Zhang H, Burn P, et al. A predominant role of acyl-CoA:monoacylglycerol acyltransferase-2 in dietary fat absorption implicated by tissue distribution, subcellular localization, and up-regulation by high fat diet. J Biol Chem. 2004 Apr 30;279(18):18878-86. PubMed PMID: 14966132.

140. Yen CL, Cheong ML, Grueter C, Zhou P, Moriwaki J, Wong JS, et al. Deficiency of the intestinal enzyme acyl CoA:monoacylglycerol acyltransferase-2 protects mice from metabolic disorders induced by high-fat feeding. Nat Med. 2009 Apr;15(4):442-6. PubMed PMID: 19287392. Pubmed Central PMCID: PMC2786494.

141. Nelson DW, Gao Y, Yen MI, Yen CL. Intestine-specific deletion of acyl-CoA:monoacylglycerol acyltransferase (MGAT) 2 protects mice from diet-induced obesity and glucose intolerance. J Biol Chem. 2014 Jun 20;289(25):17338-49. PubMed PMID: 24784138. Pubmed Central PMCID: PMC4067168.

142. Okuma C, Ohta T, Tadaki H, Hamada H, Oda T, Taniuchi H, et al. JTP-103237, a novel monoacylglycerol acyltransferase inhibitor, modulates fat absorption and prevents diet-induced obesity. Eur J Pharmacol. 2015 Jul 05;758:72-81. PubMed PMID: 25857225.

143. Smith SJ, Cases S, Jensen DR, Chen HC, Sande E, Tow B, et al. Obesity resistance and multiple mechanisms of triglyceride synthesis in mice lacking Dgat. Nat Genet. 2000 May;25(1):87-90. PubMed PMID: 10802663.

144. Sachdev V, Leopold C, Bauer R, Patankar JV, Iqbal J, Obrowsky S, et al. Novel role of a triglyceride-synthesizing enzyme: DGAT1 at the crossroad between triglyceride and cholesterol metabolism. Biochim Biophys Acta. 2016 Sep;1861(9 Pt A):1132-41. PubMed PMID: 27344248. Pubmed Central PMCID: 4948681.

145. Birch AM, Birtles S, Buckett LK, Kemmitt PD, Smith GJ, Smith TJ, et al. Discovery of a potent, selective, and orally efficacious pyrimidinooxazinyl bicyclooctaneacetic acid diacylglycerol acyltransferase-1 inhibitor. J Med Chem. 2009 Mar 26;52(6):1558-68. PubMed PMID: 19256504.

146. Eichmann TO, Kumari M, Haas JT, Farese RV, Jr., Zimmermann R, Lass A, et al. Studies on the substrate and stereo/regioselectivity of adipose triglyceride lipase, hormone-sensitive lipase, and diacylglycerol-O-acyltransferases. J Biol Chem. 2012 Nov 30;287(49):41446-57. PubMed PMID: 23066022. Pubmed Central PMCID: 3510842.

147. Ionac M. One technique, two approaches, and results: thoracic duct cannulation in small laboratory animals. Microsurgery. 2003;23(3):239-45. PubMed PMID: 12833325.

148. Aube AC, Cabarrocas J, Bauer J, Philippe D, Aubert P, Doulay F, et al. Changes in enteric neurone phenotype and intestinal functions in a transgenic mouse model of enteric glia disruption. Gut. 2006 May;55(5):630-7. PubMed PMID: 16236773. Pubmed Central PMCID: 1856141.

149. Nguyen TM, Sawyer JK, Kelley KL, Davis MA, Rudel LL. Cholesterol esterification by ACAT2 is essential for efficient intestinal cholesterol absorption: evidence from thoracic lymph duct cannulation. J Lipid Res. 2012 Jan;53(1):95-104. PubMed PMID: 22045928. Pubmed Central PMCID: PMC3243485.

150. Patankar JV, Chandak PG, Obrowsky S, Pfeifer T, Diwoky C, Uellen A, et al. Loss of intestinal GATA4 prevents diet-induced obesity and promotes insulin

sensitivity in mice. Am J Physiol Endocrinol Metab. 2011 Mar;300(3):E478-88. PubMed PMID: 21177287. Pubmed Central PMCID: 3163292.

151. Malanovic N, Leber R, Schmuck M, Kriechbaum M, Cordfunke RA, Drijfhout JW, et al. Phospholipid-driven differences determine the action of the synthetic antimicrobial peptide OP-145 on Gram-positive bacterial and mammalian membrane model systems. Biochim Biophys Acta. 2015 Oct;1848(10 Pt A):2437-47. PubMed PMID: 26210299.

152. Boesjes M, Bloks VW, Hageman J, Bos T, van Dijk TH, Havinga R, et al. Hepatic farnesoid X-receptor isoforms alpha2 and alpha4 differentially modulate bile salt and lipoprotein metabolism in mice. PLoS One. 2014;9(12):e115028. PubMed PMID: 25506828. Pubmed Central PMCID: PMC4266635.

153. Oosterveer MH, van Dijk TH, Tietge UJ, Boer T, Havinga R, Stellaard F, et al. High fat feeding induces hepatic fatty acid elongation in mice. PLoS One. 2009 Jun 26;4(6):e6066. PubMed PMID: 19557132. Pubmed Central PMCID: PMC2699051.

154. van der Veen JN, van Dijk TH, Vrins CL, van Meer H, Havinga R, Bijsterveld K, et al. Activation of the liver X receptor stimulates trans-intestinal excretion of plasma cholesterol. J Biol Chem. 2009 Jul 17;284(29):19211-9. PubMed PMID: 19416968. Pubmed Central PMCID: PMC2740545.

155. Potthoff MJ, Kliewer SA, Mangelsdorf DJ. Endocrine fibroblast growth factors 15/19 and 21: from feast to famine. Genes & development. 2012 Feb 15;26(4):312-24. PubMed PMID: 22302876. Pubmed Central PMCID: 3289879.

156. Iqbal J, Hussain MM. Intestinal lipid absorption. Am J Physiol Endocrinol Metab. 2009 Jun;296(6):E1183-94. PubMed PMID: 19158321. Pubmed Central PMCID: PMC2692399.

157. Martins IJ, Mortimer BC, Miller J, Redgrave TG. Effects of particle size and number on the plasma clearance of chylomicrons and remnants. J Lipid Res. 1996 Dec;37(12):2696-705. PubMed PMID: 9017520.

158. Lin HV, Chen D, Shen Z, Zhu L, Ouyang X, Vongs A, et al. Diacylglycerol acyltransferase-1 (DGAT1) inhibition perturbs postprandial gut hormone release.

PLoS One. 2013;8(1):e54480. PubMed PMID: 23336002. Pubmed Central PMCID: PMC3545956.

159. Kirby RJ, Howles PN, Hui DY. Rate of gastric emptying influences dietary cholesterol absorption efficiency in selected inbred strains of mice. J Lipid Res. 2004 Jan;45(1):89-98. PubMed PMID: 14563823.

160. Jia L, Ma Y, Rong S, Betters JL, Xie P, Chung S, et al. Niemann-Pick C1-Like 1 deletion in mice prevents high-fat diet-induced fatty liver by reducing lipogenesis. J Lipid Res. 2010 Nov;51(11):3135-44. PubMed PMID: 20699423. Pubmed Central PMCID: PMC2952554.

161. Vrins CL, van der Velde AE, van den Oever K, Levels JH, Huet S, Oude Elferink RP, et al. Peroxisome proliferator-activated receptor delta activation leads to increased transintestinal cholesterol efflux. J Lipid Res. 2009 Oct;50(10):2046-54. PubMed PMID: 19439761. Pubmed Central PMCID: PMC2739754.

162. Vrins CL, Ottenhoff R, van den Oever K, de Waart DR, Kruyt JK, Zhao Y, et al. Trans-intestinal cholesterol efflux is not mediated through high density lipoprotein. J Lipid Res. 2012 Oct;53(10):2017-23. PubMed PMID: 22802462. Pubmed Central PMCID: PMC3435535.

163. Kashiwa M, Masuyama Y, Miyauchi H, Uchida T, Naganuma S, Kakuta H, et al. Pharmacological properties of YM17E, an acyl-CoA:cholesterol acyltransferase inhibitor, and diarrheal effect in beagle dogs. Jpn J Pharmacol. 1997 Jan;73(1):41-50. PubMed PMID: 9032133.

164. Hussain MM, Rava P, Walsh M, Rana M, Iqbal J. Multiple functions of microsomal triglyceride transfer protein. Nutr Metab (Lond). 2012 Feb 21;9:14. PubMed PMID: 22353470. Pubmed Central PMCID: PMC3337244.

165. Collins R, Reith C, Emberson J, Armitage J, Baigent C, Blackwell L, et al. Interpretation of the evidence for the efficacy and safety of statin therapy. Lancet. 2016 Nov 19;388(10059):2532-61. PubMed PMID: 27616593.

166. Hoeke G, Kooijman S, Boon MR, Rensen PC, Berbee JF. Role of Brown Fat in Lipoprotein Metabolism and Atherosclerosis. Circ Res. 2016 Jan 08;118(1):173-82. PubMed PMID: 26837747.

167. Cannon B, Nedergaard J. Brown adipose tissue: function and physiological significance. Physiol Rev. 2004 Jan;84(1):277-359. PubMed PMID: 14715917.

168. Chechi K, Carpentier AC, Richard D. Understanding the brown adipocyte as a contributor to energy homeostasis. Trends Endocrinol Metab. 2013 Aug;24(8):408-20. PubMed PMID: 23711353.

169. Peng XR, Gennemark P, O'Mahony G, Bartesaghi S. Unlock the Thermogenic Potential of Adipose Tissue: Pharmacological Modulation and Implications for Treatment of Diabetes and Obesity. Front Endocrinol (Lausanne). 2015;6:174. PubMed PMID: 26635723. Pubmed Central PMCID: PMC4657528.

170. Heaton JM. The distribution of brown adipose tissue in the human. Journal of anatomy. 1972 May;112(Pt 1):35-9. PubMed PMID: 5086212. Pubmed Central PMCID: 1271341.

171. van Marken Lichtenbelt WD, Vanhommerig JW, Smulders NM, Drossaerts JM, Kemerink GJ, Bouvy ND, et al. Cold-activated brown adipose tissue in healthy men. N Engl J Med. 2009 Apr 09;360(15):1500-8. PubMed PMID: 19357405.

172. Virtanen KA, Lidell ME, Orava J, Heglind M, Westergren R, Niemi T, et al. Functional brown adipose tissue in healthy adults. N Engl J Med. 2009 Apr 09;360(15):1518-25. PubMed PMID: 19357407.

173. Cypess AM, Lehman S, Williams G, Tal I, Rodman D, Goldfine AB, et al. Identification and importance of brown adipose tissue in adult humans. N Engl J Med. 2009 Apr 09;360(15):1509-17. PubMed PMID: 19357406. Pubmed Central PMCID: 2859951.

174. Hany TF, Gharehpapagh E, Kamel EM, Buck A, Himms-Hagen J, von Schulthess GK. Brown adipose tissue: a factor to consider in symmetrical tracer uptake in the neck and upper chest region. European journal of nuclear medicine and molecular imaging. 2002 Oct;29(10):1393-8. PubMed PMID: 12271425.

175. Ouellet V, Labbe SM, Blondin DP, Phoenix S, Guerin B, Haman F, et al. Brown adipose tissue oxidative metabolism contributes to energy expenditure during acute cold exposure in humans. J Clin Invest. 2012 Feb;122(2):545-52. PubMed PMID: 22269323. Pubmed Central PMCID: 3266793.

176. van der Lans AA, Hoeks J, Brans B, Vijgen GH, Visser MG, Vosselman MJ, et al. Cold acclimation recruits human brown fat and increases nonshivering thermogenesis. J Clin Invest. 2013 Aug;123(8):3395-403. PubMed PMID: 23867626. Pubmed Central PMCID: 3726172.

177. Yoneshiro T, Aita S, Matsushita M, Kayahara T, Kameya T, Kawai Y, et al. Recruited brown adipose tissue as an antiobesity agent in humans. J Clin Invest. 2013 Aug;123(8):3404-8. PubMed PMID: 23867622. Pubmed Central PMCID: 3726164.

178. Brown RJ, Rader DJ. Lipases as modulators of atherosclerosis in murine models. Current drug targets. 2007 Dec;8(12):1307-19. PubMed PMID: 18220707.

179. Olivecrona G, Olivecrona T. Triglyceride lipases and atherosclerosis. Curr Opin Lipidol. 2010 Oct;21(5):409-15. PubMed PMID: 20683326.

180. Beigneux AP, Davies BS, Gin P, Weinstein MM, Farber E, Qiao X, et al. Glycosylphosphatidylinositol-anchored high-density lipoprotein-binding protein 1 plays a critical role in the lipolytic processing of chylomicrons. Cell Metab. 2007 Apr;5(4):279-91. PubMed PMID: 17403372. Pubmed Central PMCID: PMC1913910.

181. Davies BS, Beigneux AP, Barnes RH, 2nd, Tu Y, Gin P, Weinstein MM, et al. GPIHBP1 is responsible for the entry of lipoprotein lipase into capillaries. Cell Metab. 2010 Jul 07;12(1):42-52. PubMed PMID: 20620994. Pubmed Central PMCID: PMC2913606.

182. Glatz JF, Luiken JJ, Bonen A. Membrane fatty acid transporters as regulators of lipid metabolism: implications for metabolic disease. Physiol Rev. 2010 Jan;90(1):367-417. PubMed PMID: 20086080.

183. Nilsson SK, Heeren J, Olivecrona G, Merkel M. Apolipoprotein A-V; a potent triglyceride reducer. Atherosclerosis. 2011 Nov;219(1):15-21. PubMed PMID: 21831376.

184. Merkel M, Loeffler B, Kluger M, Fabig N, Geppert G, Pennacchio LA, et al. Apolipoprotein AV accelerates plasma hydrolysis of triglyceride-rich lipoproteins by

interaction with proteoglycan-bound lipoprotein lipase. J Biol Chem. 2005 Jun 03;280(22):21553-60. PubMed PMID: 15774484.

185. Schaap FG, Rensen PC, Voshol PJ, Vrins C, van der Vliet HN, Chamuleau RA, et al. ApoAV reduces plasma triglycerides by inhibiting very low density lipoprotein-triglyceride (VLDL-TG) production and stimulating lipoprotein lipase-mediated VLDL-TG hydrolysis. J Biol Chem. 2004 Jul 02;279(27):27941-7. PubMed PMID: 15090553.

186. Lichtenstein L, Kersten S. Modulation of plasma TG lipolysis by Angiopoietin-like proteins and GPIHBP1. Biochim Biophys Acta. 2010 Apr;1801(4):415-20. PubMed PMID: 20056168.

187. Peterfy M, Ben-Zeev O, Mao HZ, Weissglas-Volkov D, Aouizerat BE, Pullinger CR, et al. Mutations in LMF1 cause combined lipase deficiency and severe hypertriglyceridemia. Nat Genet. 2007 Dec;39(12):1483-7. PubMed PMID: 17994020.

188. Breckenridge WC, Little JA, Steiner G, Chow A, Poapst M. Hypertriglyceridemia associated with deficiency of apolipoprotein C-II. N Engl J Med. 1978 Jun 08;298(23):1265-73. PubMed PMID: 565877.

189. Pennacchio LA, Olivier M, Hubacek JA, Cohen JC, Cox DR, Fruchart JC, et al. An apolipoprotein influencing triglycerides in humans and mice revealed by comparative sequencing. Science. 2001 Oct 05;294(5540):169-73. PubMed PMID: 11588264.

190. Wang J, Hegele RA. Homozygous missense mutation (G56R) in glycosylphosphatidylinositol-anchored high-density lipoprotein-binding protein 1 (GPI-HBP1) in two siblings with fasting chylomicronemia (MIM 144650). Lipids Health Dis. 2007 Sep 20;6:23. PubMed PMID: 17883852. Pubmed Central PMCID: 2039732.

191. Havel RJ, Gordon RS, Jr. Idiopathic hyperlipemia: metabolic studies in an affected family. J Clin Invest. 1960 Dec;39:1777-90. PubMed PMID: 13712364. Pubmed Central PMCID: 441903.

192. Laatsch A, Merkel M, Talmud PJ, Grewal T, Beisiegel U, Heeren J. Insulin stimulates hepatic low density lipoprotein receptor-related protein 1 (LRP1) to increase postprandial lipoprotein clearance. Atherosclerosis. 2009 May;204(1):105-11. PubMed PMID: 18834984.

193. Heeren J, Niemeier A, Merkel M, Beisiegel U. Endothelial-derived lipoprotein lipase is bound to postprandial triglyceride-rich lipoproteins and mediates their hepatic clearance in vivo. J Mol Med (Berl). 2002 Sep;80(9):576-84. PubMed PMID: 12226739.

194. Foley EM, Gordts PL, Stanford KI, Gonzales JC, Lawrence R, Stoddard N, et al. Hepatic remnant lipoprotein clearance by heparan sulfate proteoglycans and low-density lipoprotein receptors depend on dietary conditions in mice. Arteriosclerosis, thrombosis, and vascular biology. 2013 Sep;33(9):2065-74. PubMed PMID: 23846497. Pubmed Central PMCID: 3821931.

195. Bartelt A, Merkel M, Heeren J. A new, powerful player in lipoprotein metabolism: brown adipose tissue. J Mol Med (Berl). 2012 Aug;90(8):887-93. PubMed PMID: 22231746.

196. Bartelt A, Bruns OT, Reimer R, Hohenberg H, Ittrich H, Peldschus K, et al. Brown adipose tissue activity controls triglyceride clearance. Nat Med. 2011 Feb;17(2):200-5. PubMed PMID: 21258337.

197. Khedoe PP, Hoeke G, Kooijman S, Dijk W, Buijs JT, Kersten S, et al. Brown adipose tissue takes up plasma triglycerides mostly after lipolysis. J Lipid Res. 2015 Jan;56(1):51-9. PubMed PMID: 25351615. Pubmed Central PMCID: PMC4274071.

198. Park JW, Jung KH, Lee JH, Quach CH, Moon SH, Cho YS, et al. 18F-FDG PET/CT monitoring of beta3 agonist-stimulated brown adipocyte recruitment in white adipose tissue. J Nucl Med. 2015 Jan;56(1):153-8. PubMed PMID: 25525187.

199. Stanford KI, Middelbeek RJ, Townsend KL, An D, Nygaard EB, Hitchcox KM, et al. Brown adipose tissue regulates glucose homeostasis and insulin

sensitivity. J Clin Invest. 2013 Jan;123(1):215-23. PubMed PMID: 23221344. Pubmed Central PMCID: PMC3533266.

200. Hao Q, Yadav R, Basse AL, Petersen S, Sonne SB, Rasmussen S, et al. Transcriptome profiling of brown adipose tissue during cold exposure reveals extensive regulation of glucose metabolism. Am J Physiol Endocrinol Metab. 2015 Mar 01;308(5):E380-92. PubMed PMID: 25516548.

201. Festuccia WT, Blanchard PG, Deshaies Y. Control of Brown Adipose Tissue Glucose and Lipid Metabolism by PPARgamma. Front Endocrinol (Lausanne). 2011;2:84. PubMed PMID: 22654830. Pubmed Central PMCID: 3356105.

202. Teperino R, Amann S, Bayer M, McGee SL, Loipetzberger A, Connor T, et al. Hedgehog partial agonism drives Warburg-like metabolism in muscle and brown fat. Cell. 2012 Oct 12;151(2):414-26. PubMed PMID: 23063129.

203. de Jesus LA, Carvalho SD, Ribeiro MO, Schneider M, Kim SW, Harney JW, et al. The type 2 iodothyronine deiodinase is essential for adaptive thermogenesis in brown adipose tissue. J Clin Invest. 2001 Nov;108(9):1379-85. PubMed PMID: 11696583. Pubmed Central PMCID: PMC209445.

204. Christoffolete MA, Linardi CC, de Jesus L, Ebina KN, Carvalho SD, Ribeiro MO, et al. Mice with targeted disruption of the Dio2 gene have cold-induced overexpression of the uncoupling protein 1 gene but fail to increase brown adipose tissue lipogenesis and adaptive thermogenesis. Diabetes. 2004 Mar;53(3):577-84. PubMed PMID: 14988240.

205. Marsili A, Aguayo-Mazzucato C, Chen T, Kumar A, Chung M, Lunsford EP, et al. Mice with a targeted deletion of the type 2 deiodinase are insulin resistant and susceptible to diet induced obesity. PLoS One. 2011;6(6):e20832. PubMed PMID: 21698184. Pubmed Central PMCID: PMC3116839.

206. Zimmermann R, Strauss JG, Haemmerle G, Schoiswohl G, Birner-Gruenberger R, Riederer M, et al. Fat mobilization in adipose tissue is promoted by adipose triglyceride lipase. Science. 2004 Nov 19;306(5700):1383-6. PubMed PMID: 15550674.

207. Bostrom P, Wu J, Jedrychowski MP, Korde A, Ye L, Lo JC, et al. A PGC1-alpha-dependent myokine that drives brown-fat-like development of white fat and thermogenesis. Nature. 2012 Jan 11;481(7382):463-8. PubMed PMID: 22237023. Pubmed Central PMCID: 3522098.

208. Collins S, Yehuda-Shnaidman E, Wang H. Positive and negative control of Ucp1 gene transcription and the role of beta-adrenergic signaling networks. Int J Obes (Lond). 2010 Oct;34 Suppl 1:S28-33. PubMed PMID: 20935662.

209. Labbe SM, Caron A, Bakan I, Laplante M, Carpentier AC, Lecomte R, et al. In vivo measurement of energy substrate contribution to cold-induced brown adipose tissue thermogenesis. FASEB J. 2015 May;29(5):2046-58. PubMed PMID: 25681456.

210. Trayhurn P. Fatty acid synthesis in mouse brown adipose tissue. The influence of environmental temperature on the proportion of whole-body fatty acid synthesis in brown adipose tissue and the liver. Biochim Biophys Acta. 1981 Jun 23;664(3):549-60. PubMed PMID: 7272321.

211. Westerberg R, Mansson JE, Golozoubova V, Shabalina IG, Backlund EC, Tvrdik P, et al. ELOVL3 is an important component for early onset of lipid recruitment in brown adipose tissue. J Biol Chem. 2006 Feb 24;281(8):4958-68. PubMed PMID: 16326704.

212. Tan CY, Virtue S, Bidault G, Dale M, Hagen R, Griffin JL, et al. Brown Adipose Tissue Thermogenic Capacity Is Regulated by Elovl6. Cell reports. 2015 Dec 15;13(10):2039-47. PubMed PMID: 26628376. Pubmed Central PMCID: 4688035.

213. Harris CA, Haas JT, Streeper RS, Stone SJ, Kumari M, Yang K, et al. DGAT enzymes are required for triacylglycerol synthesis and lipid droplets in adipocytes. J Lipid Res. 2011 Apr;52(4):657-67. PubMed PMID: 21317108. Pubmed Central PMCID: PMC3284159.

214. Irshad Z, Dimitri F, Christian M, Zammit VA. Diacylglycerol acyltransferase 2 links glucose utilization to fatty acid oxidation in the brown adipocytes. J Lipid

Res. 2017 Jan;58(1):15-30. PubMed PMID: 27836993. Pubmed Central PMCID: PMC5234708.

215. Futatsugi K, Kung DW, Orr ST, Cabral S, Hepworth D, Aspnes G, et al. Discovery and Optimization of Imidazopyridine-Based Inhibitors of Diacylglycerol Acyltransferase 2 (DGAT2). J Med Chem. 2015 Sep 24;58(18):7173-85. PubMed PMID: 26349027.

216. Pessentheiner AR, Pelzmann HJ, Walenta E, Schweiger M, Groschner LN, Graier WF, et al. NAT8L (N-acetyltransferase 8-like) accelerates lipid turnover and increases energy expenditure in brown adipocytes. J Biol Chem. 2013 Dec 13;288(50):36040-51. PubMed PMID: 24155240. Pubmed Central PMCID: 3861652.

217. Werner A, Minich DM, Havinga R, Bloks V, Van Goor H, Kuipers F, et al. Fat malabsorption in essential fatty acid-deficient mice is not due to impaired bile formation. Am J Physiol Gastrointest Liver Physiol. 2002 Oct;283(4):G900-8. PubMed PMID: 12223350.

218. Haemmerle G, Lass A, Zimmermann R, Gorkiewicz G, Meyer C, Rozman J, et al. Defective lipolysis and altered energy metabolism in mice lacking adipose triglyceride lipase. Science. 2006 May 05;312(5774):734-7. PubMed PMID: 16675698.

219. Ahmadian M, Abbott MJ, Tang T, Hudak CS, Kim Y, Bruss M, et al. Desnutrin/ATGL is regulated by AMPK and is required for a brown adipose phenotype. Cell Metab. 2011 Jun 08;13(6):739-48. PubMed PMID: 21641555. Pubmed Central PMCID: 3148136.

Abbreviations

ABC	ATP-binding cassette
ACAT	Acyl CoA:cholesterol acyltransferase
ACSL	Acyl-coenzyme A synthetase
AGPAT	1-acylglycerol- 3-phosphate acyltransferase
AMPK	AMP-activated protein kinase
apoA1	Apolipoprotein A1
apoB	Apolipoprotein B
ATGL	Adipose triglyceride lipase
BAT	Brown adipose tissue
BBM	Brush border membrane
cAMP	cyclic AMP
CD36	Cluster of differentiation 36
CE	Cholesterol esters
CLDs	Cytosolic lipid droplets
CMs	Chylomicrons
COPII	Coat protein complex II
CREB	cAMP response element binding protein
CRs	Chylomicron remnants
CVD	Cardiovascular diseases
DG	Diglycerides
DGAT	Diacylglycerol acyl transferases
DIO1	Deiodinase 1
DIO2	Deiodinase 2
DNL	De novo lipogenesis
EE	Energy expenditure
ELOVL	Very-long-chain fatty acid elongases
ELOVL	long-chain FA elongase
ER	Endoplasmic reticulum
FABP	Fatty-acid binding protein
FAS	Fatty acid synthase
FAs	Fatty acids

FAS	FA synthase
FATP4	Fatty acid transport protein 4
FC	Free cholesterol
FFA	Free fatty acid
GLP-1	Glucagon-like peptide 1
GLUT	glucose transporter
GPAT	Glycerol-3-phosphate acyl transferase
HDL-C	High-density lipoprotein cholesterol
HF/HCD	High fat/high cholesterol diet
HSL	Hormone sensitve lipase
HSPGs	Hepran sulphate proteoglycans
I-DGAT1-/-	Intestinal-DGAT1 deficiency
IFABP	Intestinal-specific FABP
LDL	Low-density lipoprotein
LFABP	Liver-specific FABP
LPL	Lipoprotein lipase
LRP1	LDL receptor-related protein
MAG	Monoacylglycerols
MAPK	Mitogen-activated Protein Kinase
MetS	Metabolic syndrome
MGAT	Monoacylglycerol acyltransferase
MGL	Monoacylglycerol lipase
MTP	Microsomal transfer protein
NEFA	Non-esterified free fatty acids
NPC1L1	Niemann Pick C1 like 1 protein
NSL	Neutral sterol
NST	Non-shivering thermogenesis
PCTVs	Pre-chylomicron transport vesicles
PET-CT	Positron emission tomography-computed tomography
PGC1α	Peroxisome proliferator-activated receptor γ coactivator 1α
PKA	Protein Kinase A
SM	Skeletal muscle
SR-B1	Scavenger receptor class B type 1

T2DM	Type 2 diabetes mellitus
TG	Triglycerides
TICE	Trans-intestinal cholesterol excretion
TRLs	Triglyceride-rich lipoproteins
UCP1	Uncoupling protein 1
VLDL	Very low-density lipoproteins
WAT	White adipose tissue
β3-AR	β3-adrenergic receptor
β-Ars	Beta-adrenergic receptors

Appendix

Permissions granted by the publishers to use their figures in this doctoral thesis

Figure or Table number	Licensed content publisher and granted license number
Figure 1	Elsevier, 4102540384930
Figure 2	American Society for Clinical Investigation, 4102550281631
Figure 3 and 4	Annual Reviews, permission not required for use in thesis
Table 1	ASBMB, permission not required for use in thesis
Figure 5	Elsevier, 4102560274877
Figure 6 and 7	ASBMB, permission not required for use in thesis
Figure 8-26	Elsevier, permission not required for author of publication
Figure 27	Front. Endocrinol., open-access journal
Figure 28	Springer, 4102561358005
Figure 29	Wolters Kluwer Health Inc., 4102570262414

Note: Detailed PDF copies of the license documents will be furbished upon request.